University of Alberta

Techniques for Improved CDMA Forward Link Performance

by

Geoffrey G. Messier 

A thesis submitted to the Faculty of Graduate Studies and Research in partial fulfillment of the requirements for the degree of **Doctor of Philosophy**.

Department of Electrical and Computer Engineering

Edmonton, Alberta, Canada
Fall 2004

Your file Votre référence
ISBN: 0-612-95987-2
Our file Notre référence
ISBN: 0-612-95987-2

For Mom and Dad.

Acknowledgements

I would like to thank Dr. Witold Krzymień for his considerable guidance and support. I am also grateful for the support I have received from everyone at TR*Labs*. Finally, I would like to thank TR*Labs*, the Alberta Informatics Circle of Research Excellence (iCORE), the Natural Sciences and Engineering Research Council (NSERC) and the University of Alberta for their funding support.

Contents

List of Figures

List of Symbols

y_i	-	ith received channel encoded symbol at the channel decoder input
$\sigma^2(i)$	-	variance of the interference and noise at the channel decoder input during symbol interval i
$\zeta(i)$	-	amplitude of the desired signal at the channel decoder input during symbol interval i
b_i	-	ith transmitted channel encoded data symbol
x_i	-	ith channel encoded data symbol along the trellis path being evaluated in the channel decoder metric calculation
N_s	-	number of channel encoded symbols in a frame
d_k	-	kth information bit
$\Lambda(d_k)$	-	log-likelihood ratio for data information symbol d_k
N_d	-	number of data bits in a frame
μ	-	channel decoder metric
μ_{ML}	-	channel decoder metric of maximum-likelihood path
N_R	-	number of channel encoded symbols per information bit
$p_\theta(k)$	-	the *a priori* probability that the kth data bit is equal to θ
$d_{k,ML}$	-	kth information bit along the maximum likelihood trellis path
S_k	-	channel encoder state during bit interval k
B_k^θ	-	set of all encoder state transitions corresponding to an information bit θ during bit interval k
$\Xi(n)$	-	large scale fading process
$c_\phi(n,l)$	-	complex small scale channel impulse response between the mobile and transmit antenna ϕ
L	-	number of impulse response terms with significant multipath energy
R	-	number of spreading sequence chips per channel encoded symbol
$b_{i,k}$	-	ith transmitted channel encoded symbol for user k
$s_{i,k}(n)$	-	nth chip of the spreading sequence for the i channel encoded symbol of user k
$\boldsymbol{d}_{i,v}^l(a,b)$	-	lth multipath replica of the vth chip during symbol interval i captured in a window between samples a and b

σ_N^2 - variance of the intercell interference plus thermal noise process at the mobile receiver input

σ_I^2 - variance of the forward link composite signal after large scale fading

F - number of fingers in the Rake receiver

S - number of samples per chip

z_f - multipath delay tracked by finger f

$w_i(f)$ - finger combining weight for finger f during symbol interval i

$\boldsymbol{E}_i$ - equalizer tap weight matrix

$e_i(v)$ - vth tap weight during symbol interval i

N_T - number of equalizer taps

K - number of forward link traffic transmissions

$G_{i,k}$ - forward link gain applied to the k traffic transmission during symbol interval i

$N(n)$ - intercell interference plus thermal noise process at the mobile receiver input

$N_{r,i}$ - a Gaussian random variable resulting from despreading $N(n)$ with an offset of r during symbol interval i

$I(n)$ - composite forward link signal after large scale channel attenuation

$I^{\alpha}(n)$ - composite forward link signal from STTD antenna α after large scale channel attenuation

$I_{r,i}$ - normalized sum of R samples of $I(n)$ multiplied by the spreading code of user 0 with an offset of r

$\delta(x)$ - delta function (1 if $x = 0$ and 0 otherwise)

$X_i^{\alpha}(n)$ - signal transmitted from STTD antenna α during symbol interval i

N_i - intercell interference plus thermal noise term at the channel decoder input

I_i - intracell interference term at the channel decoder input

$U_{f,i}$ - $U_{f,i}$ is the noise and interference at the output of the despreading stage in finger f during symbol interval i

A - amplitude representing the combination of transmit amplitude and despreading gain

$Z(n)$ - zero mean complex AWGN process at the mobile receiver input

σ_Z^2 - variance of $Z(n)$

Z_i - contribution of $Z(n)$ at the channel decoder input

$Z_{r,i}$ - normalized sum of R samples of $Z(n)$ multiplied by the spreading code of user 0 with an offset of r

$r(n)$ - total signal at the mobile receiver input

$\phi_v(n)$ - autocorrelation function of $r(n)$

N_ϕ - number of samples used to calculate the time-domain autocorrelation function of $r(n)$

N_W - observation window of the LSE estimator for σ_N^2 and σ_I^2

$\boldsymbol{I}(\boldsymbol{\Theta})$ - Fisher information matrix

μ_E - mean of the LSE estimates of either σ_I^2 or σ_N^2

σ_E - standard deviation of the LSE estimates of either σ_I^2 or σ_N^2

γ - signal to noise plus interference ratio estimated by online estimation

ρ - ratio of signal amplitude to interference plus noise variance at the channel decoder input

$\widehat{\rho}$ - estimated ratio of signal amplitude to interference plus noise variance at the channel decoder input

V_l - complex Gaussian error process with zero mean corrupting the estimate of the lth multipath component

σ_V^2 - variance of V_l

$y_{CE,i}$ - ith received channel encoded symbol at the channel decoder input when channel estimation errors are considered

$\sigma_C^2(l)$ - variance of the Gaussian process making up the lth Rayleigh fading multipath component

$\sigma_U^2(f)$ - variance of the interference plus noise term in finger f

$\Phi_{y_i}(\omega)$ - the characteristic function of the distribution of y_i

$N_{f,k}$ - partial fraction expansion coefficient of the kth characteristic function term corresponding to finger f that has a negative pole

$P_{f,k}$ - partial fraction expansion coefficient of the kth characteristic function term corresponding to finger f that has a positive pole

$f_A(y_{CE,i})$ - approximate distribution of y_{CE}

G_{CE} - processing gain of the channel estimation scheme

P_D - received power from the desired base station

ρ_P - fraction of total forward channel power allocated to the pilot signal

$P_{N,k}$ - received power from the kth neighboring base station

P_{Th} - thermal noise power

E_b - energy per bit

$f_H(y_{CE,i})$ - numerically generated histogram of the distribution of $y_{CE,i}$

$\zeta(i)_f$ - magnitude of the desired signal at the output of finger f

$\sigma^2(i)_f$ - interference plus noise variance at the output of finger f

Chapter 1

Introduction

The purpose of this thesis is to improve the forward link physical layer performance of code division multiple access (CDMA) cellular telephone systems. This is accomplished by finding new ways to improve the decoding of convolutional and turbo codes in the CDMA mobile.

This introduction will justify this thesis topic by first establishing the relevance of CDMA technology to the wireless industry and then by discussing why CDMA forward link performance, in particular, is an important issue. Finally, it will be shown that finding ways to improve CDMA mobile channel decoder performance is a particularly attractive way to improve the forward link.

Section 1.1 presents a brief overview of the wireless industry that illustrates why CDMA is an important technology. This section shows that CDMA is widely used in current wireless networks and will become even more prominent in future systems. It also points out that forward link performance is a critical issue. The voice capacity of most CDMA networks currently deployed in the field is limited by the forward link. This problem is only expected to become more serious with the introduction of download-intensive, asymmetric wireless data service.

Given the importance of CDMA technology and the severity of the forward link performance issue, improving the CDMA forward link physical layer is a very active area of research. An introduction to the CDMA forward link and a

comparison of the techniques currently being proposed to improve its performance is provided in Section 1.2. This comparison will show that there are several advantages to improving forward link performance by making improvements to the CDMA mobile channel decoding process. The techniques presented in this thesis that contribute to making these improvements are therefore an attractive way of achieving better CDMA forward link performance.

Specifically, the techniques presented in this thesis seek to improve CDMA mobile channel decoder performance by improving the accuracy of the decoder trellis path metric calculations. Before presenting this research, it is necessary to review some basic channel coding principles that outline what channel decoder trellis path metrics are and how they fit into the channel decoding process. This review is provided in Section 1.3.

Section 1.4 is an overview of the two scenarios considered when improving mobile channel decoder performance. In the first scenario, the channel estimates used for mobile Rake receiver combining are perfect and the mobile channel decoder uses conventional channel decoder metrics. The accuracy of these metrics is improved through better estimation of the channel state information (CSI) required by the metric calculations. In the second scenario, the channel estimates used by the mobile Rake receiver are subject to estimation error. The effect of this estimation error is accounted for in the channel decoder calculation either by adding a bias term to the CSI used by the conventional metric or by deriving a completely new metric that incorporates received symbol uncertainty due to Rake finger combining weight estimation error.

Finally, Section 1.5 provides a thesis overview that outlines the organization, content and research contribution of each of the chapters in this thesis.

1.1 CDMA Technology

CDMA is a multiple access technique. Multiple access techniques are methods for sharing frequency spectrum among several users in a wireless system. Users in a CDMA system multiply their signals by unique spreading sequences and transmit simultaneously on the same carrier frequency [78]. These spreading sequences make it possible to separate the signals of different users at the receiver. Other multiple access techniques include frequency division multiple access (FDMA) and time division multiple access (TDMA). In an FDMA system, different users are assigned different frequency channels. In a TDMA system, several users share the same frequency channel but transmit in different timeslots.

CDMA technology has established a strong position in the second generation (2G) digital cellular market. Second generation cellular networks were initially deployed in the mid 1990's and they are still being used extensively today. The introduction of 2G digital voice service saw the world converge on a relatively small number of standards that include: the Global System for Mobile communications (GSM), cdmaOne IS-95 and North American TDMA [15]. While GSM clearly dominates with 66% of the global market, the 11% CDMA market share is still approaching 100 million subscribers [15]. The 2G CDMA subscriber base is primarily concentrated in North America with some strong markets in Asia, particularly Korea.

Second generation cellular networks are now evolving to 2.5G and 3G technology that has the ability to provide wireless data service. As this evolution takes place, CDMA is positioned to become the dominant global multiple access technique. Naturally, the evolution of IS-95 networks is following a CDMA path [15]. In the short term, IS-95 service providers are upgrading to the IS-2000/cdma2000 standard. This system provides simultaneous voice and data service using a 1.25 MHz bandwidth CDMA interface that is backwards compatible

with IS-95. In the longer term, IS-2000 networks will evolve to the 1x Evolution, Data Only (1xEV-DO) and 1x Evolution, Data Voice (1xEV-DV) standards. These systems employ an air interface that mixes CDMA with packet data access techniques that involve link adaptation and scheduling of transmission [6, 73].

The real growth in CDMA technology will be seen as GSM networks evolve to the CDMA-based 3G Universal Mobile Telecommunications System (UMTS) [15]. To provide wireless data service in the short term, GSM providers are retaining the GSM base station to mobile air interface and upgrading their core network to conform to the General Packet Radio Service (GPRS) standard. The GPRS standard applies only to the core network and facilitates easy access to both the conventional telephone network and the Internet. In some cases, the GSM base stations and mobiles will also be replaced with ones supporting the 2.5G Edge high data rate air interface standard.

In the near future, the 2.5G GPRS/Edge technology will be upgraded to UMTS. The UMTS upgrade will replace the GSM and Edge base stations with systems that use a CDMA physical layer. In addition to the existing European and Asian GSM service providers, many of the major North American TDMA service providers, such as Cingular, are also choosing the GPRS/UMTS evolutionary path.

Clearly, CDMA will remain an important worldwide cellular network multiple access technique for the foreseeable future. As a result, research dealing with the improvement of CDMA system performance is extremely relevant to the wireless industry.

1.2 The CDMA Forward Link

Some analysis performed during the initial deployment of 2G CDMA predicted that the forward link would be the voice capacity bottleneck of CDMA systems

[30] and practical experience has proven this to be true in the vast majority of networks. The deployment of wireless data service will make CDMA forward link performance an even more important issue since many data applications feature download intensive, asymmetric traffic.

A block diagram of the CDMA forward link is shown in Fig. 1.1. The base station transmits a number of data streams in parallel. These can be transmissions to different mobiles or, in some cases, different parallel transmissions to the same mobile. Each data stream is encoded using a channel code, interleaved and multiplied by a gain factor that is adjusted based on some kind of forward link power control scheme. The signals are then spread with a unique spreading sequence. In cellular CDMA systems, the spreading sequences applied to each of the parallel signals are typically Walsh sequences [71, 72, 3]. The signals are then added together and spread with a second spreading sequence that is common to all transmissions in a particular sector. Cellular systems will construct this sector-specific spreading code using either PN sequences [71, 72] or Gold sequences [3]. The mobile receives the base station transmission and uses a receiver block to recover the desired channel encoded symbols. The symbols are then de-interleaved and passed to a channel decoder which performs some error correction in an attempt to recover the transmitted data.

Given the importance of the CDMA forward link, several interesting areas of research into improving its performance have developed. Each of these initiatives focus on improving a different aspect of the forward link shown in Fig. 1.1.

There are many techniques for improving CDMA forward link performance that require changes to the base station transmit chain. A stronger code can be used in the channel encoder block. An example is the turbo coding [8] that has been incorporated into many of the next generation CDMA standards for use with high data rate transmission [72, 1]. Another improvement is to use a

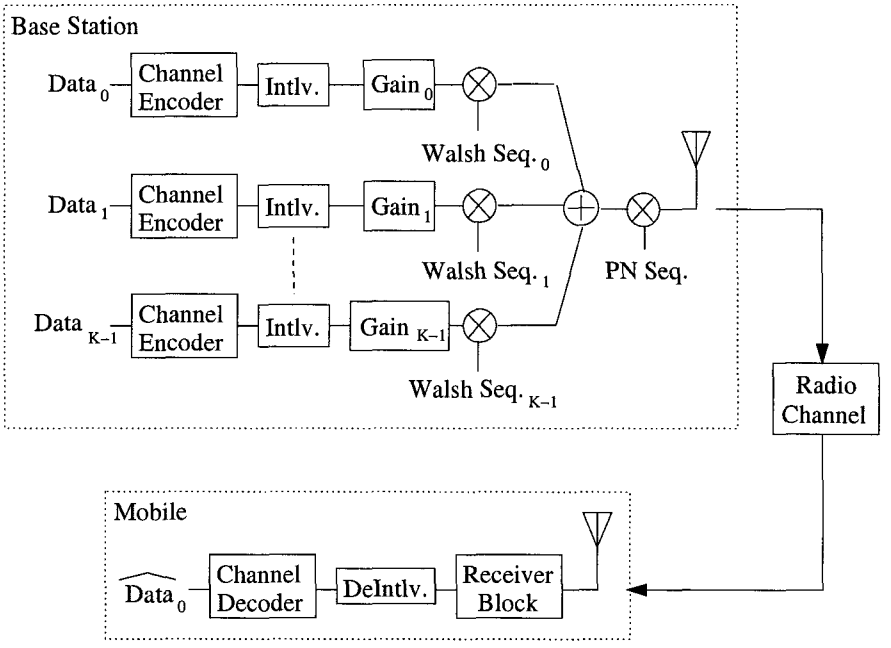

Figure 1.1: CDMA forward link.

fast forward power control scheme to adjust the transmit gains in Fig. 1.1 in an attempt to compensate for forward link fading. The spreading stages of the base station can also be changed to use sequences with improved interference suppression capability, such as the zero correlation zone (ZCZ) codes [18]. These codes allow the mobile despreading stage to completely cancel CDMA intracell interference, as long as the multipath dispersion of the forward link channel is modest. Increasing the number of base station transmit antennas has also been proposed in order to implement techniques ranging from classic adaptive beamforming [68] to transmit diversity [31] and spatial multiplexing techniques that attempt to achieve the capacity improvements shown by Foschini and Gans [19].

While these techniques do offer significant performance improvements, changes to the transmit chain of the base station almost always require a change in the industry standard that specifies the base station design. Updating these standards can be a slow process and can sometimes delay the deployment of a new technology.

Modifying existing base stations or deploying new base stations with new features can also be time consuming and expensive.

In contrast, improvements can be made to the mobile receive chain much more easily. The design of mobile and base station receiver chains are typically not regulated by industry standards. This leaves each mobile phone vendor free to implement any new receiver enhancement they wish, at any time. The turnover for phones is also much higher than for network infrastructure. This makes it easier to introduce phones with new enhancements into the market.

Research into improving the CDMA mobile receive chain has focused mainly on the development of advanced receiver designs that are capable of canceling interference. Some examples of these designs include symbol-level interference cancellation performed using a Rake receiver structure where the Rake finger combining weights are calculated according to an SNIR maximization or Neyman-Pearson detection criterion [10, 40]. This structure is called the Generalized Rake (GRake) receiver. Linear minimum mean squared error (LMMSE) equalizers have also be proposed for interference cancellation in the CDMA mobile both at the symbol-level [44, 65, 14, 37, 80] and chip-level [36, 21, 26, 14, 38, 67, 37, 41].

There has clearly been extensive work developing receiver structures like the GRake and chip-level LMMSE equalizer that are specifically designed to deal with CDMA forward link conditions. However, the channel decoder is also a major component of the mobile receive chain. While knowledge of the unique nature of CDMA forward link signals and interference has been used to develop advanced receivers, previous research has not adequately investigated whether that same knowledge can also be used to improve the channel decoding process. The contribution of this thesis is to improve CDMA forward link performance by finding new ways to improve the decoding of convolutional and turbo channel codes in the CDMA mobile. All of these new techniques are based on detailed

knowledge of CDMA forward link conditions.

1.3 Channel Decoder Trellis Metric Calculations

Convolutional and turbo channel codes are used for error correction on the CDMA forward link. This section briefly reviews the basic principles of convolutional and turbo coding with an emphasis on the trellis path metric calculations used as part of the channel decoding process.

A convolutional encoder takes the form of a simple shift register with a series of taps connected to the register storage elements. These taps are used to generate the channel encoded bits. The state of the encoder is dictated by the register contents and will change as different information bits are shifted into the register. These state transitions are represented using a trellis diagram where the nodes in the diagram indicate encoder state and the lines connecting the nodes indicate the transitions between those states [61]. A unique channel encoded information sequence corresponds to a unique path through this channel code trellis diagram.

Turbo codes typically use a parallel concatenated encoder consisting of two recursive systematic convolutional (RSC) encoders operating in parallel. The first encoder operates on the original information bits and the second encoder operates on an interleaved version of those bits [79]. The channel encoded symbols generated by the two parallel encoders are multiplexed together with some optional puncturing to control the coding rate.

The channel decoder for convolutional codes uses samples of the received channel encoded symbols to guess the trellis path used by the encoder to generate those symbols. This path is then used to recover the transmitted information. The Viterbi decoder is a computationally efficient way to calculate metrics for all possible paths through the convolutional code trellis. These metrics quantify

how similar the channel encoded symbols along a particular trellis path are to the received symbol sequence. The calculation of a path metric utilizes the channel encoded symbols that correspond to that path, samples of the received symbols and sometimes information about the desired signal and interference levels during each symbol interval. The path with the best metric is chosen as the one most likely to correspond to the encoded information.

A turbo decoder consists of two separate decoding stages. The channel encoded symbols generated by each of the parallel RSC encoders in the transmitter are processed by a different stage. These decoders typically use either the Soft Output Viterbi Algorithm (SOVA) or the Log Maximum A Posteriori (LogMAP) algorithm [79]. The first decoder uses the received channel encoded symbols to calculate metrics for the different paths through the trellis of the first RSC encoder. Those metrics are used to not only select a trellis path for decoding the transmitted information but also to generate soft information indicating the reliability of each decoded bit. That soft information is interleaved and used as *a priori* information by the second decoder as part of its own metric calculations. The calculations of the second decoder in turn produce soft information that is passed back to the first encoder. This circular sharing of soft information is repeated several times in order to produce a better estimate of the transmitted bits.

This thesis focuses on ways of improving the trellis path metric calculations performed by the CDMA mobile channel decoder for both convolutional and turbo codes. It is therefore important to first review the conventional way these metric calculations are performed.

The fundamental assumption made by conventional trellis path metric calculations is that the probability distribution of the ith received channel encoded symbol sample at the input to the channel decoder, y_i, is Gaussian. The PDF of

y_i, assuming y_i is real, is therefore written as

$$f(y_i) = \frac{1}{\sqrt{2\pi\sigma^2(i)}} \exp\left\{\frac{-[y_i - \zeta(i)b_i]^2}{\sigma^2(i)}\right\} \tag{1.1}$$

where $\zeta(i)$ is the received amplitude of the ith channel encoded symbol, $\sigma^2(i)$ is the variance of the Gaussian interference and noise during the ith symbol interval and $b_i \in \{+1, -1\}$ is the transmitted channel encoded symbol.

Under this Gaussian assumption, Viterbi decoders calculate a log-likelihood metric for several different candidate paths through the trellis according to

$$\mu = \sum_{i=0}^{N_s-1} \frac{\widehat{\zeta(i)} x_i y_i}{\widehat{\sigma^2(i)}} \tag{1.2}$$

where x_i is the ith channel encoded symbol in the trellis path being evaluated in the metric calculation, $\widehat{\zeta(i)}$ is an estimate of the amplitude of the desired signal during symbol interval i, $\widehat{\sigma^2(i)}$ is a variance estimate of the interference plus noise affecting the ith symbol and N_s is the number of channel encoded symbols in the received frame. The quantities $\widehat{\zeta(i)}$ and $\widehat{\sigma^2(i)}$ are referred to as *channel state information.*

This metric is referred to as the *correlation metric* and is a simplification of the Viterbi decoder Euclidean distance metric [61]. The simplification is achieved by removing the factors in the Euclidean distance metric that are common to all paths through the channel code trellis and do not affect the relative comparison of these paths. The Viterbi decoder selects the trellis path that maximizes (1.2) as the one corresponding to the transmitted information sequence.

Depending on the statistics of the desired signal envelope and interference plus noise variance at the input to the channel decoder, a further simplification of the correlation metric is possible. In some cases, like the time invariant AWGN channel, the ratio $\widehat{\zeta(i)}/\widehat{\sigma^2(i)}$ is constant during the frame. Any factor in the

Viterbi decoder metric that is constant can be removed since it has no effect on the relative comparison of the metrics calculated for different trellis paths [62].

In order to decode the kth information bit, d_k, the SOVA turbo decoder approximates the log-likelihood ratio $\Lambda(d_k) = \log(P\{d_k = 1|\boldsymbol{y}\}/P\{d_k = 0|\boldsymbol{y}\})$, where $P\{\cdot\}$ indicates probability and $\boldsymbol{y} = [y_0, \ldots y_{N_s-1}]$ is the received frame of channel encoded symbol samples [79]. A path metric, μ_{ML}, is calculated for the maximum likelihood (ML) path through the channel code trellis. This path corresponds to the encoded symbol sequence that maximizes

$$\mu = \sum_{k=0}^{N_d-1} \left\{ \log\left[p_{z_k}(k)\right] + \sum_{i=N_R k}^{N_R(k+1)-1} \frac{\widehat{\zeta(i)} x_i y_i}{\widehat{\sigma^2(i)}} \right\} \tag{1.3}$$

where N_d is the number of data bits per frame, N_R is the number of encoded symbols per data bit, z_k is the kth data bit that corresponds to the path being evaluated in the metric calculation and $p_\theta(k)$ is the *a priori* probability that the kth data bit is equal to θ. This *a priori* information is determined from the soft information being shared between the turbo decoding stages.

Note that the metric in (1.3) is identical to the Viterbi decoder metric in (1.2), with the addition of an *a priori* information term. As for the Viterbi decoder, if the channel state information ratio of $\widehat{\zeta(i)}/\widehat{\sigma^2(i)}$ is constant for the SOVA decoder over the frame duration, it can be removed from the metric calculation.

The SOVA decoder then uses a backwards recursion to find the path that maximizes (1.3) under the constraint that the path has the complement data bit to the kth ML data bit, $d_{k,ML}$. The metric calculated for this path is denoted $\mu_{C,k}$ and the log-likelihood ratio for the kth bit is calculated as $\Lambda(d_k) = (-1)^{d_{k,ML}}(\mu_{C,k} - \mu_{ML})$.

The MAP decoder calculates the log-likelihood ratio used to decode data bit d_k by accounting for the probability of all possible paths through the trellis according to the expression

$$\Lambda(d_k) = \frac{\sum_{(l,l')\in B_k^1} P\{S_k = l, S_{k+1} = l', \boldsymbol{y}\}}{\sum_{(l,l')\in B_k^0} P\{S_k = l, S_{k+1} = l', \boldsymbol{y}\}} \tag{1.4}$$

where S_k denotes encoder state during bit interval k and B_k^θ is the set of all encoder state transitions corresponding to an information bit θ during bit interval k [79]. The probability terms in (1.4) for information bit θ can be expressed as $P\{S_k = l, S_{k+1} = l', \boldsymbol{y}\} = \alpha_k(l)\gamma_k^\theta(l,l')\beta_{k+1}(l')$ where $\alpha_k(l) = P\{S_k = l|\boldsymbol{y}_0^k\}$, $\beta_k(l) = P\{\boldsymbol{y}_k^{N_s-1}|S_k = l\}$ and $\gamma_k^\theta(l,l') = P\{d_k = \theta, S_{k+1} = l', \boldsymbol{y}_k^{k+1}|S_k = l\}$. The term $\boldsymbol{y}_w^q = [y_{(wN_R)}, \ldots y_{(qN_R-1)}]$. Assuming that y_i is Gaussian distributed, the term $\gamma_k^\theta(l,l')$ is calculated according to

$$\gamma_k^\theta(l,l') = \begin{cases} p_\theta(k)\exp\left\{\dfrac{-\sum_{j=kN_R}^{(k+1)N_R-1}\left[y_j - \widehat{\zeta(j)}x_j\right]^2}{2\widehat{\sigma^2(j)}}\right\}, & (l,l') \in B_k^\theta \\ 0, & \text{otherwise} \end{cases}. \tag{1.5}$$

The Log-MAP decoder calculates the same metrics as the MAP decoder using a close approximation for (1.5) [79]. Both the Log-MAP and MAP algorithms require estimates of $\zeta(i)$ and $\sigma^2(i)$ for (1.5), regardless of whether or not these quantities are stationary.

1.4 Improving the Channel Decoding Process in a CDMA Mobile

This thesis improves CDMA forward link performance by presenting two approaches for improving the accuracy of the CDMA mobile trellis path metric calculations. The first approach is to use the conventional metric calculations described in Section 1.3 and to find new techniques that provide the channel decoder with more accurate channel state information. Using conventional metrics with improved channel state information offers the best performance when mobile channel estimation error is very low. The second approach applies when the chan-

nel information used in the mobile Rake receiver and channel decoder is subject to a significant level of channel estimation error. Received symbol uncertainty due to channel estimation error is accounted for in the channel decoder either by adding a bias to the CSI used by the conventional metric or by deriving a new channel decoder metric. These two strategies are discussed below.

1.4.1 Improved Channel State Estimation

For low levels of mobile channel estimation error, this thesis will show that the conventional channel decoder trellis path metrics discussed in Section 1.3 are optimal for use on the CDMA forward link. However, the calculation of these metrics still requires values of desired signal amplitude, $\zeta(i)$, and interference plus noise variance, $\sigma^2(i)$, to be calculated for each received symbol. Determining these values is referred to as channel state estimation.

Performing accurate channel state estimation in a CDMA mobile is challenging due to the complex nature of CDMA forward link interference. Three different channel state estimation techniques will be presented in this thesis that each make different assumptions about the statistics of CDMA forward link interference. It will be shown that the estimator based on the most accurate CDMA forward link model provides the most accurate channel state information. While the more accurate channel state estimators are more complex, they also result in the best forward link performance when used in the CDMA mobile.

The channel state estimation schemes in this thesis are first developed in the context of the conventional CDMA forward link with single antenna base station transmission and a standard mobile Rake receiver. However, it is also important to establish how these techniques perform with future CDMA systems that may incorporate other advanced physical layer techniques. Therefore, this thesis also adapts the three channel state estimation schemes for CDMA forward links where

the base station uses space time transmit diversity (STTD) transmission and where the mobiles use chip-level linear minimum mean squared error (LMMSE) interference cancellation.

Simulations will be used to show that more accurate channel state estimation schemes can significantly improve the overall performance of both conventional CDMA forward links and links that incorporate advanced physical layer techniques. However, the size of this improvement is sensitive to a number of factors that include channel code type, channel decoder algorithm, mobile velocity, mobile receiver architecture and base station transmission scheme.

1.4.2 Channel Decoder Metric Calculations for High Levels of Channel Estimation Error

Estimation error in the channel information used for the mobile Rake finger combining weights adds an additional source of uncertainty to the symbols at the channel decoder input. This thesis presents two approaches for dealing with this uncertainty.

The first approach uses the conventional channel decoder metric in the mobile and with a bias term added to the CSI used for the metric calculation. This bias term compensates for the additional uncertainty in the received symbols due to Rake receiver channel estimation error. The second approach uses a new channel decoder metric derived based on a received symbol distribution that incorporates uncertainty not only due to interference plus noise but also small scale fading and Rake finger estimation error.

Forward link simulations will illustrate that these approaches offer a considerable performance improvement when channel estimation error in the mobile is significant. The new metric based on the new received symbol distribution performs better than the conventional metric with bias.

1.5 Thesis Overview and Research Contributions

Chapter 2

The purpose of this chapter is to present a chip-level and symbol-level model for the CDMA forward link. These models are used in subsequent chapters to characterize the nature of CDMA forward link interference and develop new channel state estimation techniques that account for that interference. They are used to show when the distribution of the received channel encoded symbol sample can be considered Gaussian and to derive a new channel decoder metric when the symbol sample distribution is not Gaussian. The models are also used to help illustrate the construction of the simulations used in this thesis to evaluate CDMA forward link performance.

A symbol-level model is presented in addition to the chip-level model primarily to improve the efficiency of the simulations used for this thesis. The chip-level model represents CDMA forward link conditions very accurately but is also very computationally intensive to implement. It is therefore used in subsequent chapters only when advanced CDMA receivers are considered that perform interference cancellation at the chip level. The symbol-level CDMA forward link model leads to a much more efficient simulation. Symbol-level simulations are used in subsequent chapters whenever the CDMA forward link under consideration involves a Rake receiver in the mobile. The symbol-level model will also be used as part of an analysis of CDMA forward link intracell interference at the symbol level.

The primary contribution to new research made in this chapter deals with observations made concerning CDMA forward link intracell interference [51]. It is commonly assumed that CDMA forward link intercell interference can be considered Gaussian [28, 35]. However, this chapter will show that a Gaussian distribution can be used to accurately describe CDMA forward link intracell interference

for moderate spreading factors and link loads. It will also be shown that this Gaussian intracell interference assumption is highly dependent on whether the gains of the interfering forward link signals are being adjusted by some type of fast power control scheme.

Chapter 3

This chapter starts by showing that conventional trellis path metric calculations are optimal for use on the CDMA forward link when channel estimation errors are small. It then explores how to best balance accuracy and complexity when generating the channel state estimates required by these metric calculations.

Three new channel state estimation schemes are presented. The first technique, standard estimation, achieves a simple estimator structure by making some simplifying assumptions about CDMA forward link intracell interference. The second technique, online estimation, is a channel state estimation technique previously developed for the time invariant AWGN channel that has been adapted for use on the CDMA forward link. The third technique, improved estimation, accounts for the true nature of intracell interference and produces more accurate channel state estimates than the first two techniques. However, improved estimation is also more complex.

Versions of these estimators are developed not only for the conventional CDMA forward link but also for systems using STTD in the base station and chip-level LMMSE equalization in the mobile. Simulations are used to illustrate how the accuracy of the three channel state estimation schemes affect forward link performance.

The work in this chapter makes several new contributions to the area of channel state estimation for the CDMA forward link [50, 49, 48, 52, 53].

- This work is the first to evaluate and compare different alternatives for

CDMA forward link channel state estimation in detail and to show that the accuracy of these techniques can considerably affect forward link performance.

- The improved channel state estimation scheme is a novel technique that is the first to separately account for the CDMA forward link intracell interference and intercell interference plus thermal noise processes when performing channel state estimation. The improvement in accuracy that results provides a significant performance advantage over other channel state estimation schemes.

- Part of the improved estimation technique is the development of a new linear estimator that uses the second order statistics of the received forward link signal to determine how much intracell and intercell is present at the input to a CDMA mobile. While this technique is useful for improved channel state estimation, it could also be applied to interference cancellation and hand-off algorithms that would benefit from knowing how much intracell and intercell interference the mobile is receiving.

- The online estimation scheme used in this chapter was previously developed for use on the time invariant AWGN channel. This is the first work to illustrate how it can be adapted for use on the CDMA forward link.

- This chapter is the first to consider channel state estimation for a CDMA STTD system and to illustrate how multiple antenna transmission affects channel state estimation by changing the intracell interference process.

- This chapter is also the first to consider channel state estimation for a CDMA mobile using a chip-level LMMSE receiver for intracell interference cancellation. The interference process at the output of this receiver is significantly

different than at the output of a conventional Rake receiver. This thesis illustrates how this affects the channel state estimation process.

Chapter 4

This chapter shows that the effect of channel estimation error on the mobile Rake finger combining weights can be a significant source of received symbol uncertainty. Accounting for this source of uncertainty in the mobile channel decoder can significantly improve CDMA forward link performance.

Two approaches are used to compensate for Rake finger channel estimation error in the channel decoder. First, a bias factor is applied to the CSI used by the conventional channel decoder metric calculation. Second, a new metric, called an inclusive metric, is derived based on a received symbol uncertainty distribution that includes the interference plus noise, small scale fading and channel estimation error processes. Simulations show that these techniques considerably outperform conventional channel decoder metrics for a significant level of channel estimation error. The conventional metric with bias outperforms the inclusive metric with perfect knowledge of CSI. However, when CSI must be estimated, the inclusive metric offers the best performance since it is able to use longer observation windows to estimate CSI.

The work in this chapter makes several new research contributions [54].

- The inclusive metric is the first MAP channel decoder metric that accounts for the change in received symbol sample distribution due to channel estimation errors in a mobile receiver operating on a frequency selective channel. All previous MAP metrics developed to account for channel estimation error have considered only flat fading channels.

- The conventional metric with bias is the first conventional channel decoder

metric calculation to include a bias factor that accounts for receiver estimation error on a frequency selective channel.

- These metrics are the first to account for estimation error in a mobile receiver operating on the CDMA forward link. All other MAP channel decoder metrics that account for channel estimation error have been developed for AWGN only.

- This work is the first to illustrate that the benefit of accounting for channel estimation error in a channel decoder metric is sensitive to the number of resolvable multipath components in the radio channel.

Chapter 5

This chapter summarizes the main conclusions resulting from this thesis work. It also discusses some of the possibilities for future work based on this research.

Appendix A

The purpose of this appendix is to select an advanced CDMA forward link receiver design capable of intracell interference cancellation to be considered in Chapter 3. A brief survey of CDMA forward link receiver research is presented and several designs are selected for a simulation comparison. This comparison considers a number of factors, including how the receiver designs perform on both simulated and measured channels. Based on this comparison, the chip-level LMMSE receiver is selected as a good balance between performance and complexity.

The new research contribution made in this appendix is primarily in the comparison of Generalized Rake (GRake) receiver and chip-level LMMSE receiver performance on simulated and measured channels. This is the first comparison of these receivers using measured channels. It is noted that the two receivers perform almost the same on the simulated channel with uniformly spaced channel taps.

However, when used on an actual measured channel, the GRake performs worse than the chip-level LMMSE receiver due to degradation caused by difficulty in placing the GRake fingers.

Chapter 2

The CDMA Forward Link

This chapter introduces chip-level and symbol-level models for the CDMA forward link that represent a system transmitting synchronous CDMA signals using concatenated Walsh/PN-sequence spreading. These models are used in subsequent chapters to develop and evaluate new ways to improve CDMA mobile channel decoder performance through more accurate trellis path metric calculations.

The goal of this thesis is to improve the forward link performance of both current generation and future CDMA systems. It is very likely that future CDMA systems will incorporate a number of advanced physical layer techniques. It is important to ensure that the ideas developed in this thesis will work well not only with a conventional CDMA forward link design but also with designs that incorporate some of these advanced techniques. Therefore, the models presented in this chapter consider not only single antenna base station transmission to a standard mobile Rake receiver but also multiple antenna base station transmission and advanced mobile receivers capable of interference cancellation.

Section 2.2 presents a linear chip-level model of the CDMA forward link. This model offers a very accurate characterization of CDMA forward link conditions. It considers single antenna base station transmission and either the Rake or chip-level LMMSE mobile receiver structures. The Rake receiver performs maximal ratio combining on the received components of the forward link signal [61] and is

the receiver most commonly used in commercial CDMA systems. The chip-level LMMSE equalizer attempts to cancel intracell interference by equalizing multipath dispersion and restoring the orthogonality of the Walsh spreading sequences [36, 21, 26, 14, 38, 67, 37, 41]. This receiver structure was selected from a number of advanced CDMA mobile receiver structures compared in Appendix A as a good compromise between complexity and performance.

While very accurate, the chip-level model in Section 2.2 is computationally intensive to implement. Therefore, a second symbol-level model is presented in Section 2.3 that is much more efficient to use in simulation. It will also be used in Chapters 3 and 4 to make some important observation about the nature of CDMA forward link interference at the symbol level.

Since the chip-level LMMSE receiver has to operate at the chip level, the symbol level model presented in Section 2.3 considers only the mobile Rake receiver. However, the symbol level model does incorporate single antenna transmission and space time transmit diversity (STTD). STTD is based on the space time block codes originally developed by Alamouti [4]. This transmit diversity technique is considered because it offers a substantial system performance improvement [70, 31] and has already been adopted into the IS-2000 and UMTS 2.5G/3G CDMA standards [72, 2].

The symbol-level model presented in Section 2.3 is based on the assumption that intracell interference can be modeled as a coloured Gaussian process [51]. The idea of using a Gaussian process to model CDMA forward link intracell interference has been used for system comparisons [29] and to develop advanced forward link receiver structures [10]. However, previous research has not verified that the Gaussian assumption is accurate for the wide range of spreading factors and traffic loads being proposed for current and next generation CDMA systems. This verification is performed in Section 2.3 by examining interference distributions and by

comparing simulation results generated using the symbol-level model with results from a full chip-level simulation based on the model presented in Section 2.2.

Common to both the chip-level and symbol-level models is the forward link radio channel. The radio channel model is presented in Section 2.1.

2.1 Radio Channel Model

A general block diagram for the CDMA forward link is shown for single antenna and transmit diversity in Figs. 2.1 and 2.2, respectively. The radio channel model in this diagram is divided into two components that represent large scale and small channel effects.

Large scale path loss and shadowing are represented using the real valued function $\Xi(n)$, where n is discrete time. If the base station is using multiple antenna transmission, it is assumed that large scale channel attenuation is the same between each base station transmit antenna and the mobile.

For multiple antenna transmission, the complex valued small scale channel impulse response between base station antenna ϕ and the mobile is denoted $c_\phi(n,l)$, $l = 0, \ldots L-1$, where l signifies excess delay. The channel term $c_\phi(n,l)$ can be considered the small scale channel impulse response at discrete time n due to an impulse applied at time $n-l$. Assuming a receiver operating at S samples per chip, the number of impulse response samples with significant signal energy is equal to L. The excess delay of each resolvable multipath component in the channel impulse response is assumed to be an integer multiple of $1/S$ chip duration. It is also assumed that the small scale fading between base station transmit antennas is independent and that the small scale channel impulse response is normalized such that

$$\left\langle \sum_{l=0}^{L-1} |c_\phi(n,l)|^2 \right\rangle = 1 \tag{2.1}$$

where $\langle \cdot \rangle$ indicates expectation taken with respect to discrete time n.

For brevity in the following sections, $c_\phi(l)$ will be used to refer to $c_\phi(iR, l)$, where i is channel encoded symbol interval and R is the number of spreading chips per channel encoded symbol. It is assumed that small scale fading remains approximately constant over one encoded symbol interval. The subscript ϕ will also be dropped for systems using only single antenna transmission.

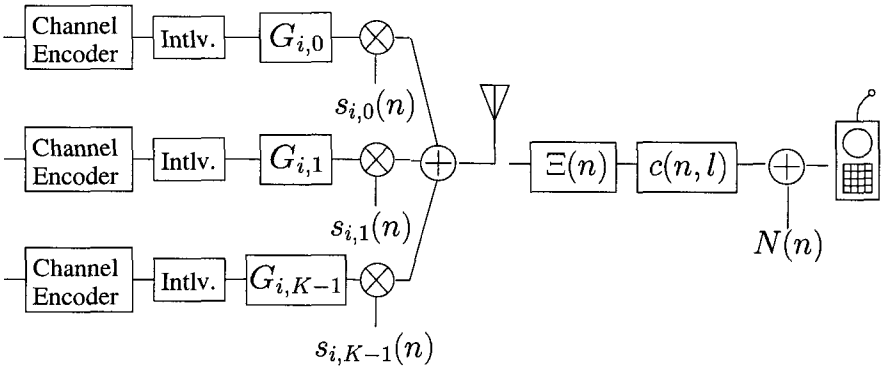

Figure 2.1: CDMA forward link, single antenna transmission.

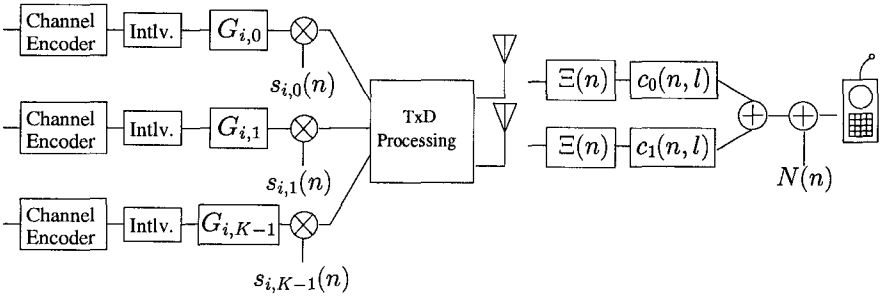

Figure 2.2: CDMA forward link, transmit diversity.

2.2 Chip-Level CDMA Forward Link Model

2.2.1 Received Signal for Single Antenna Transmission

This section presents a linear chip-level expression for the signal received by a CDMA mobile from a base station with a single transmit antenna, as shown in

Fig. 2.1. The notation used for this model is similar to that used by Hooli *et. al.* [26]. However, it has been modified somewhat to allow the number of taps in the chip-level LMMSE equalizer to be reduced to less than the spreading factor. This allows LMMSE receiver performance to be evaluated in subsequent chapters using a modest number of taps that would be more practical to implement in a battery powered handset.

In the following, $\mathcal{R}^{b\times c}$ and $\mathcal{C}^{b\times c}$ denote $b \times c$ real and complex matrices, respectively. The symbols $\mathcal{R}^b$ and $\mathcal{C}^b$ denote b-element real and complex vectors, respectively.

The CDMA base station shown in Fig. 2.1 generates K parallel, synchronous CDMA signals. The signal received by the CDMA mobile is given by

$$\boldsymbol{r}_i(a,b) = \sum_{k=0}^{K-1} G_{i,k}\boldsymbol{D}_i(a,b)\boldsymbol{C}_i\boldsymbol{S}_{i,k}\boldsymbol{b}_{i,k} + \boldsymbol{n}_i(a,b) \tag{2.2}$$

where $\boldsymbol{r}_i(a,b) \in \mathcal{C}^{(b-a)}$ is a vector of received signal samples starting at sample a and ending at sample $b-1$ and i is the index of the channel encoded symbol that is currently being detected.

The real-valued scalar term $G_{i,k}$ is a gain factor applied to the ith data symbol transmitted to user k. For a CDMA traffic channel, this gain factor is typically adjusted according to some kind of forward link power control scheme. For a CDMA overhead channel, this gain factor is typically fixed.

The vector $\boldsymbol{b}_{i,k}$ contains the channel encoded data symbols. For user k, this vector is $\boldsymbol{b}_{i,k} = [b_{i-1,k}\ b_{i,k}\ b_{i+1,k}]^T \in \mathcal{C}^3$, where $b_{i,k}$ is the desired channel encoded symbol currently being detected and the symbols $b_{i-1,k}$ and $b_{i+1,k}$ cause inter-symbol interference (ISI). Note that in very high data rate systems, ISI could be caused by more symbols than just those adjacent to the desired symbol. However, in this thesis, the maximum data rate considered is 153.7 kb/s, which corresponds to a symbol duration of 6.5 μs. Therefore, in order to get ISI from symbols other

than the ones adjacent to the desired symbol, the channel delay spread would have to be larger than 6.5 μs. This is longer than the delay spreads of the channels that were considered in this thesis and are, in general, quite rare [66].

The forward link spreading sequence of user k is contained in the matrix $\boldsymbol{S}_{i,k} \in \mathcal{C}^{3R\times 3}$. The matrix

$$\begin{aligned}\boldsymbol{S}_{i,k} &= \text{diag}\left\{\boldsymbol{s}_{i-1,k}, \boldsymbol{s}_{i,k}, \boldsymbol{s}_{i+1,k}\right\} \\ &= \begin{bmatrix} \uparrow & 0 & 0 \\ \boldsymbol{s}_{i-1,k} & \vdots & \vdots \\ \downarrow & 0 & 0 \\ 0 & \uparrow & 0 \\ \vdots & \boldsymbol{s}_{i,k} & \vdots \\ 0 & \downarrow & 0 \\ 0 & 0 & \uparrow \\ \vdots & \vdots & \boldsymbol{s}_{i+1,k} \\ 0 & 0 & \downarrow \end{bmatrix}\end{aligned} \tag{2.3}$$

where the vector $\boldsymbol{s}_{i,k} = [s_{i,k}(0)\cdots s_{i,k}(R-1)]^T \in \mathcal{C}^R$ is the spreading sequence for the ith encoded symbol of user k and R is the number of spreading sequence chips per symbol (spreading gain). This spreading sequence is the product of a Walsh sequence specific to the kth traffic transmission and a PN-sequence based code common to all transmissions in a specific sector. The codes $\boldsymbol{s}_{i-1,k}$ and $\boldsymbol{s}_{i+1,k}$ spread the adjacent data symbols that cause ISI.

The complex multipath channel tap weights are contained in matrix $\boldsymbol{C}_i \in$

$\mathcal{C}^{3RL\times 3R}$ defined as

$$\boldsymbol{C}_i = \text{diag}\{\boldsymbol{c}_{i-1,0}, \boldsymbol{c}_{i-1,1}, \cdots \boldsymbol{c}_{i-1,R-1}, \boldsymbol{c}_{i,0} \cdots \boldsymbol{c}_{i,R-1}, \boldsymbol{c}_{i+1,0} \cdots \boldsymbol{c}_{i+1,R-1}\}$$

$$= \begin{bmatrix} \uparrow & 0 & \dots & 0 \\ \boldsymbol{c}_{i-1,0} & 0 & \dots & 0 \\ \downarrow & 0 & \dots & 0 \\ 0 & \uparrow & \dots & 0 \\ 0 & \boldsymbol{c}_{i-1,1} & \dots & 0 \\ 0 & \downarrow & \dots & 0 \\ \vdots & \vdots & \vdots & \vdots \\ 0 & 0 & \dots & \uparrow \\ 0 & 0 & \dots & \boldsymbol{c}_{i+1,R-1} \\ 0 & 0 & \dots & \downarrow \end{bmatrix} \tag{2.4}$$

where the vector $\boldsymbol{c}_{i,v} \in \mathcal{C}^L$ contains the complex values of the L multipath components during the interval of the vth chip of symbol i. The elements of this vector are written as $\boldsymbol{c}_{i,v} = [c_{i,v}(0) \cdots c_{i,v}(L-1)]^T$, where $c_{i,v}(l) = \Xi(iR+v)c(iR+v,l)$ according to the channel model defined in Section 2.1. This notation accounts for the time variation of the large scale channel attenuation from chip to chip. However, this variation is extremely small.

The columns of matrix $\boldsymbol{D}_i(a,b) \in \mathcal{R}^{(b-a)\times 3RL}$ contain the chip waveforms. For each chip, there are L consecutive columns that represent the L samples of the multipath channel impulse response with significant signal energy. The time delay of the chip waveform in each column is determined by the transmit time of the chip and its multipath delay. Only the portion of the chip falling into the window defined by the sample indices a and b is retained. The matrix is written as

$$\boldsymbol{D}_i(a,b) = \begin{bmatrix} \uparrow & & \uparrow & \uparrow & & \uparrow & \uparrow \\ \boldsymbol{d}^0_{i-1,0}(a,b) & \cdots & \boldsymbol{d}^{L-1}_{i-1,0}(a,b) & \boldsymbol{d}^0_{i-1,1}(a,b) & \cdots & \boldsymbol{d}^{L-1}_{i-1,R-1}(a,b) & \boldsymbol{d}^0_{i,0}(a,b) \\ \downarrow & & \downarrow & \downarrow & & \downarrow & \downarrow \end{bmatrix}$$
$$\begin{bmatrix} \uparrow \\ \cdots \quad \boldsymbol{d}^{L-1}_{i+1,R-1}(a,b) \\ \downarrow \end{bmatrix} \tag{2.5}$$

where the vector $\boldsymbol{d}_{i,v}^{l}(a,b) \in \mathcal{R}^{b-a}$ represents the chip waveform of the vth chip of symbol i delayed by l samples. This vector is windowed such that only the portion of the waveform that falls within the window defined by samples a and b is retained. Note that these columns contain only a delayed version of the chip waveform. The actual fading value of each multipath component is contained in matrix $\boldsymbol{C}_i$.

The vector $\boldsymbol{n}_i(a,b) \in \mathcal{C}^{(b-a)}$ represents intercell interference plus thermal noise and is a complex, additive Gaussian noise term with variance σ_N^2.

2.2.2 Rake Receiver

Fig 2.3 shows an F finger Rake receiver with finger 0 shown in detail. Assuming BPSK, the channel encoded symbol at the output of the receiver is given by

$$y_i = \mathcal{R}(\frac{1}{\sqrt{R}} \boldsymbol{s}_{i,0}^H \boldsymbol{W}_i^H \boldsymbol{M}_i(a,b)^H \boldsymbol{r}_i(a,b)) \tag{2.6}$$

where the columns of $\boldsymbol{M}_i(a,b)$ contain copies of the chip waveforms with time delays corresponding to the time offsets tracked by each finger, $\boldsymbol{W}_i$ contains the complex finger combining taps for symbol i and $\boldsymbol{s}_{i,0}$ is the spreading sequence for the desired user. If QPSK modulation is employed, the received channel encoded symbols equal the real component of (2.6) for i even and the imaginary component for i odd.

The Rake receiver chip level matched filtering is performed by multiplying the received signal vector by $\boldsymbol{M}_i(a,b)^H$, the finger combining by multiplying by $\boldsymbol{W}_i^H$ and despreading by multiplying by $\boldsymbol{s}_{i,0}^H$. Note that (2.6) performs finger combining and despreading in opposite order to that of a conventional Rake receiver. This simplifies notation somewhat and does not affect performance since the receiver is linear.

The Rake receiver despreads all significant multipath components of the received symbol such that the signal vector processed by the receiver, $\boldsymbol{r}_i(a,b)$, con-

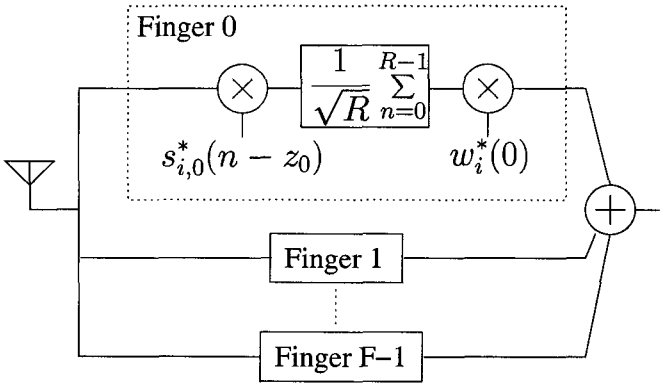

Figure 2.3: Rake receiver

tains all the samples defined by the window $a = iRS$ and $b = [(i+1)RS - 1] + (L - S)$, where S is the number of samples per chip and $(L - S)$ is the number of samples the current symbol overlaps with the next symbol due to multipath delay. The multipath time delays tracked by each finger are denoted $z_0, \ldots z_{F-1}$. It is assumed that these delays correspond to the arrivals of the strongest forward link multipath components and that they are updated for each received symbol. The matrix $\boldsymbol{M}_i(a,b) \in \mathcal{R}^{(b-a)\times FR}$ contains chip waveforms delayed according to these finger time offsets such that

$$\boldsymbol{M}_i(a,b) = \begin{bmatrix} \uparrow & & \uparrow & \uparrow & & \uparrow \\ \boldsymbol{d}^{z_0}_{i,0}(a,b) & \cdots & \boldsymbol{d}^{z_{F-1}}_{i,0}(a,b) & \boldsymbol{d}^{z_0}_{i,1}(a,b) & \cdots & \boldsymbol{d}^{z_{F-1}}_{i,R-1}(a,b) \\ \downarrow & & \downarrow & \downarrow & & \downarrow \end{bmatrix} \tag{2.7}$$

The matrix $\boldsymbol{W}_i$ is written as

$$\begin{aligned}\boldsymbol{W}_i &= \text{diag}\{\boldsymbol{w}_i, \ldots \boldsymbol{w}_i\} \in \mathcal{C}^{FR\times R} \\ &= \begin{bmatrix} \uparrow & 0 & \ldots & 0 \\ \boldsymbol{w}_i & 0 & \ldots & 0 \\ \downarrow & 0 & \ldots & 0 \\ 0 & \uparrow & \ldots & 0 \\ 0 & \boldsymbol{w}_i & \ldots & 0 \\ 0 & \downarrow & \ldots & 0 \\ \vdots & \vdots & \vdots & \vdots \\ 0 & 0 & \ldots & \uparrow \\ 0 & 0 & \ldots & \boldsymbol{w}_i \\ 0 & 0 & \ldots & \downarrow \end{bmatrix}\end{aligned} \tag{2.8}$$

where $\boldsymbol{w}_i = [w_i(0) \ldots w_i(F-1)]^T \in \mathcal{C}^F$ and $w_i(f)$ is the combining weight for finger f during encoded symbol interval i. Assuming the channel remains constant over a single symbol interval, the elements of the finger combining weight matrix are $w_i(f) = c_{i,0}(z_f)$.

2.2.3 Chip-Level LMMSE Receiver

The chip-level LMMSE receiver seeks to equalize the multipath dispersion of the received forward link signal and restore the orthogonality of the Walsh spreading sequences. This is performed by finding the matrix $\boldsymbol{E}_i$ that minimizes

$$\left\langle \left| \boldsymbol{E}_i^H \boldsymbol{r}_i(a,b) - \sum_{k=0}^{K-1} G_{i,k} \overline{\boldsymbol{D}}_i(a,b) \boldsymbol{S}_{i,k} \boldsymbol{b}_{i,k} \right|^2 \right\rangle . \tag{2.9}$$

The matrix $\overline{\boldsymbol{D}}_i(a,b) \in \mathcal{R}^{(b-a)\times 3R}$ corresponds to the chip waveforms of the transmitted CDMA signal when uncorrupted by multipath and is written as

$$\overline{\boldsymbol{D}}_i(a,b) = \begin{bmatrix} \uparrow & \uparrow & & \uparrow & \uparrow & & \uparrow \\ \boldsymbol{d}^0_{i-1,0}(a,b) & \boldsymbol{d}^0_{i-1,1}(a,b) & \cdots & \boldsymbol{d}^0_{i-1,R-1}(a,b) & \boldsymbol{d}^0_{i,0}(a,b) & \cdots & \boldsymbol{d}^0_{i+1,R-1}(a,b) \\ \downarrow & \downarrow & & \downarrow & \downarrow & & \downarrow \end{bmatrix} \tag{2.10}$$

where the vector $\boldsymbol{d}^0_{i,v}(a,b)$ is defined in Section 2.2.1 as the chip waveform of the vth chip of symbol i with a multipath index of 0 (no multipath delay). The number

of rows in $\boldsymbol{E}_i$ is equal to the number of samples in the observation window defined by a and b and the number of columns equals the number of complete chips that fall in that observation window.

This receiver first equalizes the received signal using the matrix $\boldsymbol{E}_i$ and then passes the result to a single despreading stage that recovers the channel encoded symbols. While the receiver is derived in block form, it can be converted to the FIR equalizer form shown in Fig. 2.4 by using one of the middle columns of $\boldsymbol{E}_i$ as the filter coefficients [26]. The column vector of equalizer taps is $\boldsymbol{e}_i = [e_i(0) \cdots e_i(N_T - 1)]^T \in \mathcal{C}^{N_T}$, where $N_T = b - a$ is the number of equalizer taps. Convolution of the received signal with $\boldsymbol{e}_i$ is used to equalize all chips in the (a, b) observation window after which, the taps must be recalculated.

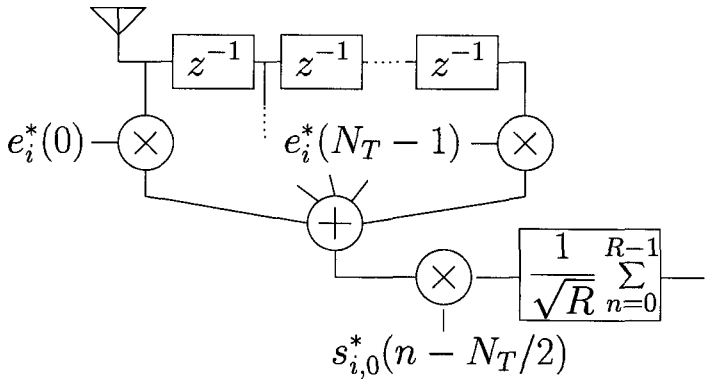

Figure 2.4: Chip-level LMMSE equalizer.

The tap weight matrix of an LMMSE receiver is determined according to

$$\boldsymbol{E}_i = \boldsymbol{C}_{br}\boldsymbol{C}_{rr}^{-1} \tag{2.11}$$

where $\boldsymbol{C}_{br}$ is the cross-covariance matrix between the received signal and the desired transmitted chip sequence, free of multipath dispersion. The matrix $\boldsymbol{C}_{rr}$ is the covariance matrix of the received signal [33].

The cross-covariance matrix $\boldsymbol{C}_{br}$ is given by

$$
\begin{aligned}
\boldsymbol{C}_{br} &= \left\langle \left[\sum_{k=0}^{K-1} G_{i,k}\overline{\boldsymbol{D}}_i(a,b)\boldsymbol{S}_{i,k}\boldsymbol{b}_{i,k}\right]\left[\sum_{k=0}^{K-1} G_{i,k}\boldsymbol{D}_i(a,b)\boldsymbol{C}_i\boldsymbol{S}_{i,k}\boldsymbol{b}_{i,k}\right]^H\right\rangle \\
&= \overline{\boldsymbol{D}}_i(a,b)\left\langle \sum_{k=0}^{K-1} G_{i,k}^2\boldsymbol{S}_{i,k}\boldsymbol{b}_{i,k}\boldsymbol{b}_{i,k}^H\boldsymbol{S}_{i,k}^H\right\rangle \boldsymbol{C}_i^H\boldsymbol{D}_i(a,b)^H \\
&= \overline{\boldsymbol{D}}_i(a,b)\boldsymbol{R}_{SS}\boldsymbol{C}_i^H\boldsymbol{D}_i(a,b)^H
\end{aligned} \tag{2.12}
$$

where the matrix $\boldsymbol{R}_{SS} \in \mathcal{C}^{3R\times 3R}$ is the covariance matrix of the channel encoded data symbols multiplied by their spreading sequences [27].

The covariance matrix of the received signal during symbol interval i, $\boldsymbol{C}_{rr}$, is calculated directly from (2.2) as

$$
\begin{aligned}
\boldsymbol{C}_{rr} &= \left\langle \boldsymbol{r}_i(a,b)\boldsymbol{r}_i(a,b)^H\right\rangle \\
&= \left\langle \left[\sum_{k=0}^{K-1} G_{i,k}\boldsymbol{D}_i(a,b)\boldsymbol{C}_i\boldsymbol{S}_{i,k}\boldsymbol{b}_{i,k} + \boldsymbol{n}_i(a,b)\right]\right. \\
&\quad \left.\left[\sum_{k=0}^{K-1} G_{i,k}\boldsymbol{D}_i(a,b)\boldsymbol{C}_i\boldsymbol{S}_{i,k}\boldsymbol{b}_{i,k} + \boldsymbol{n}_i(a,b)\right]^H\right\rangle \\
&= \boldsymbol{D}_i(a,b)\boldsymbol{C}_i\left\langle \sum_{k=0}^{K-1} G_{i,k}^2\boldsymbol{S}_{i,k}\boldsymbol{b}_{i,k}\boldsymbol{b}_{i,k}^H\boldsymbol{S}_{i,k}^H\right\rangle \boldsymbol{C}_i^H\boldsymbol{D}_i(a,b)^H \\
&\quad + \left\langle \boldsymbol{n}_i(a,b)\boldsymbol{n}_i(a,b)^H\right\rangle \\
&= \boldsymbol{D}_i(a,b)\boldsymbol{C}_i\boldsymbol{R}_{SS}\boldsymbol{C}_i^H\boldsymbol{D}_i(a,b)^H + \sigma_N^2\boldsymbol{I}.
\end{aligned} \tag{2.13}
$$

The dependence of $\boldsymbol{C}_{br}$ and $\boldsymbol{C}_{rr}$ on knowledge of the forward link spreading codes can be removed by approximating the spreading sequences as white, binomial random variables [26]. With this simplification, the matrix $\boldsymbol{R}_{SS}$ in (2.12) and (2.13) can be replaced by the diagonal matrix $\boldsymbol{R}_{SS} = \text{diag}\{A,\ldots,A\} \in \mathcal{R}^{3R\times 3R}$, where $A = \sum_{k=0}^{K-1} G_{i,k}^2$ is the transmit energy of the composite forward link signal. While the diagonals of this matrix will fluctuate due to the power control adjustments of individual gain values, the matrix can be approximated as constant for a large number of forward link traffic signals.

The complexity of this receiver is governed by the number of computations required to solve (2.11), either by direct calculation or using a recursive algorithm. This complexity can be changed by varying the number of receiver taps. While reducing the number of taps reduces the complexity of the equalizer, it also degrades the equalization operation. This means the multipath dispersion will not

be completely removed and some amount of intracell interference will appear at the output of the despreading stage.

2.3 Symbol-Level CDMA Forward Link Model

2.3.1 Single Antenna Transmission with Rake Receiver

As in Section 2.2, the symbol level CDMA forward link model presented in this section assumes the forward link can be represented as shown in Fig. 2.1 where the base station transmits K parallel CDMA signals using a single transmit antenna. The data symbol $b_{i,k}$, forward link gain factor $G_{i,k}$ and spreading sequence $s_{i,k}(n)$ notation used in this section is defined in Section 2.2.1.

It is assumed that each mobile uses a conventional Rake receiver with F fingers for tracking the strongest multipath components of the forward channel signal. A diagram of the receiver is shown in Fig. 2.3, with finger 0 shown in detail. As in Section 2.2.2, the Rake finger time offsets are denoted $z_0, z_1, \ldots z_{F-1}$, which corresponds to the arrivals of the strongest received signal components. These signal components are despread and then combined using maximal ratio combining.

The envelope of the desired signal at the output of the Rake receiver during the ith symbol interval is denoted $\zeta(i)$ and is given by

$$\zeta(i) = \sqrt{R} G_{i,0} \Xi(iR) \sum_{f=0}^{F-1} |c(z_f)|^2 . \tag{2.14}$$

Intercell interference and thermal noise are typically lumped together and modeled as a single, additive Gaussian process, $N(n)$, at the Rake receiver input [28, 35]. It is assumed that $N(n)$ is a complex Gaussian process with zero mean and variance σ_N^2. Accounting for the maximal ratio combining and despreading performed within the Rake receiver, the intercell interference plus thermal noise at the Rake receiver output during symbol interval i is

$$\begin{aligned} N_i &= \sum_{f=0}^{F-1} c^*(z_f) \\ &\quad \cdot \frac{1}{\sqrt{R}} \sum_{r=0}^{R-1} s_{i,0}^*(r) N(iR + z_f + r) \\ &= \sum_{f=0}^{F-1} c^*(z_f) N_{z_f,i} \end{aligned} \tag{2.15}$$

where $N_{z_f,i}$ is a Gaussian random variable resulting from despreading $N(n)$ with a time offset of z_f during symbol interval i. The despreading stage in each Rake finger does not alter the Gaussian distribution of the intercell interference and thermal noise. Samples of a complex Gaussian process that are multiplied by a pseudo-random spreading code with real and imaginary components equal to 1 or -1 retain a Gaussian distribution. The Gaussian process at the output of the normalized summation block in each Rake finger has the same variance as the Gaussian process at the input to the summation [61]. Therefore, $N_{z_f,i}$ in (2.15) is a complex Gaussian random variable with zero mean and variance σ_N^2, the same variance as $N(n)$.

Intracell interference consists of the $K-1$ forward link signals that are transmitted by the base station to other users plus the self interference of the desired signal caused by its multipath replicas. To characterize this interference, the forward link signal transmitted by the base station is represented as a complex random process with zero mean. The term $I(n)$ represents this transmitted forward link signal attenuated by large scale channel effects. The signal $I(n)$ is a complex random process with zero mean and variance σ_I^2. In order to determine the intracell interference at the output of finger f, the signal $I(n)$ is convolved with the small scale channel impulse response $c(n,l)$ and applied to the Rake receiver input. Accounting for despreading and multiplication by the maximal ratio combining weights, the intracell interference at the output of finger f can be written as

$$\begin{aligned} I'_{f,i} &= c^*(z_f) \frac{1}{\sqrt{R}} \sum_{r=0}^{R-1} s_{0,i}^*(r) \\ &\quad \cdot \sum_{l=0}^{L-1} c(l) I(iR + z_f - l + r). \end{aligned} \tag{2.16}$$

Rake finger f will extract the desired signal from the component of $I(n)$ arriving at delay z_f. The Walsh sequences used for spreading on the forward link enable the despreading performed by finger f to completely cancel the signals of the $K-1$ interfering users that also arrive at delay z_f. Therefore, (2.16) can be simplified to

$$I'_{f,i} = c^*(z_f) \sum_{l=0}^{L-1} c(l) I_{z_f-l,i}[1-\delta(l-z_f)] \tag{2.17}$$

where the term $I_{z_f-l,i}$ is the normalized sum of R samples of the process $I(n)$ multiplied by the spreading sequence of user 0 with a time offset of $z_f - l$ during symbol interval i. The $[1-\delta(\cdot)]$ term represents the Walsh sequence cancellation of intracell interference, where $\delta(z)$ equals 1 if $z=0$ and is 0 otherwise. As was the case for the intercell interference plus thermal noise process $N(n)$, it is assumed that the despreading operation does not alter the variance of the random process $I(n)$. Therefore, the random variable $I_{z_f-l,i}$ also has a variance of σ_I^2. Using (2.17), the overall intracell interference process at the Rake output is

$$\begin{aligned} I_i &= \textstyle\sum_{f=0}^{F-1} I'_{f,i} \\ &= \textstyle\sum_{f=0}^{F-1} c^*(z_f) \sum_{l=0}^{L-1} c(l) I_{z_f-l,i}[1-\delta(l-z_f)] \end{aligned} \tag{2.18}$$

When this model is implemented in simulation, the term $I_{z_f-l,i}$ in (2.18) is considered a complex Gaussian random variable with zero mean and variance σ_I^2. This assumption is verified in Section 2.3.3.

2.3.2 Space Time Transmit Diversity Transmission with Rake Receiver

This section presents a symbol-level CDMA forward link model for space time transmit diversity (STTD) [48]. As illustrated in Fig. 2.2, an STTD CDMA base station transmits K synchronous CDMA signals using two base station antennas. The signals transmitted from these two antennas are denoted $X_i^{\alpha}(n)$, where i is encoded symbol interval and $\alpha \in \{0,1\}$ is antenna number. Based on the STTD

scheme adopted for use in the UMTS CDMA system [2], these signals can be written as

$$X_i^0(n) = \sum_{k=0}^{K-1} G_{i,k} b_{i,k} s_{i,k}(n - iR)$$
$$X_i^1(n) = \begin{cases} \sum_{k=0}^{K-1} G_{i,k} b_{i+1,k}^* s_{i,k}(n - iR), i \text{ even} \\ -\sum_{k=0}^{K-1} G_{i,k} b_{i-1,k}^* s_{i,k}(n - iR), i \text{ odd} \end{cases} \quad (2.19)$$

where the transmitted channel encoded symbol $b_{i,k}$, forward link gain factor $G_{i,k}$ and spreading code $s_{i,k}(n)$ are all defined in Section 2.2.1. This scheme is a direct adaptation of Alamouti's space time block codes that allow the mobile to perform maximal ratio combining (MRC) on the signals it receives from the two transmit antennas [4].

Some modifications of the Rake receiver are required in order to process an STTD signal and perform the dual antenna MRC. The STTD Rake receiver is illustrated in Fig. 2.5 with finger 0 shown in detail. The desired signal component at the output of the despreading stage in Fig. 2.5 is given by

$$\Psi_{\text{DS}}(i) = \begin{cases} \Xi(iR)\sqrt{R}G_{i,0}\left[c_0(z_0)b_{k,i} + c_1(z_0)b_{k,i+1}^*\right], i \text{ even} \\ \Xi(iR)\sqrt{R}G_{i,0}\left[c_0(z_0)b_{k,i} - c_1(z_0)b_{k,i-1}^*\right], i \text{ odd} \end{cases} \quad (2.20)$$

The desired signal component at the finger output for i even can then be written as

$$\begin{aligned} \Psi_{\text{OUT}}(i) &= c_0^*(z_0)\Psi_{\text{DS}}(i) - c_1(z_0)\Psi_{\text{DS}}^*(i+1) \\ &= \Xi(iR)\sqrt{R}G_{i,0}(|c_0(z_0)|^2 + |c_1(z_0)|^2)b_{i,k} \end{aligned} \quad (2.21)$$

and for i odd as

$$\begin{aligned} \Psi_{\text{OUT}}(i) &= c_0^*(z_0)\Psi_{\text{DS}}(i) + c_1(z_0)\Psi_{\text{DS}}^*(i-1) \\ &= \Xi(iR)\sqrt{R}G_{i,0}(|c_0(z_0)|^2 + |c_1(z_0)|^2)b_{i,k} \end{aligned} \quad (2.22)$$

Therefore, the envelope of the desired signal at the Rake output during symbol interval i for STTD transmission is

$$\zeta(i) = \Xi(iR)\sqrt{R}G_{i,0}\sum_{f=0}^{F-1}\left[|c_0(z_f)|^2 + |c_1(z_f)|^2\right]. \tag{2.23}$$

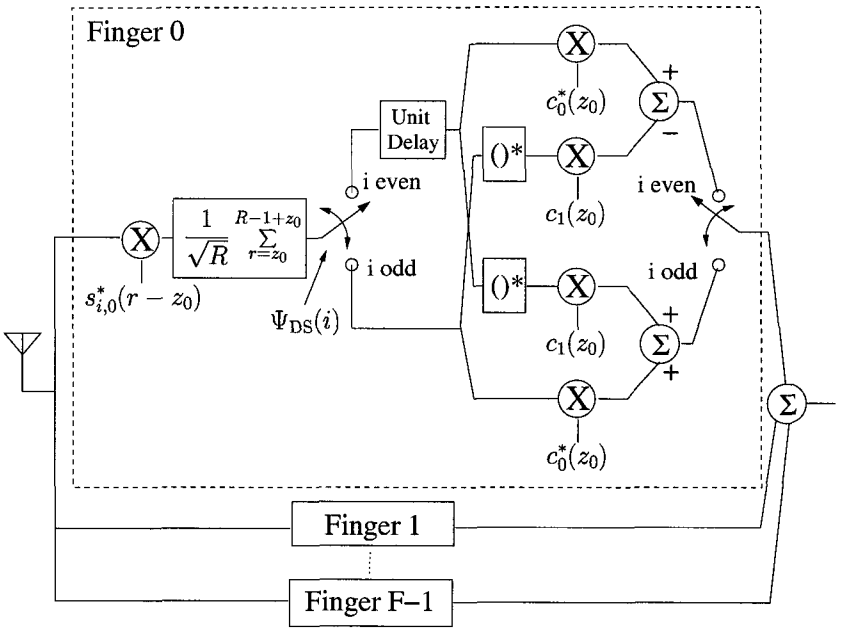

Figure 2.5: STTD Rake receiver.

As for single antenna transmission in Section 2.3.1, intercell interference plus thermal noise is modeled at the input to the Rake receiver as an additive complex Gaussian process with zero mean and variance σ_N^2. The result of passing this process through a normalized despreading block synchronized to a finger time offset of r is denoted $N_{r,i}$ which is a complex Gaussian random variable that also has zero mean and variance σ_N^2. Accounting for the STTD Rake combining shown in Fig. 2.5, the intercell interference plus thermal noise at the output of the Rake receiver for during symbol interval i is

$$N_i = \begin{cases} \sum_{f=0}^{F-1}\left[c_0^*(z_f)N_{z_f,i} - c_1(z_f)N^*_{z_f,i+1}\right], i \text{ even} \\ \sum_{f=0}^{F-1}\left[c_0^*(z_f)N_{z_f,i} + c_1(z_f)N^*_{z_f,i-1}\right], i \text{ odd} \end{cases} \tag{2.24}$$

The composite forward link signal transmitted by base station antenna α and

attenuated by large scale channel effects is considered a zero mean, complex random process, $I^{\alpha}(n)$, with variance σ_I^2. The composite forward link signal at the output of the Rake finger despreading stage is denoted $I^{\alpha}_{r,i}$, which is equal to the normalized sum of R samples of $I^{\alpha}(n)$ multiplied by $s_{0,i}(n)$ with a time offset of r during symbol interval i. Since the normalized despreading process does not alter the mean or variance of the received forward channel signal, $I^{\alpha}_{r,i}$ is a zero-mean random variable with variance σ_I^2. These random variables are independent for different transmit antennas and different values of r and i. Accounting for the STTD processing performed in the Rake receiver, the intracell interference at the output of finger f is

$$I'_{f,i} = \begin{cases} \sum_{l=0}^{L-1} \Big(c_0^*(z_f)\left[c_0(l)I^0_{z_f-l,i} + c_1(l)I^1_{z_f-l,i}\right] \\ \qquad -c_1(z_f)\left[c_0(l)I^0_{z_f-l,i+1} + c_1(l)I^1_{z_f-l,i+1}\right]^*\Big)[1-\delta(l-z_f)], i \text{ even} \\ \sum_{l=0}^{L-1} \Big(c_0^*(z_f)\left[c_0(l)I^0_{z_f-l,i} + c_1(l)I^1_{z_f-l,i}\right] \\ \qquad +c_1(z_f)\left[c_0(l)I^0_{z_f-l,i-1} + c_1(l)I^1_{z_f-l,i-1}\right]^*\Big)[1-\delta(l-z_f)], i \text{ odd.} \end{cases} \tag{2.25}$$

The overall intracell interference at the Rake receiver output is given by $I_i = \sum_{f=0}^{F-1} I'_{f,i}$. As for the single base station antenna model, it is assumed that the intracell interference terms $I^{\alpha}_{z_f-l,i}$ in (2.25) can be modeled using complex Gaussian variables with zero mean and variance σ_I^2.

2.3.3 Validation of the Gaussian Intracell Interference Assumption

One of the key assumptions made by the symbol-level CDMA forward link models presented in Sections 2.3.1 and 2.3.2 is that the intracell interference contribution from any forward link multipath component can be described as Gaussian at the output of a Rake finger despreading stage. This is equivalent to assuming the random variable, $I_{z_f-l,i}$ in (2.17) and $I^{\alpha}_{z_f-l,i}$ in (2.25) are Gaussian random

variables.

When similar Gaussian intracell interference assumptions have been made in previous research [29, 10], a fully loaded link with a spreading factor of 64 or 128 is typically assumed. However, in order to support high speed data service, modern CDMA systems will use much smaller spreading factors on links with a small number of high power CDMA traffic signals. The purpose of this section is to determine whether the Gaussian intracell interference assumption will hold for this type of low spreading factor, high data rate link [51].

Two approaches are used to verify the Gaussian intracell interference assumption. First, actual CDMA forward link intracell interference distributions are generated using a chip-level simulation. These distributions are compared to an ideal Gaussian distribution both graphically and using a Chi-square goodness of fit test [39]. Second, simulations are performed with the single base station antenna symbol-level model presented in Section 2.3.1 using the Gaussian intracell interference assumption. The results from these simulations are compared to results generated using a full chip-level simulation. The purpose of this simulation comparison is to ensure that a model based on the Gaussian intracell interference assumption can be used to accurately characterize CDMA forward link performance.

Model Verification by Comparing Distributions

To verify the Gaussian intracell interference assumption, a chip-level simulation is used to generate distributions of $I_{1,i}$. As defined in Section 2.3.1, this term corresponds to the intracell interference that appears at the output of a Rake finger despreading stage due to a multipath component that arrives 1 chip after the finger time offset. This numerically generated intracell interference distribution is then compared with an ideal Gaussian distribution.

A chip-level IS-2000 CDMA forward link simulation is used to numerically generate the actual distribution of $I_{1,i}$. During the simulation, samples of the $I_{1,i}$ interference term are collected at the Rake finger despreading stage output for every symbol received during a 30 s interval. The distribution is then determined by generating a histogram using these samples.

The forward link interfering signals in the chip-level simulation used to generate samples of $I_{1,i}$ consist of both traffic and overhead CDMA channels. These signals are spread using the Walsh codes and PN-sequence short code of an IS-2000 CDMA base station [72]. The forward link transmit gains of the interfering traffic signals are adjusted by 800 Hz fast forward power control commands. These commands are independent and random power control adjustments that attempt to compensate for fast Rayleigh fading are generated for each traffic signal. The overhead signals include the pilot, paging and sync channels specified in the IS-2000 standard and their gains are set so that they transmit at 8%, 4% and 1% of maximum forward link power, respectively. These overhead channel gains are constant and remain at the same level regardless of the number of traffic channels or Walsh sequence length used in the simulation.

Distributions of $I_{1,i}$ generated for CDMA forward links using traffic channel Walsh sequences of length 64 and 8 are shown in Fig. 2.6. For the length 64 Walsh sequences, distributions are shown for 61 and 20 traffic channel signals which corresponds to a traffic load of 100% and approximately 30%. For the length 8 codes, distributions are shown for 6 and 2 traffic channel signals which also corresponds to 100% and approximately 30% traffic loading.

When a chi-square goodness-of-fit test is performed, only the distributions generated for the length 64 Walsh codes satisfy the Gaussian assumption. It is clear from Fig. 2.6 that intracell interference on a CDMA forward link with a spreading factor of 8 does not satisfy the Gaussian assumption, even for full traffic

loading. The individual interfering signals on the forward link are essentially binomial random variables with the gains of the traffic signals randomly adjusted by forward link power control. When the number of forward link signals is small, the binomial nature of the interfering signals becomes apparent in the distribution of the overall forward link signal. This is the cause of the spikes in the distribution of the forward link signal in Fig. 2.6 generated with length 8 codes and 2 interfering users.

Even though the intracell interference distributions for the low spreading factor channels are not Gaussian, it will be shown in the next section that a symbol-level CDMA forward link model that uses a Gaussian intracell interference assumption can still provide accurate simulation results.

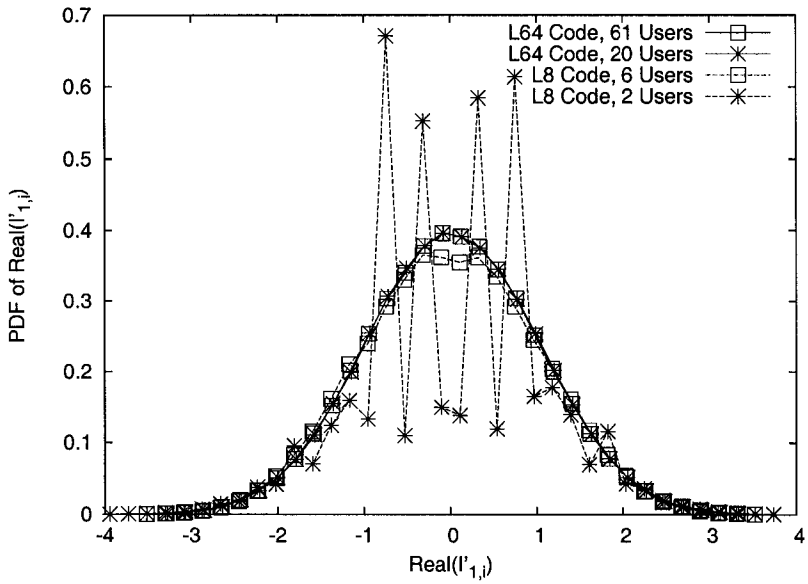

Figure 2.6: $\mathcal{R}(I'_{1,i})$ distributions.

Model Verification using Link Simulations

This section compares CDMA forward link simulation results generated using a full IS-2000 chip-level simulation to results generated with a symbol level simu-

lation with Gaussian intracell interference. The chip-level simulation is based on the model presented in Section 2.2 and the symbol level simulation on Section 2.3. The results from both simulations show bit error rate (BER) versus the ratio of desired signal energy per information bit, E_b, to the variance of intercell interference plus thermal noise at the mobile receiver input, σ_N^2. The level of intracell interference used for each simulation run remains fixed for all values of E_b/σ_N^2.

Simulation results with and without channel coding are produced for CDMA forward links using length 64 and length 8 Walsh sequences. The channel code is a rate 1/2, constraint length 3 (5,7) convolutional code. Soft decision Viterbi decoding is used. For the length 64 Walsh sequences, the bit rate with channel coding is 9.6 kb/s and the bit rate without channel coding is 19.2 kb/s. For the length 8 Walsh sequences, the bit rates are 76.8 kb/s and 153.6 kb/s for the coded and uncoded cases, respectively. Frames are 20 ms long and the radio channel is Rayleigh with average relative path powers equal to -2 dB, -6 dB and -10 dB. A mobile velocity of 100 km/h is assumed which, at a carrier frequency of 1.9 GHz, corresponds to a Doppler frequency of approximately 176 Hz. The forward link power control adjustments of the traffic channels and the fixed overhead channel gains are modeled as described in the previous section. The results generated for the length 64 and length 8 Walsh codes are shown in Figs. 2.7 and 2.8, respectively. The intracell interference levels used to generate these simulation results correspond to a forward link signal consisting of the pilot, paging and sync overhead channels plus a number of traffic channels equal to 100% and approximately 30% traffic loading.

Figs. 2.7 and 2.8 show good agreement between the results generated using the chip-level and symbol-level models when channel coding is not used in the simulations. The agreement is excellent for the length 64 Walsh sequences and, as expected, degrades somewhat when the traffic channels use the lower spreading

factor, length 8 Walsh sequences. However, the agreement between the two models is still much better than the non-Gaussian interference distributions in Fig. 2.6 would suggest, particularly for the extreme case of length 8 traffic channel Walsh sequences and only 2 traffic transmissions.

Figs. 2.7 and 2.8 also show that the agreement between the chip-level and symbol-level models degrades when channel coding is used in the simulations. The degradation is mild for the link using length 64 Walsh sequences but becomes more pronounced for the link using length 8 Walsh sequences. This behavior provides some insight into the nature of the Gaussian intracell interference assumption. The intracell interference term $I_{z_w-l,i}$ would not approach a Gaussian distribution even for large spreading factors if the forward link traffic channel gains remained fixed. The independent and random gain variations in each traffic channel due to fast forward power control smooth the distribution of the traffic signal interference and make the overall intracell interference process closer to Gaussian. However, since only 16 fast forward power control adjustments can occur in each 20 ms frame, there is not enough variation for Gaussian statistics to develop within a single frame duration. Since the Viterbi decoder operates on a frame-by-frame basis, a discrepancy develops between the symbol-level model and the chip-level simulation results when channel coding is used. This discrepancy is not as pronounced in the uncoded simulations that average BER over many frames at the Rake receiver output.

Overall, the simulation results indicate that the Gaussian intracell interference assumption can be used in a symbol-level simulation to produce accurate results even for low spreading factors. However, a bias in the simulation will result if channel codes are combined with a lightly loaded low spreading factor link in the simulation.

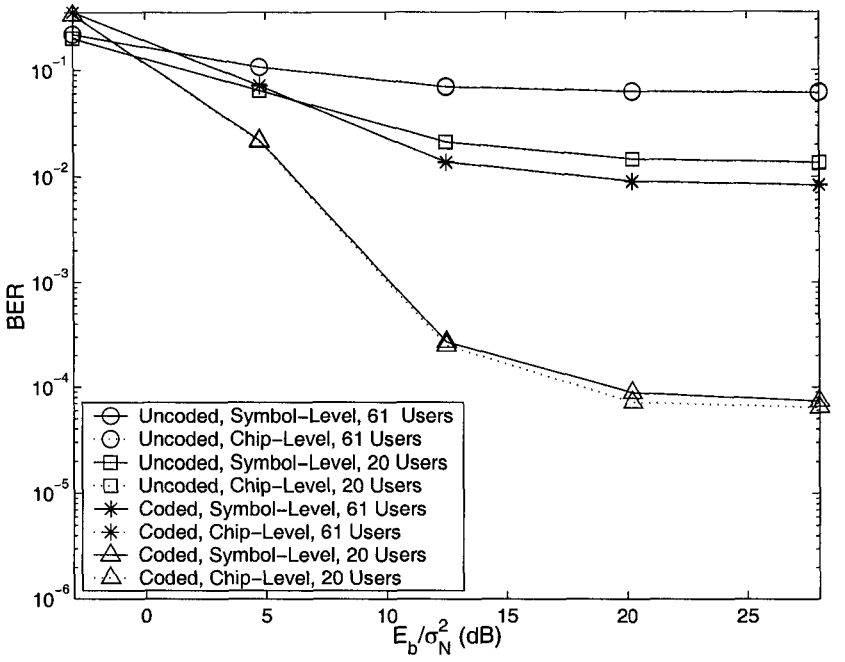

Figure 2.7: Chip-level and symbol-level simulations, length 64 codes.

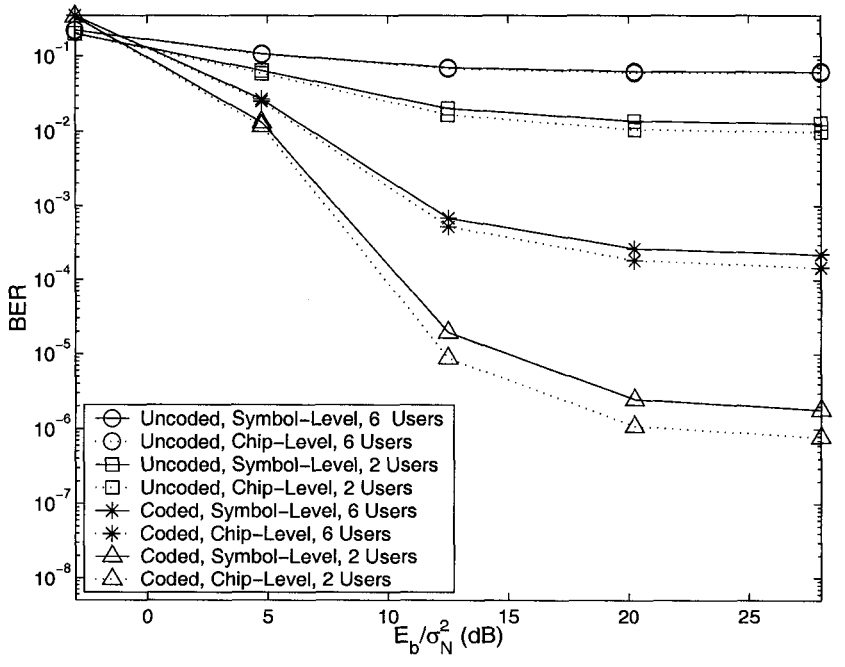

Figure 2.8: Chip-level and symbol-level simulations, length 8 codes.

Chapter 3

CDMA Forward Link Channel State Estimation for Conventional Trellis Path Metrics

This chapter improves CDMA forward link performance through the development of new channel state estimation techniques for the CDMA mobile. Channel state estimation is the calculation of the desired signal amplitude and interference plus noise variance values required by the conventional channel decoder metric calculations described in Chapter 1.

Before developing new channel state estimation techniques for the CDMA mobile, it must first be established whether the conventional channel decoder trellis path metrics are optimal for use on the CDMA forward link. Section 1.3 states that the primary assumption made by the conventional Viterbi, SOVA and MAP algorithms is that the probability density function (PDF) of the ith channel encoded symbol sample at the input to the channel decoder, y_i, is Gaussian. Since the de-interleaving process does not alter the statistics of individual symbols, this is equivalent to assuming the PDF of the symbol sample at the Rake receiver output is Gaussian. Assuming BPSK modulation, an expression for y_i at the output of a CDMA mobile Rake receiver with F fingers can be written as

$$y_i = \mathcal{R}(\sum_{f=0}^{F-1} [c(z_f)Ax_i + U_{f,i}]\, \widehat{c(z_f)}^*) \tag{3.1}$$

where $U_{f,i}$ is the noise and interference at the output of the despreading stage in finger f during symbol interval i, the amplitude A represents the combination of transmit amplitude and despreading gain, $c(z_f)$ is the complex channel impulse response value at delay z_f and $\widehat{c(z_f)}$ is the mobile's estimate of that channel impulse response value. Using the symbol-level CDMA forward link model presented in Section 2.3, the $U_{f,i}$ term can be written as

$$U_{f,i} = N_{f,i} + \sum_{l=0}^{L-1} c(l) I_{z_f-l,i}[1 - \delta(l - z_f)] \tag{3.2}$$

where both the intercell interference plus thermal noise term, $N_{f,i}$, and the intracell interference term $I_{z_f-l,i}$ were shown to be Gaussian for moderate to high spreading factors and traffic loads. As long as channel estimation error is small, the term $\widehat{c(z_f)}$ in (3.1) can be considered equal to the instantaneous value of $c(z_f)$ and the uncertainty in y_i is due only to the Gaussian interference and noise term $U_{f,i}$. Therefore, the distribution for y_i is Gaussian and the conventional channel decoder trellis path metrics are optimal for use on the CDMA forward link.

Even if the conventional channel decoder metrics are optimal for use in a CDMA mobile, the calculation of these metrics still requires estimates of the desired signal amplitude, $\zeta(i)$, and interference plus noise variance, $\sigma^2(i)$, to be determined at the input to the mobile channel decoder. These two terms can be estimated separately or together as a signal to noise plus interference ratio. This estimation is sometimes referred to as channel state estimation and sometimes as SNIR estimation.

It is well known that the desired signal envelope $\zeta(i)$ varies from symbol to symbol due to small scale fading. It is therefore accepted that this signal amplitude must be estimated by the mobile and incorporated into the channel decoder

metric calculations. However, the CDMA forward link discussion in Chapter 2 points out that small scale fading can also cause $\sigma^2(i)$ to fluctuate from symbol to symbol due to non-stationary intracell interference. As a result, the channel state estimation schemes presented in this chapter will focus on improving channel decoder performance by providing good symbol-by-symbol estimates of both $\zeta(i)$ and $\sigma^2(i)$.

In a channel state estimation scheme that calculates $\zeta(i)$ and $\sigma^2(i)$ separately, the estimation of $\zeta(i)$ can be performed using relatively straightforward techniques that operate on fixed transmit energy power control bits or pilot symbols embedded in the traffic transmission [13, 2]. However, the estimation of $\sigma^2(i)$ is more challenging due to the complex nature of forward link interference in a CDMA system. For the channel state estimation techniques presented in this chapter that separately calculate $\zeta(i)$ and $\sigma^2(i)$ in the mobile, most of the discussion is devoted to correctly performing the estimation of $\sigma^2(i)$.

While it is necessary to produce accurate channel state estimates, it is also desirable to keep the structure of the estimator as simple as possible. This simplicity is necessary to minimize the computations that must be performed by the battery-powered mobile. This chapter presents two techniques for estimating $\zeta(i)$ and $\sigma^2(i)$ separately that make different tradeoffs between the sometimes conflicting requirements of accuracy and complexity. They are referred to as *standard estimation* and *improved estimation* [50, 49, 48, 52, 53].

Standard estimation is presented in Section 3.1. This scheme estimates $\zeta(i)$ using a moving average filter that operates on pilot symbols embedded in the traffic stream. The variance $\sigma^2(i)$ is estimated based on the assumption that CDMA forward link intracell interference, intercell interference and thermal noise can be lumped together and modeled as an additive white Gaussian noise (AWGN) process at the mobile receiver input. This is an assumption often made by CDMA

forward link studies [9, 25] and it will be shown that it leads to a very simple estimator structure. However, the estimates of $\sigma^2(i)$ produced by standard estimation are somewhat inaccurate. This is because assuming that all CDMA forward link interference and noise can be represented using a single AWGN process prevents the estimator from accounting for the non-stationarity and partial Walsh sequence cancellation of intracell interference.

Improved estimation is presented in Section 3.2. Like standard estimation, $\zeta(i)$ is estimated using pilot signals embedded in the traffic transmission. The variance $\sigma^2(i)$ is determined using a new technique that separately estimates the variance of the intracell interference and intercell interference plus thermal noise processes at the input to the mobile channel decoder. This approach results in a more complex estimator structure. However, it also produces more accurate estimates of $\sigma^2(i)$ since this method is able to account for the non-stationarity and partial Walsh sequence cancellation of intracell interference.

While the standard and improved estimation schemes presented in this chapter estimate $\zeta(i)$ and $\sigma^2(i)$ separately, some techniques have been proposed for simultaneously estimating $\zeta(i)$ and $\sigma^2(i)$ as a signal to noise plus interference ratio. Summers and Wilson present an "online" technique for estimating SNR at the turbo decoder input based on the second order statistics of the received signal [69]. Ramesh, *et. al.* extend this technique for a Nakagami fading channel with both flat fading and equal gain diversity combining [63, 64]. The technique developed by Ramesh cannot be applied to the CDMA forward link since it produces average SNR estimates that do not capture the symbol-to-symbol fluctuations in $\zeta(i)$ and $\sigma^2(i)$ due to small scale fading. This chapter will show that capturing these variations significantly improves CDMA mobile channel decoder performance.

However, this chapter will demonstrate that it is possible to adapt the original online SNR estimation technique developed by Summers and Wilson for use in

a CDMA mobile. In [69], the authors start by considering SNR estimation in a time invariant AWGN channel with a constant desired signal envelope and noise variance. It has been established in Chapter 2 that CDMA forward link interference and noise can be considered Gaussian and that both the desired signal level and interference variance will fluctuate with small scale fading. Therefore, during time intervals less than the channel coherence time, the CDMA forward link is approximately equivalent to a time invariant AWGN channel with constant desired signal envelope and Gaussian interference plus noise variance. As a result, the original AWGN channel version of online estimation can be applied to the CDMA forward link as long as it operates on an observation window shorter than the channel coherence time. This is a novel application of the online estimation technique and is discussed in more detail in Section 3.3.

This chapter makes a new contribution to CDMA research since this is the first work to perform a detailed investigation of channel state estimation on a frequency selective CDMA forward link that employs Walsh/PN-sequence concatenated spreading. This is an important contribution since this forward link model represents conditions on all commercial CDMA systems. Research into multi-code CDMA systems that combine channel coding with concatenated Walsh/PN-sequence spreading and a frequency selective channel has considered only a single multi-code CDMA user [32] or the reverse link of a multi-code system [45]. The work by Unal modifies turbo decoding metrics to account for non-stationary intracell interference variance estimates on the CDMA forward link but assumes a flat fading channel with signals spread using only PN sequences [75]. The work by Elezabi and Duel-Hallen calculates non-stationary interference variance estimates for use in a Viterbi decoder [16]. However, the authors consider subtractive interference cancellation rather than the more practical Rake receiver or chip-level LMMSE equalizer. They also consider only a flat fading channel with PN-sequence

spreading codes. Other channel coding papers for the CDMA forward link use an AWGN process to represent all interference and noise and do not model the actual statistics of CDMA forward link interference [9, 25].

It is clear from the discussion in Section 1.2 that enhancing the performance of the CDMA forward link is a very active area of research and a wide range of new techniques for improving forward link performance have been proposed. Many of these techniques, like transmit diversity and advanced receivers capable of interference cancellation, will change the nature of the interference and noise at the input to the mobile channel decoder. This can make it necessary to modify the channel state estimation techniques that are used to supply the information required by the channel decoder metric calculations.

In order to be relevant not only to current CDMA systems but also to future systems, the channel state estimation schemes presented in Sections 3.1 through 3.3 must not only be applied to the conventional CDMA forward link but also to forward link designs that incorporate advanced physical layer techniques. As a result, the following forward link configurations will be used to evaluate the performance of the online, standard and improved channel state estimation schemes:

1. Single antenna base station transmission, mobile Rake receiver.

2. Space time transmit diversity base station transmission, mobile Rake receiver.

3. Single antenna base station transmission, mobile chip-level LMMSE equalizer receiver.

Some of the channel state estimation schemes presented in this chapter will require modification to be used with these different forward link designs and some will not.

CDMA forward link simulations are used in Section 3.4 to investigate the performance of these three forward link configurations when standard, improved and online channel state estimation is employed in the mobile. Both convolutional and turbo channel codes are considered. The results will indicate that improved estimation provides the most accurate channel state estimates and always results in the best forward link performance. Standard estimation tends to perform better than online estimation when the two schemes are used with either the Viterbi or SOVA decoders. However, online estimation can outperform standard estimation when the LogMAP decoder is used in the mobile.

The simulations will also show that the relative performance difference between these channel state estimation techniques depends on a number of factors. These factors include mobile velocity, channel decoder algorithm, mobile receiver architecture and whether the base station uses single antenna transmission or transmit diversity. It is important to understand these sensitivities since they determine whether the performance improvement provided by a more accurate channel state estimation technique is sufficient to justify the increase in complexity.

3.1 Standard Channel State Estimation

Standard estimation assumes that all interference and noise at the mobile receiver input can be lumped together and modeled as a complex AWGN process, $Z(n)$, with zero mean and variance σ_Z^2. This assumption is equivalent to assuming that the CDMA forward link can be represented as a frequency selective fading channel with AWGN.

The standard estimation scheme must be modified for different forward link designs. Section 3.1.1 considers a conventional CDMA forward link where the base station uses single antenna transmission and the mobile uses a Rake receiver. Section 3.1.2 derives standard estimation for the combination of space time transmit

diversity and a Rake receiver in the mobile. Section 3.1.3 considers single antenna base station transmission combined with the chip-level LMMSE mobile receiver. Note that while these sections all consider different link configurations, they all derive estimators for $\sigma^2(i)$ based on the assumption that all forward link interference and noise can be represented using the AWGN process $Z(n)$. These different versions of standard estimation also all assume that desired signal envelope, $\zeta(i)$, is estimated by applying a simple moving average filter to pilot symbols embedded in the transmitted traffic signal.

3.1.1 Single Antenna Transmission, Mobile Rake Receiver

In order to derive an expression for estimating $\sigma^2(i)$, it is necessary to first derive an expression for the interference plus noise at the Rake receiver output during symbol interval i, Z_i. It is assumed that the total forward link interference and noise received by the mobile can be represented using a single Gaussian source, $Z(n)$, added to the desired signal at the input to the mobile Rake receiver shown in Fig. 2.3. Accounting for the Rake finger despreading and finger maximal ratio combining, an expression for Z_i can be written as

$$\begin{aligned} Z_i &= \frac{1}{\sqrt{R}} \sum_{f=0}^{F-1} c^*(z_f) \sum_{r=0}^{R-1} s_{i,0}^*(r) Z(iR - z_f + r) \\ &= \sum_{f=0}^{F-1} c^*(z_f) Z_{z_f,i} \end{aligned} \tag{3.3}$$

where the channel response, spreading code and Rake receiver notation used in (3.3) is defined in Chapter 2. The term $Z_{z_f,i}$ is the interference plus noise at the output of the despreading stage in finger f during symbol interval i. As in Section 2.3.1, it is assumed that the spreading code multiplication and normalized summation making up the despreading operation in each finger does not alter the variance or distribution of an additive Gaussian interference and noise process at the Rake input. Therefore, $Z_{z_f,i}$ can be considered a zero mean complex Gaussian random variable with variance σ_Z^2.

The standard estimator assumes that $\sigma^2(i)$ can be estimated by the mobile using an expression for the variance of Z_i. As long as the Rake finger time offsets are separated by at least one chip, the $Z_{f,i}$ terms in (3.3) can be considered independent. This is because $Z_{f,i}$ consists of the summation of samples of $Z(n)$ multiplied by $s_{i,0}(n)$ with different time offsets and $s_{i,0}(n)$ is uncorrelated at time offsets of more than one chip. The variance expression is therefore written as

$$\sigma^2(i) = \left\langle |Z_i|^2 \right\rangle = \sigma_Z^2 \sum_{f=0}^{F-1} |c(z_f)|^2. \tag{3.4}$$

Section 2.3 provides an expression in (2.14) for the desired signal amplitude, $\zeta(i)$, at the output of the Rake receiver. Note that the ratio of this expression and the estimated variance $\sigma^2(i)$ in (3.4) is equal to a constant. The channel decoder path metric discussion in Section 1.3 points out that when the estimated ratio $\zeta(i)/\sigma^2(i)$ is constant for the duration of the encoded frame, it can be removed from the Viterbi and SOVA decoder metric calculations. Therefore the "standard estimation" scheme when combined with the Viterbi or SOVA decoders is not to estimate $\sigma^2(i)$ and $\zeta(i)$ at all but instead use the Viterbi/SOVA correlation metric without any channel state information. However, when standard estimation is combined with the LogMAP decoder, estimates of $\zeta(i)$ and $\sigma^2(i)$ are still determined. These values are always required by the LogMAP path metric calculations, even if they are stationary.

The complexity of the standard estimation scheme is very low. For the Viterbi and SOVA decoders, no estimation is required at all. When estimation of $\sigma^2(i)$ is performed for the LogMAP decoder, the estimation equation (3.4) is complexity order $O(F)$, using Landau symbol notation [11]. The channel terms required by (3.4) are already being determined by the mobile for Rake finger combining and the input variance term σ_Z^2 is easily estimated by assuming it is equal to the total signal power at the mobile receiver input. This estimate of σ_Z^2 will also contain

a small contribution from the desired signal. However, this contribution can be neglected for links with moderate to high traffic loading since the amplitude of the desired signal before despreading is small relative to the total received interference plus noise.

3.1.2 STTD Transmission, Mobile Rake Receiver

The derivation of standard estimation for a CDMA forward link using STTD starts by determining an expression for the interference plus noise at the output of the STTD Rake receiver shown in Fig. 2.5. It is assumed that the interference and noise process at the input to the Rake receiver is the AWGN process $Z(n)$. Accounting for the finger despreading and STTD combining performed by the Rake and using the notation in Section 2.3.2, an expression for Z_i is written as

$$
\begin{aligned}
& Z_i \\
&= \begin{cases} \frac{1}{\sqrt{R}} \sum_{f=0}^{F-1} \sum_{r=0}^{R-1} \left\{ c_0^*(z_f) Z(iR - z_f + r) - c_1(z_f) Z^* \left[(i+1)R - z_f + r \right] \right\}, \\ i \text{ even} \\ \frac{1}{\sqrt{R}} \sum_{f=0}^{F-1} \sum_{r=0}^{R-1} \left\{ c_0^*(z_f) Z(iR - z_f + r) + c_1(z_f) Z^* \left[(i-1)R - z_f + r \right] \right\}, \\ i \text{ odd} \end{cases} \\
&= \begin{cases} \sum_{f=0}^{F-1} \left[c_0^*(z_f) Z_{z_f,i} - c_1(z_f) Z_{z_f,i+1}^* \right], i \text{ even} \\ \sum_{f=0}^{F-1} \left[c_0^*(z_f) Z_{z_f,i} + c_1(z_f) Z_{z_f,i-1}^* \right], i \text{ odd} \end{cases}
\end{aligned}
\tag{3.5}
$$

where, as in Section 3.1.1, $Z_{z_f,i}$ is a zero mean complex Gaussian random variable with variance σ_Z^2 which represents the interference plus noise at the output of the despreading stage in finger f during symbol interval i.

The standard estimator for a mobile in an STTD system determines $\sigma^2(i)$ using an expression for the variance of Z_i. If the Rake fingers are separated by at least one chip, this variance can be written for both the even and odd symbol intervals as

$$\sigma^2(i) = \sigma_Z^2 \sum_{f=0}^{F-1} \left[|c_0(z_f)|^2 + |c_1(z_f)|^2 \right] \tag{3.6}$$

where the channel impulse response terms are already being estimated for use in the mobile Rake receiver. As in Section 3.1.1, σ_Z^2 can be estimated by assuming it is equal to the total received power.

Desired signal envelope at the output of a mobile Rake receiver, $\zeta(i)$, in an STTD system is given by (2.23) in Section 2.3.2. The ratio of this envelope expression and the variance estimated by (3.6) is a constant. Therefore, as was the case in Section 3.1.1, estimation of the ratio $\zeta(i)/\sigma^2(i)$ is not required for the Viterbi and SOVA decoders and the mobile can revert to using the correlation metric calculation without channel state information. However, calculation of $\zeta(i)$ and $\sigma^2(i)$ is still required for the LogMAP decoder.

3.1.3 Single Antenna Transmission, Mobile Chip-level LMMSE Equalizer

Standard estimation for a mobile using the chip-level LMMSE equalizer is derived by first finding an expression for the interference plus noise, Z_i, at the output of the equalizer shown in Fig. 2.4. In the following, it is assumed that the equalizer operates at one sample per chip, $S = 1$. Using the equalizer receiver notation from Section 2.2.3 and assuming that the Gaussian process $Z(n)$ is applied to the equalizer input, the interference plus noise component at the equalizer output is

$$\begin{aligned} Z_i &= \sum_{v=0}^{N_T-1} \frac{1}{\sqrt{R}} \sum_{r=0}^{R-1} s_{i,0}^*(r) e_i^*(v) Z(iR - v + r) \\ &= \sum_{v=0}^{N_T-1} e_i^*(v) Z_{v,i} \end{aligned} \tag{3.7}$$

where $Z_{v,i}$ is a zero mean, complex Gaussian random variable with variance σ_Z^2 that represents $Z(n)$ after despreading with a time offset of v. This term is identical to $Z_{f,i}$ in (3.3) and (3.5).

The standard estimator for the chip-level LMMSE equalizer determines $\sigma^2(i)$

using an expression for the variance of Z_i in (3.7). Assuming the equalizer taps are separated by at least one chip, the $Z_{v,i}$ terms in (3.7) are independent and the variance of Z_i can be written as

$$\sigma^2(i) = \sigma_Z^2 \sum_{v=0}^{N_T-1} |e_i(v)|^2. \tag{3.8}$$

The tap weight values are already known to the receiver and, as for the previous two sections, σ_Z^2 is estimated by assuming it is equal to the total signal power at the equalizer input.

The standard estimators presented in Sections 3.1.1 and 3.1.2 were both developed for use with a Rake receiver and in both cases it was found that the estimated ratio $\zeta(i)/\sigma^2(i)$ was constant. This made it unnecessary to estimate either $\zeta(i)$ or $\sigma^2(i)$ for the Viterbi and SOVA decoders. However, in the case of the chip-level LMMSE equalizer, the desired signal amplitude $\zeta(i)$ is proportional to the double convolution of the channel impulse response and the equalizer taps. The variance $\sigma^2(i)$ in (3.8) is proportional to the summation of the equalizer tap energies. It is not obvious that the ratio of $\zeta(i)/\sigma^2(i)$ at the output of the equalizer will be constant as it was for the Rake receiver. Therefore, the standard estimation scheme for the chip-level LMMSE equalizer must estimate both $\zeta(i)$ and $\sigma^2(i)$ at all times, regardless of what channel decoder algorithm is being used by the mobile.

3.2 Improved Channel State Estimation

Improved estimation determines $\sigma^2(i)$ by separately calculating the variances of the intracell interference and intercell interference plus thermal noise processes at the mobile receiver output. This approach assumes that $\sigma^2(i) = \langle |N_i|^2 \rangle + \langle |I_i|^2 \rangle$, where I_i and N_i are defined in the symbol-level model presented in Section 2.3 as the intracell interference and intercell interference plus thermal noise process at the mobile receiver output during symbol interval i, respectively.

Improved estimation assumes that interference and noise on the CDMA forward link can be represented as shown in Fig. 3.1. As defined in Section 2.3.1, $I(n)$ is a complex, zero mean random process with variance σ_I^2 that represents the composite forward link signal after large scale channel attenuation but before convolution with the small scale channel impulse response. The term $N(n)$ is a complex, zero mean Gaussian random process with variance σ_N^2 that represents intercell interference plus thermal noise and is added directly to the signal at the mobile input.

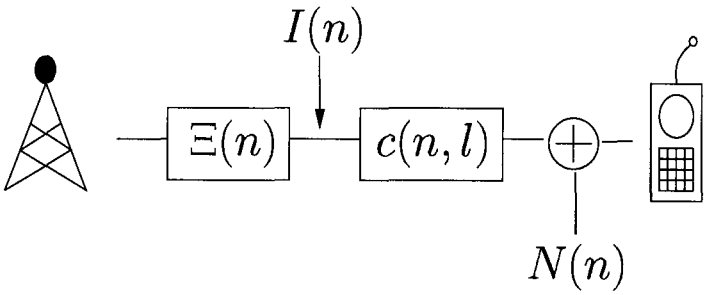

Figure 3.1: CDMA forward link interference.

The improved estimation scheme must be modified for different forward link configurations. Section 3.2.1 presents a variant of improved estimation that considers a CDMA forward link where the base station uses single antenna transmission and the mobile uses a Rake receiver. Section 3.2.2 considers the combination of space time transmit diversity and a Rake receiver in the mobile. Section 3.2.3 considers single antenna base station transmission combined with the chip-level LMMSE mobile receiver.

It will be shown that the improved estimators developed in all three cases require knowledge of the variances σ_I^2 and σ_N^2. Section 3.2.4 presents a linear estimator for determining these values. As for standard estimation, it is assumed that the three different versions of improved estimation discussed below all estimate $\zeta(i)$ using a moving average filter that operates on pilot symbols embedded in the

traffic transmission.

3.2.1 Single Antenna Transmission, Mobile Rake Receiver

Improved estimation for single antenna transmission individually calculates $\langle |I_i|^2 \rangle$ and $\langle |N_i|^2 \rangle$ and then adds these two values to determine $\sigma^2(i)$. Expressions for these variances are derived using the expressions for N_i and I_i presented as part of the symbol-level model in Section 2.3.

The expression for N_i is given by (2.15) in Section 2.3.1. If the Rake fingers are separated by at least one chip, the terms $N_{f,i}, f = 0, \ldots F-1$ in (2.15) are independent and $\langle |N_i|^2 \rangle$ can be estimated according to

$$\left\langle |N_i|^2 \right\rangle = \sigma_N^2 \sum_{f=0}^{F-1} |c(z_f)|^2 . \tag{3.9}$$

The expression for I_i is given by (2.18) in Section 2.3.1 as

$$I_i = \sum_{f=0}^{F-1} c^*(z_f) \sum_{l=0}^{L-1} c(l) I_{z_f - l, i} [1 - \delta(l - z_f)] \tag{3.10}$$

where the $[1 - \delta(l - z_f)]$ term accounts for the Walsh sequence cancellation of intracell interference. Accounting for correlation between interference terms, the variance of this intracell interference term can be estimated according to

$$\begin{aligned} \langle |I_i|^2 \rangle &= \left\langle \left(\sum_{f=0}^{F-1} c^*(z_f) \sum_{l=0}^{L-1} c(l) I_{z_f - l, i} [1 - \delta(l - z_f)] \right) \right. \\ &\quad \left. \left(\sum_{v=0}^{F-1} c^*(z_v) \sum_{q=0}^{L-1} c(q) I_{z_v - q, i} [1 - \delta(q - z_v)] \right)^* \right\rangle \\ &= \sum_{f=0}^{F-1} \sum_{l=0}^{L-1} \sum_{v=0}^{F-1} \sum_{q=0}^{L-1} c^*(z_f) c(l) \left[c^*(z_v) c(q) \right]^* \\ &\quad \left\langle I_{z_f - l, i} I^*_{z_v - q, i} \right\rangle [1 - \delta(l - z_f)][1 - \delta(q - z_v)] \\ &= \sigma_I^2 \sum_{f=0}^{F-1} \sum_{l=0}^{L-1} \sum_{v=0}^{F-1} \sum_{q=0}^{L-1} c^*(z_f) c(l) \left[c^*(z_v) c(q) \right]^* \\ &\quad \cdot \delta \left[(l - z_f) - (q - z_v) \right] \left[1 - \delta(l - z_f) \right] \left[1 - \delta(q - z_v) \right] . \end{aligned} \tag{3.11}$$

Unlike standard estimation, the improved estimation approach accounts for the non-stationary fluctuations and partial Walsh sequence cancellation of intracell interference. As a result, the ratio of the desired signal envelope expression

for $\zeta(i)$ in (2.14) and the estimated variance $\sigma^2(i)$ given by the summation of (3.9) and (3.11) is no longer constant. This means the estimated ratio $\zeta(i)/\sigma^2(i)$ must now be included in the Viterbi and SOVA metric calculations. Improved estimation therefore always calculates estimates of $\zeta(i)$ and $\sigma^2(i)$ regardless of channel decoder algorithm.

The complexity of improved estimation is higher than standard estimation. Estimation of $\zeta(i)$ and $\sigma^2(i)$ must now be performed for all channel decoding algorithms and calculating $\sigma^2(i)$ using the summation of (3.9) and (3.11) has a complexity order $O(F^2L^2)$. This is a significant complexity increase over standard estimation. However, the computations required by improved estimation will remain manageable in practice since the numbers F and L are typically quite low for standard Rake receivers and modest multipath dispersion. The channel terms required in (3.9) and (3.11) are estimated by the mobile using the forward channel pilot signal. The input variances σ_I^2 and σ_N^2 required in (3.9) and (3.11) can be calculated using the least-squares estimator derived in Section 3.2.4.

3.2.2 STTD Transmission, Mobile Rake Receiver

The equation used to estimate intercell interference plus thermal noise variance, $\langle |N_i|^2 \rangle$ is derived based on the expression for intercell interference plus thermal noise at the output of the STTD Rake receiver, given by (2.24) in Section 2.3.2. If the Rake fingers are separated by at least one chip, the terms $N_{f,i}, f = 0, \ldots F-1$ in (2.24) are independent and $\langle |N_i|^2 \rangle$ can be calculated by the mobile according to

$$\left\langle |N_i|^2 \right\rangle = \sigma_N^2 \sum_{f=0}^{F-1} \left[|c_0(z_f)|^2 + |c_1(z_f)|^2 \right] \tag{3.12}$$

for both even and odd symbol intervals.

Using the expression for STTD intracell interference at the output of the de-

spreading stage in Rake finger f in (2.25), the overall intracell interference at the output of the Rake receiver is

$$I_i = \begin{cases} \sum_{f=0}^{F-1}\sum_{l=0}^{L-1}\left\{c_0^*(z_f)\left[c_0(l)I^0_{z_f-l,i}+c_1(l)I^1_{z_f-l,i}\right]\right. \\ \qquad \left.-c_1(z_f)\left[c_0(l)I^0_{z_f-l,i+1}+c_1(l)I^1_{z_f-l,i+1}\right]^*\right\} \\ \qquad \cdot[1-\delta(z_f-l)] & ,i \text{ even} \\ \sum_{f=0}^{F-1}\sum_{l=0}^{L-1}\left\{c_0^*(z_w)\left[c_0(l)I^0_{z_w-l,i}+c_1(l)I^1_{z_w-l,i}\right]\right. \\ \qquad \left.+c_1(z_w)\left[c_0(l)I^0_{z_w-l,i-1}+c_1(l)I^1_{z_w-l,i-1}\right]^*\right\} \\ \qquad \cdot[1-\delta(z_w-l)] & ,i \text{ odd.} \end{cases} \tag{3.13}$$

For the even symbols, the variance of the intracell interference process can be estimated according to

$$\begin{aligned} \langle |I_i|^2 \rangle &= \left\langle \left(\begin{array}{l} \sum_{f=0}^{F-1}\sum_{l=0}^{L-1}\left\{c_0^*(z_f)\left[c_0(l)I^0_{z_f-l,i}+c_1(l)I^1_{z_f-l,i}\right]\right. \\ \qquad \left.-c_1(z_f)\left[c_0(l)I^0_{z_f-l,i+1}+c_1(l)I^1_{z_f-l,i+1}\right]^*\right\} \\ \qquad \cdot[1-\delta(z_f-l)] \end{array} \right) \right. \\ &\quad \left. \left(\begin{array}{l} \sum_{v=0}^{F-1}\sum_{q=0}^{L-1}\left\{c_0^*(z_v)\left[c_0(q)I^0_{z_v-q,i}+c_1(q)I^1_{z_v-q,i}\right]\right. \\ \qquad \left.-c_1(z_v)\left[c_0(q)I^0_{z_v-q,i+1}+c_1(q)I^1_{z_v-q,i+1}\right]^*\right\} \\ \qquad \cdot[1-\delta(z_f-l)] \end{array} \right)^* \right\rangle \\ &= \sum_{f=0}^{F-1}\sum_{l=0}^{L-1}\sum_{v=0}^{F-1}\sum_{q=0}^{L-1} \\ &\quad \left[c_0^*(z_f)c_0(l)c_0(z_v)c_0^*(q)\left\langle I^0_{z_f-l,i}I^{0*}_{z_v-q,i}\right\rangle\right. \\ &\quad +c_0^*(z_f)c_1(l)c_0(z_v)c_1^*(q)\left\langle I^1_{z_f-l,i}I^{1*}_{z_v-q,i}\right\rangle \\ &\quad +c_1(z_f)c_0^*(l)c_1^*(z_v)c_0(q)\left\langle I^0_{z_f-l,i+1}I^{0*}_{z_v-q,i+1}\right\rangle \\ &\quad \left.+c_1(z_f)c_1^*(l)c_1^*(z_v)c_1(q)\left\langle I^1_{z_f-l,i+1}I^{1*}_{z_v-q,i+1}\right\rangle\right] \\ &\quad \cdot[1-\delta(z_f-l)][1-\delta(z_v-q)] \\ &= \sigma_I^2\sum_{f=0}^{F-1}\sum_{l=0}^{L-1}\sum_{v=0}^{F-1}\sum_{q=0}^{L-1} \\ &\quad [c_0^*(z_f)c_0(l)c_0(z_v)c_0^*(q)+c_0^*(z_f)c_1(l)c_0(z_v)c_1^*(q) \\ &\quad +c_1(z_f)c_0^*(l)c_1^*(z_v)c_0(q)+c_1(z_f)c_1^*(l)c_1^*(z_v)c_1(q)] \\ &\quad \cdot\delta[(z_f-l)-(z_v-q)][1-\delta(z_f-l)][1-\delta(z_v-q)]. \end{aligned} \tag{3.14}$$

Performing the same derivation for the odd symbol intervals yields the same expression for $\langle |I_i|^2 \rangle$.

The channel terms required in (3.12) and (3.14) can be estimated by the mobile using the forward link pilot signals transmitted from the two base station antennas.

The σ_N^2 and σ_I^2 variance terms are determined using the linear estimator described in Section 3.2.4. As for the single antenna case described in Section 3.2.1, the estimated ratio $\zeta(i)/\sigma^2(i)$ is no longer constant when improved estimation is used in an STTD system. As a result, improved estimation in an STTD system must calculate values of $\zeta(i)$ and $\sigma^2(i)$ for all channel decoder algorithms.

3.2.3 Single Antenna Transmission, Mobile Chip-level LMMSE Equalizer

In the following, it is assumed that the equalizer operates at one sample per chip, $S = 1$. The intercell interference plus thermal noise term at the output of the chip-level LMMSE receiver, N_i, can be determined by convolving the intercell interference plus thermal noise process $N(n)$ defined in Section 2.3 with the equalizer taps and passing the result through the despreading stage. This expression for N_i is written as

$$\begin{aligned} N_i &= \sum_{v=0}^{N_T-1} e_i(v) \frac{1}{\sqrt{R}} \sum_{r=0}^{R-1} s_{0,i}^*(r) N(iR - v + r) \\ &= \sum_{v=0}^{N_T-1} e_i(v) N_{v,i} \end{aligned} \tag{3.15}$$

where $N_{v,i}$ is a zero-mean, complex Gaussian random variable with variance σ_N^2. The term $N_{v,i}$ represents the intercell interference plus thermal noise at the output of a despreading stage that despreads $N(n)$ with an offset of v during symbol interval i. Since the equalizer taps are separated by one chip, the $N_{v,i}$ terms are independent and the variance of N_i can be calculated by the mobile according to

$$\left\langle |N_i|^2 \right\rangle = \sigma_N^2 \sum_{v=0}^{N_T-1} |e_i(v)|^2. \tag{3.16}$$

For the chip-level LMMSE receiver, I_i is equal to $I(n)$ first convolved with both the small scale channel impulse response and the equalizer and then processed by the despreading stage. The result is written as

$$
\begin{aligned}
I_i &= \sum_{l=0}^{L-1} c_{i,0}(l) \sum_{v=0}^{N_T-1} e_i^*(v) \tfrac{1}{\sqrt{R}} \sum_{r=0}^{R-1} s_{i,0}^*(r) I(iR - l - v + N_T/2 + r) \\
&= \sum_{l=0}^{L-1} c_{i,0}(l) \sum_{v=0}^{N_T-1} e_i^*(v) I_{l+v-N_T/2,i} \left[1 - \delta(l - (v - N_T/2))\right]
\end{aligned}
\tag{3.17}
$$

where $I_{l+v-N_T/2,i}$ is a zero mean Gaussian random variable with variance σ_I^2 that represents $I(n)$ after despreading with an offset of $l + v - N_T/2$ during symbol interval i. The $[1 - \delta(\cdot)]$ term accounts for the Walsh code cancellation of any intracell interference components that are synchronous with the desired signal. The chip-level LMMSE receiver attempts to equalize multipath dispersion such that all intracell interference is synchronous with the desired signal and is canceled by the $[1 - \delta(\cdot)]$ term. Using (3.17), the variance of I_i can be estimated by the mobile according to

$$
\begin{aligned}
\langle |I_i|^2 \rangle &= \left\langle \left(\sum_{l=0}^{L-1} c_{i,0}(l) \sum_{v=0}^{N_T-1} e_i^*(v) I_{l+v-N_T/2,i} \left[1 - \delta(l - (v - N_T/2))\right] \right) \right. \\
&\quad \left. \left(\sum_{q=0}^{L-1} c_{i,0}(q) \sum_{w=0}^{N_T-1} e_i^*(w) I_{q+w-N_T/2,i} \left[1 - \delta(q - (w - N_T/2))\right] \right)^* \right\rangle \\
&= \sum_{l=0}^{L-1} \sum_{v=0}^{N_T-1} \sum_{q=0}^{L-1} \sum_{w=0}^{N_T-1} c_{i,0}(l) e_i^*(v) \left[c_{i,0}(q) e_i^*(w)\right]^* \\
&\quad \cdot \left\langle I_{l+v-N_T/2,i} I_{q+w-N_T/2,i}^* \right\rangle \\
&\quad \{1 - \delta\left[l - (v - N_T/2)\right]\} \{1 - \delta\left[q - (w - N_T/2)\right]\} \\
&= \sigma_I^2 \sum_{l=0}^{L-1} \sum_{v=0}^{N_T-1} \sum_{q=0}^{L-1} \sum_{w=0}^{N_T-1} c_{i,0}(l) e_i^*(v) \left[c_{i,0}(q) e_i^*(w)\right]^* \\
&\quad \cdot \delta\left\{\left[l - (v - N_T/2)\right] - \left[q - (w - N_T/2)\right]\right\} \\
&\quad \{1 - \delta\left[l - (v - N_T/2)\right]\} \{1 - \delta\left[q - (w - N_T/2)\right]\}
\end{aligned}
\tag{3.18}
$$

where the equalizer tap weights are known to the receiver and the channel terms are estimated using the forward link pilot signal. The technique described in Section 3.2.4 for estimating σ_I^2 and σ_N^2 can also be used for improved estimation for the chip-level LMMSE equalizer. As was the case for the chip-level LMMSE equalizer version of the standard estimator, the ratio $\zeta(i)/\sigma^2(i)$ is non-constant and the amplitude and variance values must be estimated for the metric calculations of all channel decoder algorithms.

3.2.4 Estimating Mobile Receiver Input Interference Levels

Derivation of Estimator

This section derives an estimator for the variances of the intracell interference and intercell interference plus thermal noise processes at the input to the mobile. These values correspond to the variances σ_I^2 and σ_N^2 of the interference processes illustrated in Fig. 3.1 and are required by the improved estimation techniques described in Sections 3.2.1 through 3.2.3. The estimator presented in this section will calculate σ_I^2 and σ_N^2 using the second order statistics of the aggregate signal received by the mobile, $r(n)$.

Based on Fig. 3.1, the signal $r(n)$ can be written as

$$r(n) = c(n,l) \star I(n) + N(n) \tag{3.19}$$

where $\star$ indicates convolution. The autocorrelation function of $r(n)$ is written as $\phi_v(n) = \langle r(n)r^*(n-v) \rangle$.

It is assumed that the random processes $I(n)$ and $N(n)$ are white such that the samples of $I(n)$ and $N(n)$ are independent for different values of N. This corresponds to a flat, stationary power spectral density. However, convolution with $c(n,l)$ colours $I(n)$. Therefore, $\phi_v(n)$ will be a function of $c(n,l)$, σ_I^2 and σ_N^2 for $v = 0$ but will only be a function of $c(n,l)$ and σ_I^2 for $v \neq 0$. This observation can be used to determine σ_I^2 and σ_N^2 from samples of $r(n)$.

Most CDMA mobiles determine $c(n,l)$ using the forward link pilot signal. If $c(n,l)$ is known, the channel terms in the convolution $c(n,l) \star I(n)$ can be treated as constants rather than random variables when calculating $\phi_v(n)$. The autocorrelation function of $r(n)$ therefore can be written as

$$\phi_v(n) = \begin{cases} \sum_{i=0}^{L-1}\sum_{m=0}^{L-1} c(n,i)c^*(n-v,m)\left\langle I(n-i)I^*(n-m-v)\right\rangle \\ +\left\langle N(n)N^*(n-v)\right\rangle & ,v \leq L \\ 0 & ,\text{otherwise.} \end{cases} \tag{3.20}$$

Since the spreading code chip rate is typically much higher than the maximum Doppler shift of the channel, $c(n,l) \simeq c(n-v,l)$ for $v \leq L$. Hence, the expression in (3.20) can be simplified to

$$\phi_v(n) = \sigma_I^2 \sum_{i=0}^{L-1}\sum_{m=0}^{L-1} c(n,i)c^*(n,m)\delta\left[(i-m)-v\right] + \sigma_N^2\delta(v). \tag{3.21}$$

It is noted that (3.21) is a linear function of the variances that are to be estimated. The autocorrelation values for $0 \leq v \leq L-1$ can be written as a series of linear equations such that

$$\boldsymbol{\phi} = \boldsymbol{H\Theta} \tag{3.22}$$

where $\boldsymbol{\phi} = [\phi_0(n), \ldots \phi_{L-1}(n)]^T$, $\boldsymbol{\Theta} = [\sigma_N^2 \sigma_I^2]^T$ and

$$\boldsymbol{H} = \begin{bmatrix} 1 & \sum_{i=0}^{L-1}\sum_{m=0}^{L-1} c(n,i)c^*(n,m)\delta(i-m) \\ 0 & \sum_{i=0}^{L-1}\sum_{m=0}^{L-1} c(n,i)c^*(n,m)\delta\left[(i-m)-1\right] \\ \vdots & \vdots \\ 0 & \sum_{i=0}^{L-1}\sum_{m=0}^{L-1} c(n,i)c^*(n,m) \cdot\delta\left[(i-m)-(L-1)\right] \end{bmatrix}. \tag{3.23}$$

The elements of $\boldsymbol{\phi}$ can be determined from the received signal using a sliding window time average, where

$$\phi_v(n) \simeq \frac{1}{N_\phi} \sum_{k=0}^{N_\phi-1} r(n+k)r^*(n+k-v). \tag{3.24}$$

and the window used to collect the N_ϕ samples is short enough to assume the channel remains approximately constant during the summation.

It is clear that linear estimation techniques can be applied to (3.22) in order to estimate σ_I^2 and σ_N^2. The Best Linear Unbiased Estimator (BLUE) finds the

minimum variance unbiased estimator when the observation vector is a linear function of the quantities to be estimated [33]. However, the BLUE requires the covariance matrix of the additive random process corrupting $\boldsymbol{\phi}$. This matrix is not trivial to determine so the Least-Squares Estimator (LSE) is applied as a simplification [33]. The LSE determines σ_I^2 and σ_N^2 according to

$$[\hat{\sigma_N^2}\hat{\sigma_I^2}]^T = (\boldsymbol{H}^T\boldsymbol{H})^{-1}\boldsymbol{H}\boldsymbol{\phi}. \tag{3.25}$$

The total number of samples processed by the estimator, N_W, is called the observation window. If the observation window is shorter than the channel coherence time, the number of samples used in the time domain correlation in (3.24), N_ϕ, is equal to N_W. If an observation window longer than the coherence time is required, N_W is divided up into several consecutive segments of length N_ϕ that are equal to the channel coherence time. The samples in each segment are processed according to (3.24) and used to generate estimates of σ_I^2 and σ_N^2 as indicated in (3.25). The variance estimates produced using each segment are then averaged together. Since the estimator is linear, averaging the variance estimates produced from each segment yields the same performance as processing all N_W samples directly in the estimator.

The extra error caused by using the sub-optimal LSE can be quantified by comparing the estimator performance to the Cramer-Rao Lower Bound (CRLB) [33]. The CRLB provides a lower bound that represents the variance of the error that can be expected from the minimum variance unbiased estimator of a particular quantity. Kay provides a CRLB expression for the general Gaussian case where the PDF of the received signal is

$$\boldsymbol{r} \sim \mathcal{N}(\boldsymbol{\mu}(\boldsymbol{\Theta}), \boldsymbol{C}(\boldsymbol{\Theta})) \tag{3.26}$$

where $\boldsymbol{r} = [r(0), \ldots r(N_W - 1)]$ is a vector containing samples of the signal

received by the mobile, $\boldsymbol{\mu}(\boldsymbol{\Theta}) \in \mathcal{R}^{N_W}$ is the mean of the signal vector and $\boldsymbol{C}(\boldsymbol{\Theta}) \in \mathcal{R}^{N_W \times N_W}$ is the covariance matrix of the signal vector. Since the interference, noise and desired signal processes received by the mobile are zero mean, $\boldsymbol{\mu}(\boldsymbol{\Theta})$ is zero. The covariance matrix of $\boldsymbol{r}$, $\boldsymbol{C}(\boldsymbol{\Theta})$, is a symmetric Toeplitz matrix whose elements are a function of the intracell and intercell interference processes and can be determined using (3.21).

The CRLB for a particular quantity $\boldsymbol{\Theta}$ is given by $\left\langle \widehat{\Theta}_i^2 \right\rangle \geq \left[\boldsymbol{I}^{-1}(\boldsymbol{\Theta})\right]_{ii}$, where $\boldsymbol{I}(\boldsymbol{\Theta})$ is the Fisher information matrix. For this estimator, $\Theta_0 = \sigma_I^2$ and $\Theta_1 = \sigma_N^2$. According to Kay's expression, the elements of the 2×2 Fisher information matrix are given by

$$[\boldsymbol{I}(\boldsymbol{\Theta})]_{ij} = \frac{1}{2}\mathrm{tr}\left[\boldsymbol{C}^{-1}(\boldsymbol{\Theta})\frac{\delta \boldsymbol{C}(\boldsymbol{\Theta})}{\delta \Theta_i}\boldsymbol{C}^{-1}(\boldsymbol{\Theta})\frac{\delta \boldsymbol{C}(\boldsymbol{\Theta})}{\delta \Theta_j}\right]. \tag{3.27}$$

It is difficult to find an analytical expression for the Fisher information matrix given by (3.27) when the elements of the autocorrelation matrix $\boldsymbol{C}(\boldsymbol{\Theta})$ are given by (3.21). However, given a particular set of channel impulse response values, it is possible to calculate the numerical values of the elements of $\boldsymbol{C}(\boldsymbol{\Theta})$ using (3.21). The Fisher information matrix can then determined according to (3.27) and inverted numerically to find the CRLB of σ_I^2 and σ_N^2 specific to those channel impulse response values.

The limitation of this numerical approach to finding the CRLB is the number of computations required to invert the matrix $\boldsymbol{C}(\boldsymbol{\Theta})$ in (3.27). The LSE estimator for σ_I^2 and σ_N^2 will typically process received signal vectors where the number of samples in the observation window, N_W, is quite large. Since the autocorrelation matrix $\boldsymbol{C}(\boldsymbol{\Theta})$ that must be inverted in (3.27) is $N_W \times N_W$, it may not be practical to use this technique for some of the larger values of N_W.

Evaluation of Estimator

Simulation is used to evaluate the accuracy of this LS estimator of σ_N^2 and σ_I^2. The simulation generates samples of the received signal, $r(n)$, at one sample per chip according to (3.19). These signal samples are then processed using the time domain autocorrelation function in (3.24) in order to find the elements of the vector $\boldsymbol{\phi}$. The vector $\boldsymbol{\phi}$ is then used in (3.25) to determine estimates of σ_I^2 and σ_N^2. A time invariant multipath channel is assumed so that the total number of samples processed by the estimator N_W is equal to N_ϕ in (3.24). The average received relative powers of the resolvable paths of this multipath channel are -2 dB, -6 dB and -10 dB.

One simulation run uses 10,000 trials to determine the mean and standard deviation of the estimates produced by (3.25). Several simulation runs are performed for values of N_W equal to 500, 1536, 3072, 24576 and 245760 chips. For IS-95 and IS-2000 CDMA signals, the chip rate is 1.2288 Mchip/s so that 1536 samples corresponds to one 1.25 ms power control group, 3072 samples to two power control groups, 24576 samples to one 20 ms frame and 245760 samples to ten 20 ms frames. The error in the estimates produced with these 10,000 trials is expressed as normalized deviation from the mean, $(\mu_E + \sigma_E)/\mu_E$, where μ_E is the mean of the estimates and σ_E is the standard deviation of the estimates. This normalized deviation is expressed in dB and plotted versus N_W.

To examine estimator sensitivity to different levels of intracell interference and intercell interference plus thermal noise, simulations are performed for $\sigma_I^2 = 5/\sigma_N^2 = 5$, $\sigma_I^2 = 10/\sigma_N^2 = 1$ and $\sigma_I^2 = 1/\sigma_N^2 = 10$. The results are shown in Figs. 3.2, 3.3 and 3.4. Note that the CRLB is only shown for N_W up to 3072 since the matrix inversions required to numerically determine the bound become impractical for larger values of N_W.

For equal levels of σ_I^2 and σ_N^2, the LSE estimation is quite close to the CRLB

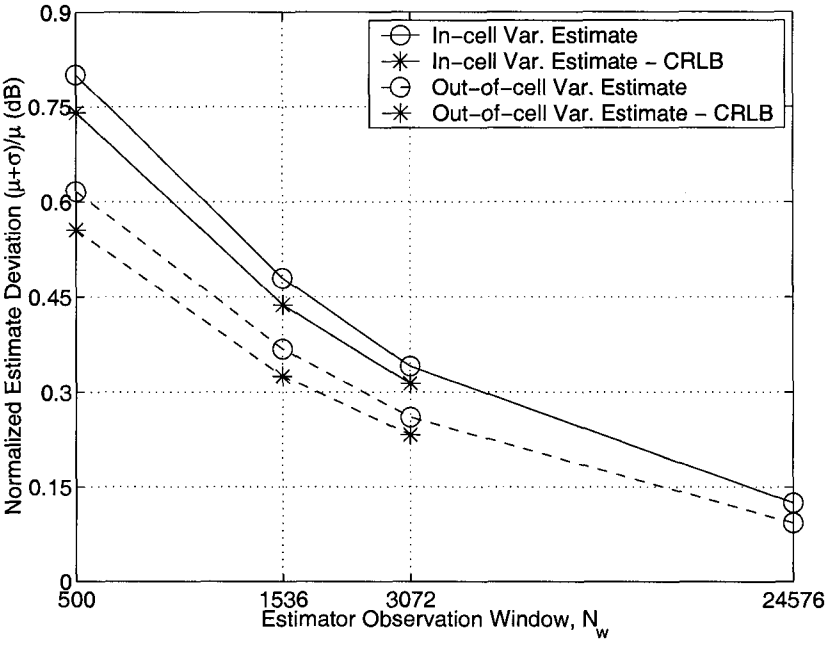

Figure 3.2: Estimator accuracy, $\sigma_I^2 = 5$ & $\sigma_I^2 = 5$.

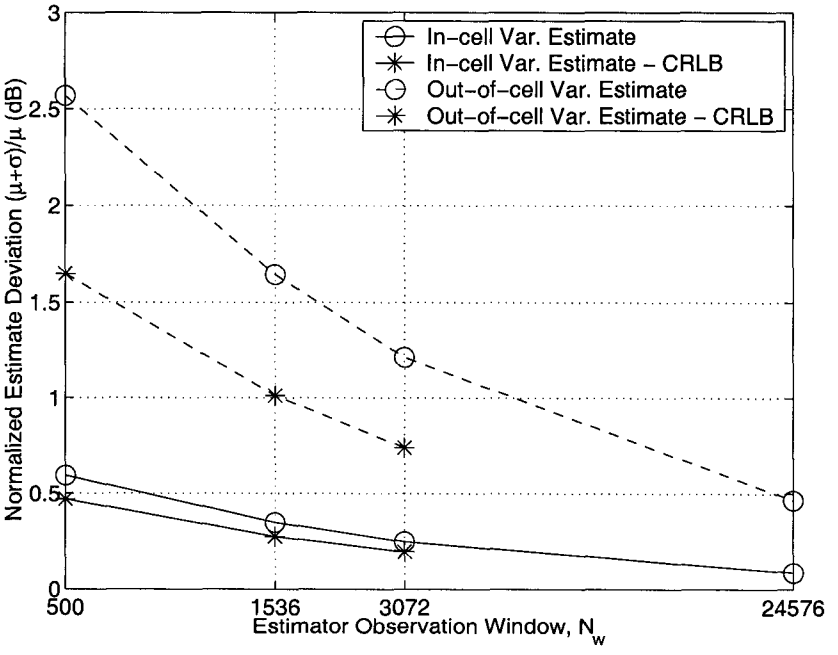

Figure 3.3: Estimator accuracy, $\sigma_I^2 = 10$ & $\sigma_N^2 = 1$.

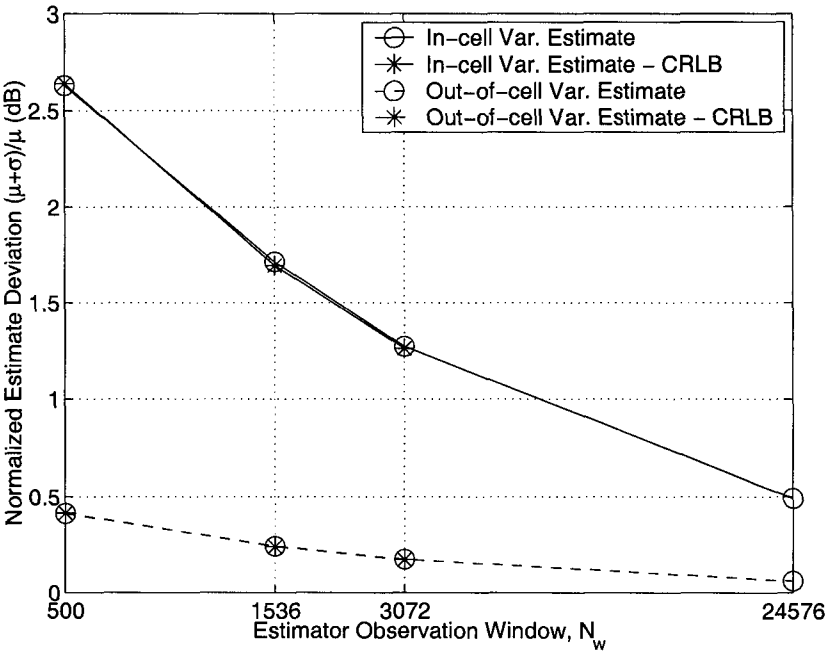

Figure 3.4: Estimator accuracy, $\sigma_I^2 = 1$ & $\sigma_N^2 = 10$.

with very good accuracy possible if the observation window of the estimator is at least one 20 ms frame. If one source of interference dominates, Figs. 3.3 and 3.4 show that the error increases for estimates of the weaker interference source. The LSE estimator diverges most significantly from the CRLB for high levels of σ_I^2. For high levels of σ_N^2, the estimator actually achieves the CRLB.

The simulations also show that the performance of the LSE gets closer to the CRLB for increasing values of N_W. In a practical system, the length of N_W is limited by how long the variance values σ_I^2 and σ_N^2 remain unchanged. Since these variance values will remain constant for at least a few frames, large values of N_W are possible and LSE performance will be close to the optimal CRLB. This means that the incremental benefit of finding a better estimator for σ_I^2 and σ_N^2 is small.

3.3 Online Channel State Estimation

This section shows how the online SNR estimation technique presented by Summers and Wilson can be adapted for use on the CDMA forward link [69]. The technique presented below can be used without modification on a conventional CDMA forward link and on links incorporating STTD transmission and chip-level LMMSE mobile receivers.

The online estimation technique assumes that the signal at the channel decoder input during symbol interval i can be represented as

$$r_i = \zeta b_i + n_i \tag{3.28}$$

where b_i is the transmitted channel encoded symbol, the signal envelope is denoted ζ and the additive noise term n_i is zero mean Gaussian. Both the signal envelope and the variance of the noise, σ^2 are unknown but are assumed to remain constant.

The online SNR estimation scheme produces an estimate of the ratio $\gamma = \zeta^2/\sigma^2$. In order to estimate γ, Summers and Wilson show that the second order statistics of r_i satisfy the following relationship

$$\frac{\langle r_i^2 \rangle}{\langle |r_i| \rangle^2} = \frac{1+\gamma}{\left[\sqrt{\frac{2}{\pi}} e^{-\gamma/2} + \sqrt{\gamma}\,\mathrm{erf}\left(\sqrt{\frac{\gamma}{2}}\right)\right]^2}. \tag{3.29}$$

The mean values $\langle r_i^2 \rangle$ and $\langle |r_i| \rangle$ are calculated at the input to the channel decoder using time averaging. The estimated SNR factor γ is then determined using the inverse function for (3.29) implemented using a lookup table.

This technique provides the ratio of desired signal envelope power to interference plus noise variance. However, the conventional channel decoder metrics presented in Chapter 1 require signal envelope values, not envelope power. As a result, when this channel state estimation technique is used for the wireless channel, it must be implemented using sub-optimal channel decoder metric calcu-

lations [63]. The Viterbi decoder metric in (1.2) is replaced by (3.30), the SOVA metric in (1.3) with (3.31) and the MAP metric in (1.5) with (3.32).

$$\mu = \sum_{i=0}^{N_s-1} \gamma x_i y_i \tag{3.30}$$

$$\mu = \sum_{k=0}^{N_d-1} \left[\log\left(p_{z_k}(k)\right) + \sum_{i=N_R k}^{N_R(k+1)-1} \gamma x_i y_i \right] \tag{3.31}$$

$$\gamma_k^{\theta}(l,l') = \begin{cases} p_{\theta}(k) \exp\left(-\sum_{j=kN_R}^{(k+1)N_R-1} \gamma (y_j - x_j)^2/2\right), & (l,l') \in B_k^{\theta} \\ 0, & \text{otherwise} \end{cases} \tag{3.32}$$

The complexity of online channel state estimation can be considered similar to standard estimation. The calculation of the time domain averages $\langle r_i^2 \rangle$ and $\langle |r_i| \rangle$ is similar to the averaging required to determine the input interference plus noise variance σ_Z^2. While online estimation does not require an $O(F)$ calculation to determine a final channel state estimate, the implementation of the lookup table will consume memory resources in the mobile and require a similar level of computational effort to implement.

3.4 Forward Link Performance

3.4.1 Single Antenna Transmission, Mobile Rake Receiver

CDMA forward link simulations are used to quantify the performance difference between mobiles using online, standard and improved estimation. This section considers single antenna transmission where the mobile uses a standard Rake receiver. The simulation results show bit error rate (BER) plotted versus signal to noise ratio E_b/σ_N^2, where E_b is energy per bit and σ_N^2 is defined in Chapter 2 as the variance of the intercell interference plus thermal noise at the receiver input. The simulation results in this section are generated using the symbol-level CDMA forward link model described in Section 2.3.1.

A spreading factor of 16 is assumed. The simulation generates a constant level of intracell interference for all values of E_b/σ_N^2 that is equivalent to a fully loaded link carrying 16 equal power traffic transmissions. Results are generated assuming a data rate of 38.4 kbps, 40 ms frames and a 1.9 GHz carrier frequency. Mobile velocities of 5 km/h and 100 km/h are considered and the radio channel has three resolvable Rayleigh fading paths with average received powers of -2 dB, -6 dB and -10 dB.

Convolutional code results are generated with a rate 1/2 (23,35) constraint length 5 code and soft decision Viterbi decoding in the mobile. The turbo code results use a punctured rate 1/2 code with rate 1/2 (1,17/15) RSC component encoders [79]. A random interleaver is used in the turbo encoder and the turbo decoder uses up to 8 iterations. The LogMAP and SOVA algorithms are both considered for turbo decoding.

Comparing Channel State Estimation Techniques with Known Input Parameters

The first scenario considered in this section compares standard and improved estimation under the assumption that the mobile has perfect knowledge of the channel impulse response, $c(n,l)$, and the interference variances σ_I^2, σ_N^2 and σ_Z^2. The purpose of these simulations is to remove any parameter estimation error and to compare the performance difference between standard and improved estimation simply due to the different assumptions the techniques make about CDMA forward link interference. The results are shown in Figs. 3.5 and 3.6. Section 3.1.1 points out that the Viterbi and SOVA metric calculations for standard estimation are equivalent to simply using correlation metric calculation without any channel state information at all. This is indicated in the simulation plots.

Figs. 3.5 and 3.6 show that the more accurate channel state estimates produced by improved estimation result in better performance. Separately considering the

contribution of intracell interference and intercell interference plus thermal noise allows the calculation of $\sigma^2(i)$ to account for both the non-stationary nature of the intracell interference and its partial cancellation due to the Walsh spreading sequences. The result is a more accurate estimate of $\sigma^2(i)$ that significantly improves channel decoder performance, particularly in the case of the LogMAP decoder.

Generally, turbo codes with a LogMAP decoder tend to outperform turbo codes with a SOVA decoder [79]. However, Figs. 3.5 and 3.6 indicate that when standard estimation is used in the mobile, turbo codes with LogMAP decoding perform worse than turbo codes with SOVA decoding and even convolutional codes. Valenti and Woerner have compared the sensitivity of the LogMAP and SOVA turbo decoders to channel state estimation error on the flat Rayleigh fading channel with AWGN [76]. The authors show that the LogMAP decoder is more sensitive to channel state estimation errors than the SOVA decoder. The degradation of the LogMAP decoder seen in Figs. 3.5 and 3.6 is worse than demonstrated in [76] because the error standard estimation makes in estimating the non-stationary variance $\sigma^2(i)$ is worse that the channel tap weight estimation errors considered in [76]. Standard estimation is a valuable technique due to its simple structure and the acceptable performance results it can achieve with the Viterbi and SOVA decoders. However, it should clearly not be used with the LogMAP decoder.

Fig. 3.5 also shows that the performance difference between standard and improved estimation is largest at high values of E_b/σ_N^2, where intracell interference dominates. Under these conditions, separately accounting for the intracell interference process by using improved estimation provides the maximum benefit. At low E_b/σ_N^2, the additive Gaussian intercell interference plus thermal noise process dominates and the estimates of $\sigma^2(i)$ returned by standard and improved esti-

mation are very similar. This is because standard estimation assumes that all interference and noise can be represented using an AWGN source. The result is a reduction in the performance gap between the two techniques at low values of E_b/σ_N^2.

Comparing Figs. 3.5 and 3.6 shows that the gap between standard and improved estimation shrinks for the Viterbi and SOVA decoders as velocity is reduced. Section 1.3 notes that any parameter in the Viterbi or SOVA decoder metric calculations that remains constant over the encoded frame duration has no effect on decoder performance. At low velocities, the radio channel is approximately constant during the frame duration. Since fluctuations in intracell interference power are caused by changes in the radio channel, the $\langle |I_i|^2 \rangle$ term used by improved estimation to calculate $\sigma^2(i)$ also becomes more stationary at lower mobile velocities. Since standard and improved estimation are both producing estimates of $\sigma^2(i)$ that remain approximately constant at low mobile speeds, both techniques result in approximately the same performance with the Viterbi and SOVA decoders.

In contrast, Figs. 3.5 and 3.6 show that the performance gap between standard and improved estimation is not velocity dependent for the LogMAP decoder. The trellis path metrics for the LogMAP decoder require accurate estimates of $\zeta(i)$ and $\sigma^2(i)$, regardless of whether or not these quantities are stationary. Even though both standard and improved estimation produce stationary estimates of $\sigma^2(i)$ at low velocities, improved estimation is always more accurate since it accounts for the partial Walsh sequence cancellation of intracell interference and standard estimation does not. The result is better LogMAP decoder performance even at low mobile speeds.

Comparing Channel State Estimation Techniques with Estimated Input Parameters

The second simulation scenario in this section compares forward link performance when standard estimation, improved estimation and online estimation are used in the mobile and all information required by these channel state estimation techniques must be estimated. It is assumed that $c(n,l)$ is estimated from the base station forward channel pilot signal. The forward link pilot signal is allocated 16% of the maximum base station transmit power and the mobile averages the pilot for 1 ms before producing a channel impulse response estimate. The variance σ_Z^2 required by standard estimation is calculated by performing a 40 ms sliding window time average on the energy of the received signal at the mobile receiver input. The variances σ_I^2 and σ_N^2 required by improved estimation are determined using the LSE described in Section 3.2.4, where the estimator observation window is 40 ms. At 1.2288 Mcps, this corresponds to 49152 samples. The CDMA forward link results for convolutional coding are shown in Fig. 3.7, turbo coding with SOVA decoding in Fig. 3.8 and turbo coding with LogMAP decoding in Fig. 3.9.

To help interpret the results in Figs. 3.7 through 3.9, the accuracy of the different channel state estimation schemes are shown in Figs. 3.10 and 3.11. These plots show the mean (bias) and standard deviation of the channel state estimation error $\hat{\rho} - \rho$, where ρ is the true value of the ratio $\zeta(i)/\sigma^2(i)$ at the mobile channel decoder input and $\hat{\rho}$ is the ratio calculated using the channel state estimation technique.

The channel decoder metric discussion in Chapter 1 points out that any factor in the Viterbi or SOVA metric calculation that remains constant over the frame duration will have no effect on the performance of these decoders. This also means that any channel state estimation error that remains constant over the frame duration will not affect Viterbi and SOVA performance. Therefore, when using

the channel state accuracy plots in Figs. 3.10 and 3.11 to interpret the Viterbi and SOVA performance results in Figs. 3.7 and 3.8, only the error standard deviation results need to be considered. The value of the bias plots have no effect on Viterbi or SOVA decoder performance.

The channel state estimation plots show online estimation with the largest channel state estimation error standard deviation, followed by standard estimation and then improved estimation. This supports the Viterbi and SOVA simulation results in Figs. 3.7 and 3.8 where online estimation results in the worst performance and improved estimation in the best. Comparing Figs. 3.10 and 3.11 also shows that the error standard deviation of online, standard and improved estimation is reduced at lower velocity. The error standard deviation values produced by these techniques also becomes more similar at low mobile speeds. As a result, the forward link BER curves achieved with online, standard and improved estimation in Figs. 3.7 and 3.8 are closer together at 5 km/h than they are at 100 km/h.

The performance of the LogMAP decoder is influenced by both the bias and the standard deviation of channel state estimation error. Figs. 3.10 and 3.11 show improved estimation with almost no bias, online estimation with a large positive bias and standard estimation with a smaller negative bias. Previous research has shown that the LogMAP decoder performs better when the SNR values it uses for its trellis metric calculations are over-estimated rather than under-estimated [69]. As a result of its positive bias, online estimation performs better than standard estimation in Fig. 3.9 for a mobile velocity of 5 km/h. However, the larger online estimation error standard deviation at 100 km/h means that standard estimation performs better than online estimation at higher mobile speeds, despite the favorable bias of online estimation.

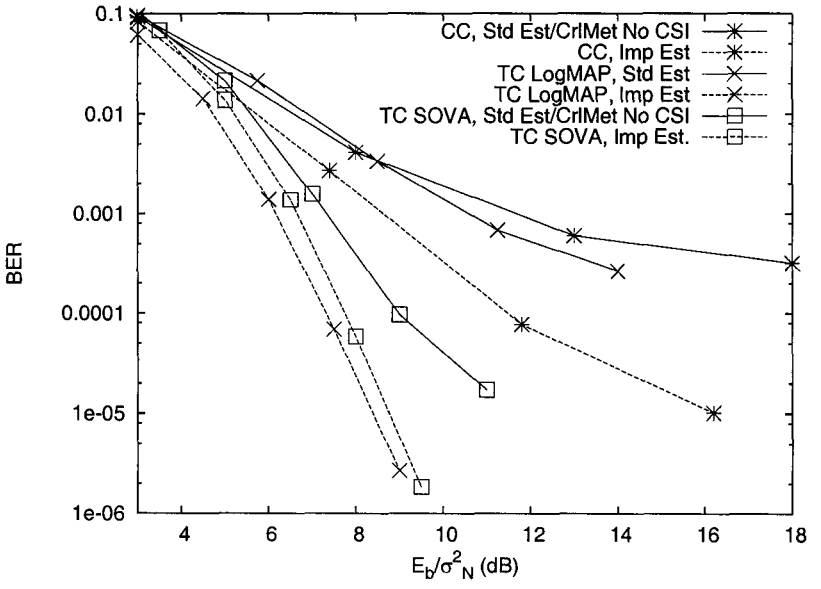

Figure 3.5: Ideal standard and improved estimation comparison, 100 km/h.

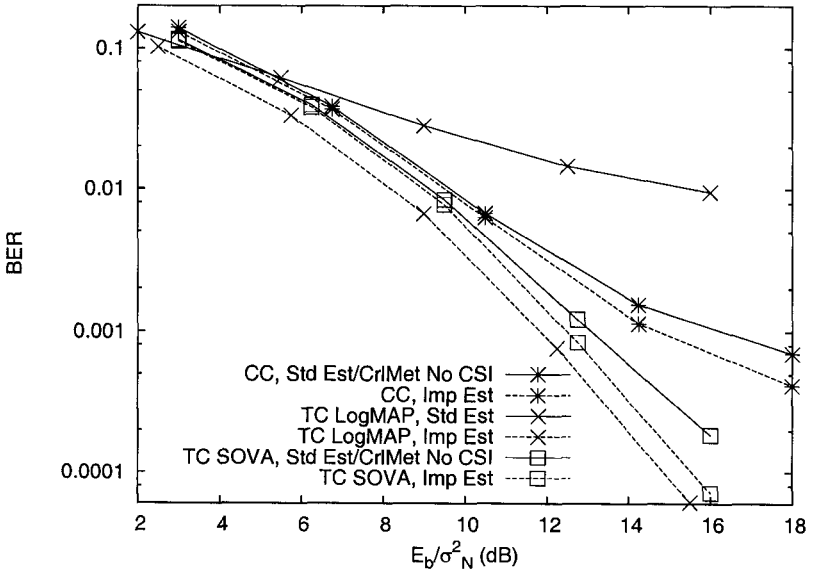

Figure 3.6: Ideal standard and improved estimation comparison, 5 km/h.

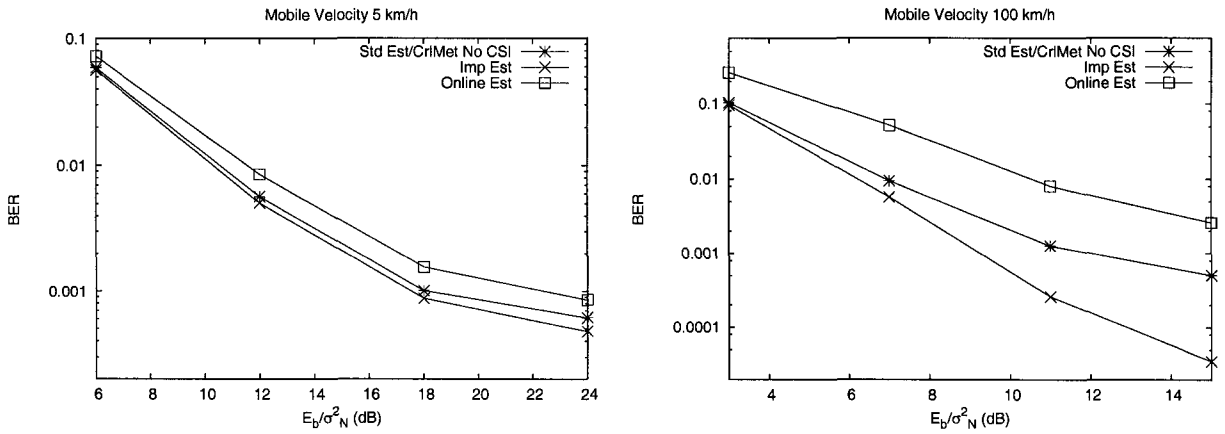

Figure 3.7: Channel state estimation performance, convolutional codes.

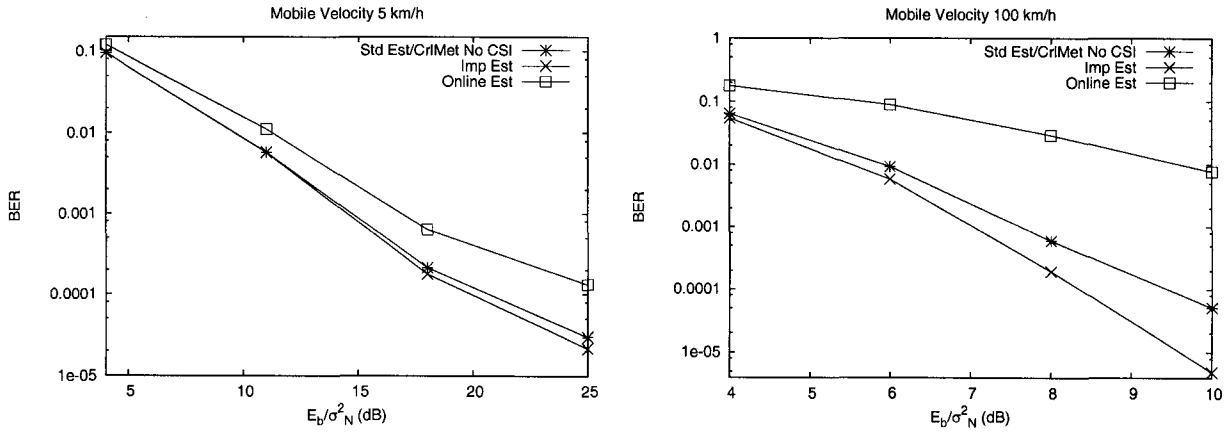

Figure 3.8: Channel state estimation performance, turbo codes with SOVA decoding.

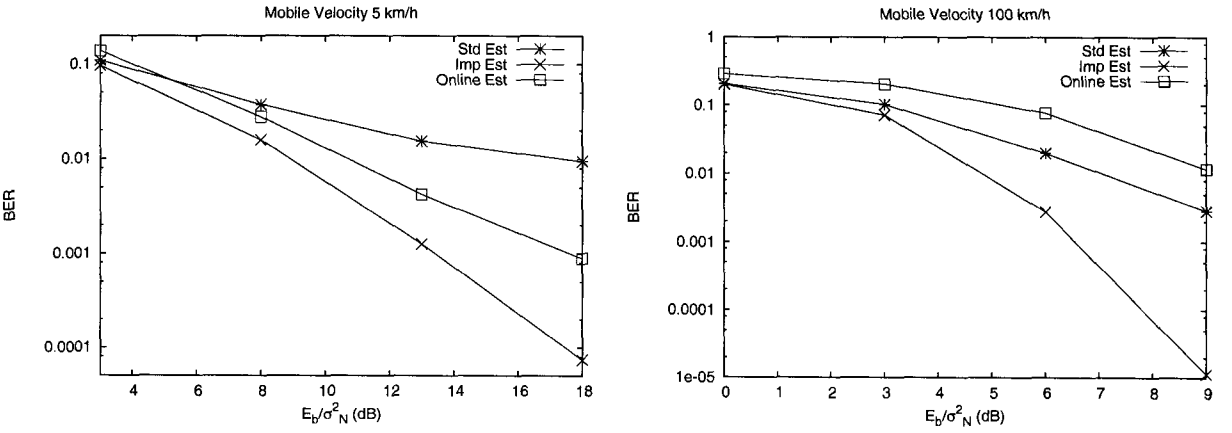

Figure 3.9: Channel state estimation performance, turbo codes with LogMAP decoding.

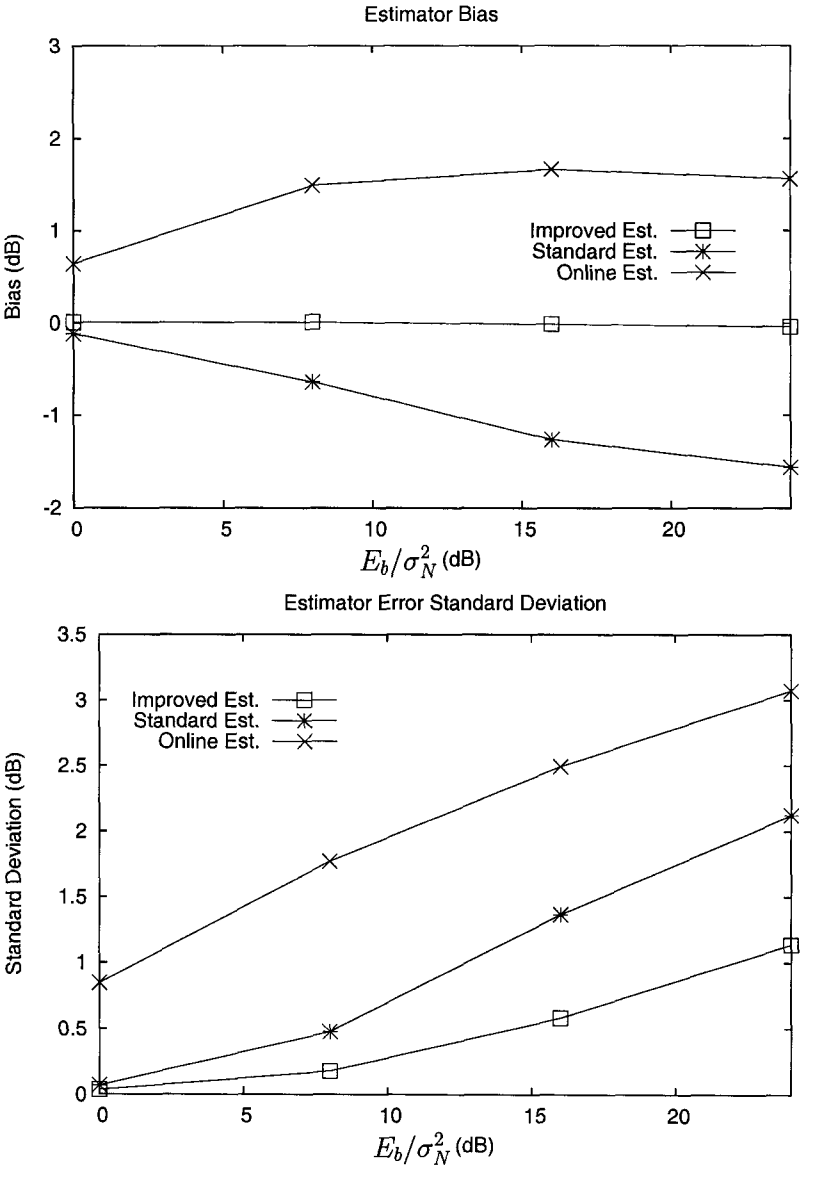

Figure 3.10: Estimator accuracy, 100 km/h.

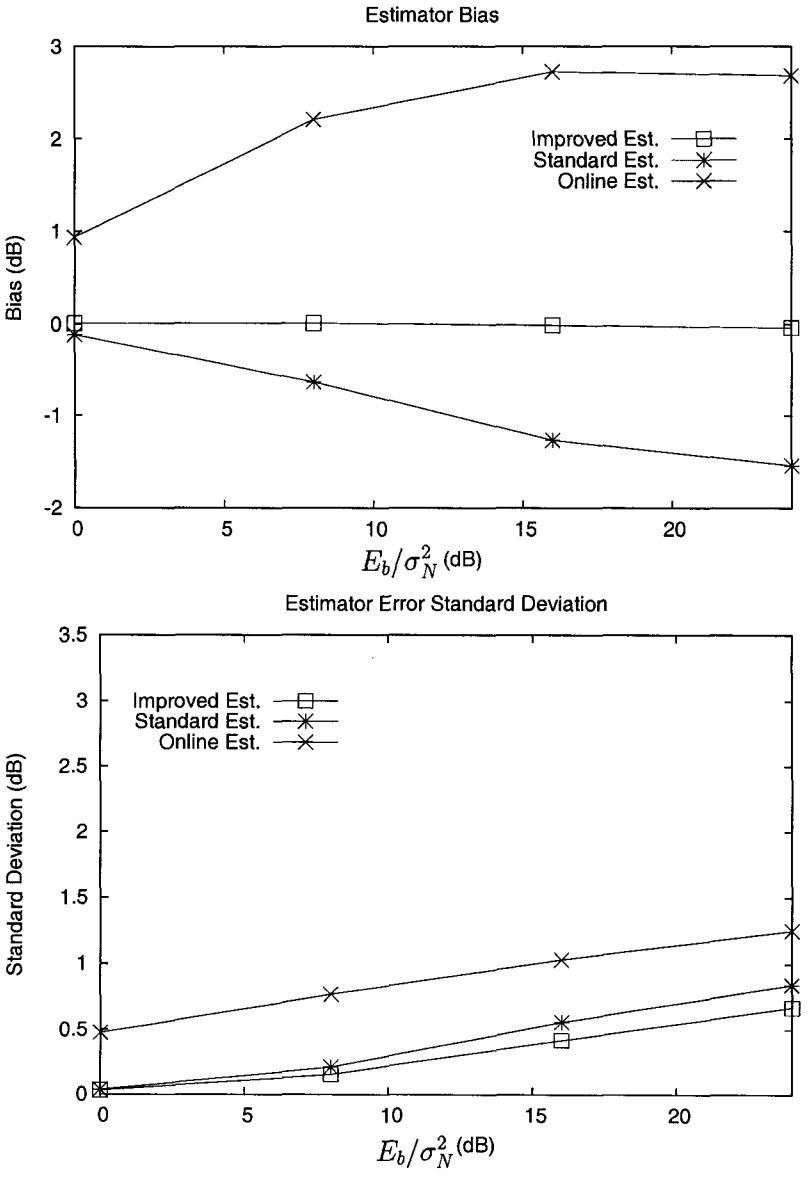

Figure 3.11: Estimator accuracy, 5 km/h.

3.4.2 STTD Transmission, Mobile Rake Receiver

This section evaluates CDMA forward link performance when online, standard and improved channel state estimation is used in the mobile and STTD is used at the base station. It is assumed the mobile uses the STTD Rake receiver structure discussed in Section 2.3.2. The simulation results are generated using the symbol-level model described in Section 2.3.2.

The simulation results show bit error rate (BER) plotted versus signal to noise ratio, E_b/σ_N^2. Intracell interference is equivalent to 16 equal power traffic transmissions on a link with a spreading factor of 16. The level of intracell interference remains constant for all values of E_b/σ_N^2. Data rate is 38.4 kbps, frames are 40 ms long and the radio channel is Rayleigh faded with average relative received path powers of -2 dB, -6 dB and -10 dB. Convolutional code results are generated with a rate 1/2 (23,35) constraint length 5 code and soft decision Viterbi decoding in the mobile. The turbo code results use a rate 1/2 code with punctured rate 1/2 (1,17/15) RSC component encoders [79]. The turbo encoder uses a random interleaver and the turbo decoders use up to 8 iterations. LogMAP and SOVA decoders are both used for the turbo code simulations.

The channel impulse response information used by the mobile Rake receiver is estimated from the forward channel pilot signal. As in Section 3.4.1, it is assumed the pilot transmit power is equivalent to 16% of the maximum base station transmit power and that the mobile averages the pilot for 1 ms before producing a channel impulse response estimate. The variance σ_Z^2 required by standard estimation is calculated by performing a 40 ms sliding window time average on the energy of the received signal at the mobile receiver input. The variances σ_I^2 and σ_N^2 required by improved estimation are determined using the LSE described in Section 3.2.4 with the estimator operating with a 40 ms observation window.

Convolutional code forward link performance at mobile speeds of 100 km/h

and 5 km/h is shown in Fig. 3.12. Forward link performance for turbo coding is shown in Figs. 3.13 and 3.14 for the SOVA and LogMAP decoders, respectively. Single antenna results from Section 3.4.1 are also included in the figures for comparison. Plots indicating the bias and error standard deviation of the channel state estimation techniques for mobile velocities of 100 km/h and 5 km/h are shown in Figs. 3.15 and 3.16, respectively.

Fig. 3.16 shows that the relative differences between the error standard deviation of online, standard and improved estimation are similar at 5 km/h in systems using single antenna and STTD transmission. As a result, the relative performance difference between these techniques at 5 km/h in the Viterbi and SOVA results in Figs. 3.12 and 3.13 is approximately the same for single antenna and STTD transmission.

At 100 km/h, the relative difference between the error standard deviation of standard and improved estimation increases slightly in an STTD system. This increase is most pronounced in Fig. 3.15 at higher values of E_b/σ_N^2. As a result, the relative performance difference between standard and improved estimation increases when the estimation techniques are used with the Viterbi and SOVA decoders in an STTD system. This increase is most visible for the higher values of E_b/σ_N^2 considered for the convolutional coding results in Fig. 3.12.

The error standard deviation of online estimation increases somewhat in an STTD system at the low values of E_b/N_o where an STTD system operates. As a result, the performance of online estimation relative to standard and improved estimation in an STTD system is degraded for the STTD results in Figs. 3.12 and 3.13. It should be noted that the BER performance of online estimation at 100 km/h in Figs. 3.12 and 3.13 is better for STTD than for single antenna transmission. However, this is due to the diversity gains of STTD, not because online estimation performs better in an STTD system.

The accuracy plots show that the negative bias of standard estimation is reduced in an STTD system. This is due to the nature of STTD intracell interference. The increased number of intracell interference terms in (3.13) means that Walsh sequence cancellation has a smaller effect on reducing the overall level of intracell interference at the STTD Rake output. The inaccuracy of standard estimation is due primarily to the fact that it neglects the Walsh sequence cancellation of intracell interference. As this cancellation becomes less significant, the bias of standard estimation improves. As a result, the performance of the LogMAP decoder when combined with standard estimation improves for the STTD results in Fig. 3.14. This improvement is most pronounced at 100 km/h.

In contrast, the bias of online estimation increases slightly in an STTD system, resulting in a degradation in performance. This degradation is more pronounced at 100 km/h where online estimation in an STTD system exhibits both a more unfavorable bias and a larger error standard deviation. Online estimation also has a more unfavorable bias in an STTD system at 5 km/h but the error standard deviation is much lower so the degradation in BER performance is not as significant.

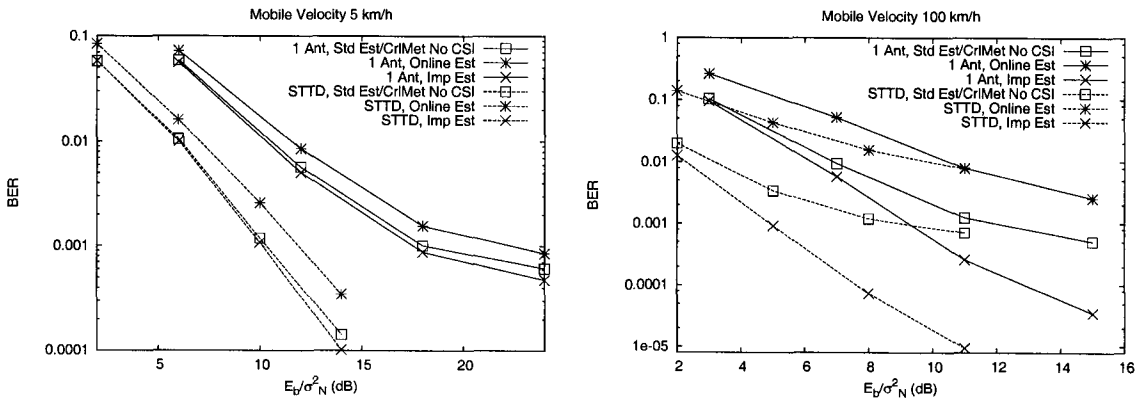

Figure 3.12: Forward link performance with convolutional codes.

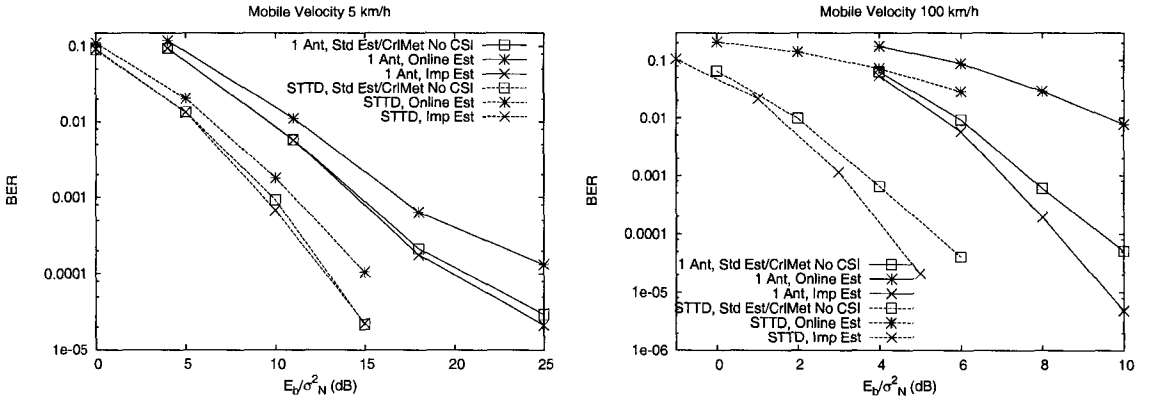

Figure 3.13: Forward link performance with turbo codes, SOVA decoder.

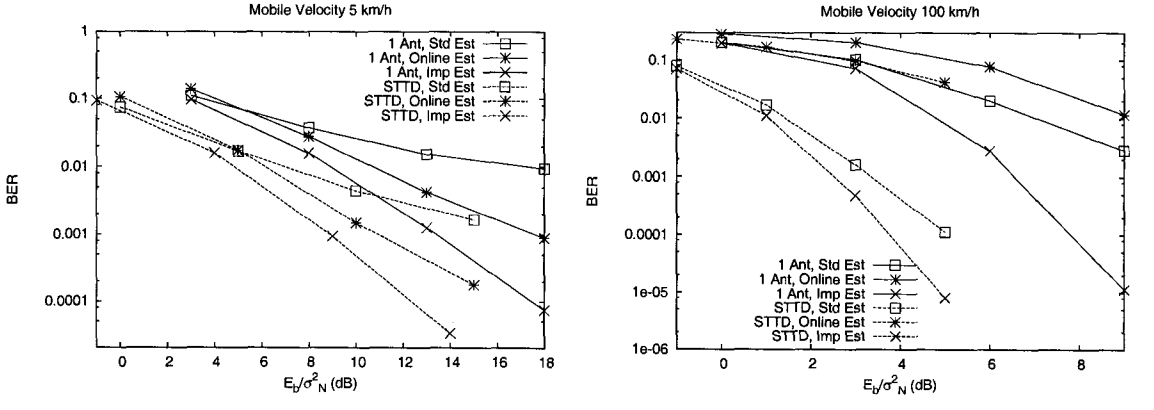

Figure 3.14: Forward link performance with turbo codes, LogMAP decoder.

3.4.3 Single Antenna Transmission, Chip-level LMMSE Equalizer

This section compares CDMA forward link performance for the Rake and chip-level LMMSE mobile receivers when the mobile employs Viterbi/SOVA correlation channel decoder metrics with no channel state information, online channel state estimation, standard channel state estimation and improved channel state estimation.

The simulations used in this section are conducted according to the chip-level CDMA forward link model described in Section 2.2. Received BER is generated for user 0 and plotted versus E_b/σ_N^2. The number of spreading sequence chips per bit, R, is 8 and intracell interference equivalent to 8 equal power forward link users is simulated. This level of intracell interference remains constant for all values of E_b/σ_N^2. Chip rate is equal to 1.2288 Mcps, data rate is 153.6 kbit/s and frame length is 20 ms.

Convolutional code results are generated with a rate 1/2 (23,35) constraint length 5 code and soft decision Viterbi decoding in the mobile. The turbo code results use a punctured rate 1/2 code with rate 1/2 (1,17/15) RSC component encoders [79]. A random interleaver is used in the turbo encoder and a maximum of 8 iterations is used in the turbo decoder. Both the LogMAP and SOVA channel decoder algorithms are considered.

A three path, Rayleigh faded channel model with average relative path powers equal to -2 dB, -6 dB and -10 dB is used. A mobile velocity of 100 km/h is assumed with a 1.9 GHz carrier frequency. The channel impulse response information used by the channel state estimation techniques, for calculating the Rake finger combining weights and for calculating the chip-level LMMSE equalizer taps is estimated using a forward link pilot signal. It is assumed the pilot transmit power is equivalent to 16% of the maximum base station transmit power and

that the mobile averages the pilot for 1 ms before producing a channel impulse response estimate. The variance σ_Z^2 required by standard estimation is calculated by performing a 40 ms sliding window time average on the received signal at the mobile receiver input. The variances σ_I^2 and σ_N^2 required by improved estimation are determined using the least squares estimator (LSE) described in Section 3.2.4 with the estimator operating with a 40 ms observation window.

The simulation uses a 3 finger Rake receiver and 5 tap chip-level LMMSE equalizer. A modest number of taps was chosen for the equalizer in order to reflect a receiver complexity that is practical to implement in a battery powered handset. The simulation calculates the equalizer taps directly from the LMMSE receiver equations rather than using a recursive algorithm.

Simulation results for convolutional coding and turbo coding with the SOVA decoding algorithm are shown in Figs. 3.17 and 3.18. These figures show performance curves for the Rake and chip-level LMMSE receivers when the mobile channel decoder uses online estimation, standard estimation and improved estimation. Note that standard estimation is shown in Figs. 3.17 and 3.18 to be equivalent to the correlation metric with no channel state information when the Rake is used in the mobile. However, as pointed out in Section 3.2.3, it is not obvious that standard estimation is equivalent to using the correlation metric with no channel state information when the chip-level LMMSE receiver is used in the mobile. As a result, they are shown as two separate performance curves in Figs. 3.17 and 3.18.

The estimation error in the channel impulse response information used to calculate the chip-level LMMSE equalizer taps degrades the performance of the equalizer. It is difficult to quantify the effect of equalizer degradation due to channel estimation error when calculating the SNR at the output of the equalizer. Since the actual SNR at the output of the equalizer used in these simulations

cannot be determined, no channel state estimation accuracy plots are shown in this section. However, the knowledge gained in Sections 3.4.1 and 3.4.2 can be used to interpret the results in Figs. 3.17 through 3.19.

The Viterbi and SOVA decoder results in Figs. 3.17 and 3.18 show that while improved estimation performs considerably better than standard estimation for the Rake receiver, the performance of the two techniques is very close when they are used with the chip-level LMMSE receiver. The primary difference between standard and improved estimation is that standard estimation does not accurately account for intracell interference. Since the chip-level LMMSE receiver removes a significant portion of the intracell interference, it is not surprising that standard and improved estimation should perform approximately the same in Figs. 3.17 and 3.18.

The chip-level LMMSE results in Figs. 3.17 and 3.18 also show that using the correlation metric calculation without any channel state information performs slightly better than standard estimation and almost as well as improved estimation. Sections 3.1.3 and 3.2.3 suggest that the estimated ratio $\zeta(i)/\sigma^2(i)$ used in the Viterbi and SOVA metric calculations will not be a constant when standard and improved channel state estimation is used with the chip-level LMMSE receiver. This accounts for the reason why CDMA forward link performance in Figs. 3.17 and 3.18 for standard and improved estimation is slightly different than for when the correlation metrics are used with no channel state information. However, this difference is so small that it is best to simply use the correlation metrics without channel state information when a Viterbi or SOVA decoder is combined with a chip-level LMMSE receiver, rather than investing extra complexity to implement a channel estimation scheme.

The performance of online estimation in Figs. 3.17 and 3.18 also improves somewhat for the chip-level LMMSE receiver. However, the other techniques con-

tinue to offer better performance. This suggests that the channel state estimate standard deviation of online estimation continues to be larger than that of standard and improved estimation, even when the mobile uses the chip-level LMMSE receiver.

Even with the equalizer removing much of the intracell interference, the simulation results in Fig. 3.19 show that improved estimation still offers a significant performance improvement when used with the LogMAP decoder.

Unlike Sections 3.4.1 and 3.4.2, online estimation performs better than standard estimation in Fig. 3.19 over all values of E_b/N_o for the Rake receiver and at high values of E_b/N_o for the chip-level LMMSE equalizer. Chip-level simulations are used in this section and the transmit gains of the traffic signals making up the intracell interference are fixed. Section 2.3.3 showed that the transmit gains of the forward link interfering signals must be adjusted by random fast forward power control commands before it is valid to assume the intracell interference process is Gaussian. Therefore, the intracell interference in these simulations is quite different than the Gaussian intracell interference used in the symbol-level simulations in Sections 3.4.1 and 3.4.2. This causes a change in the relative performance of standard and online channel state estimation.

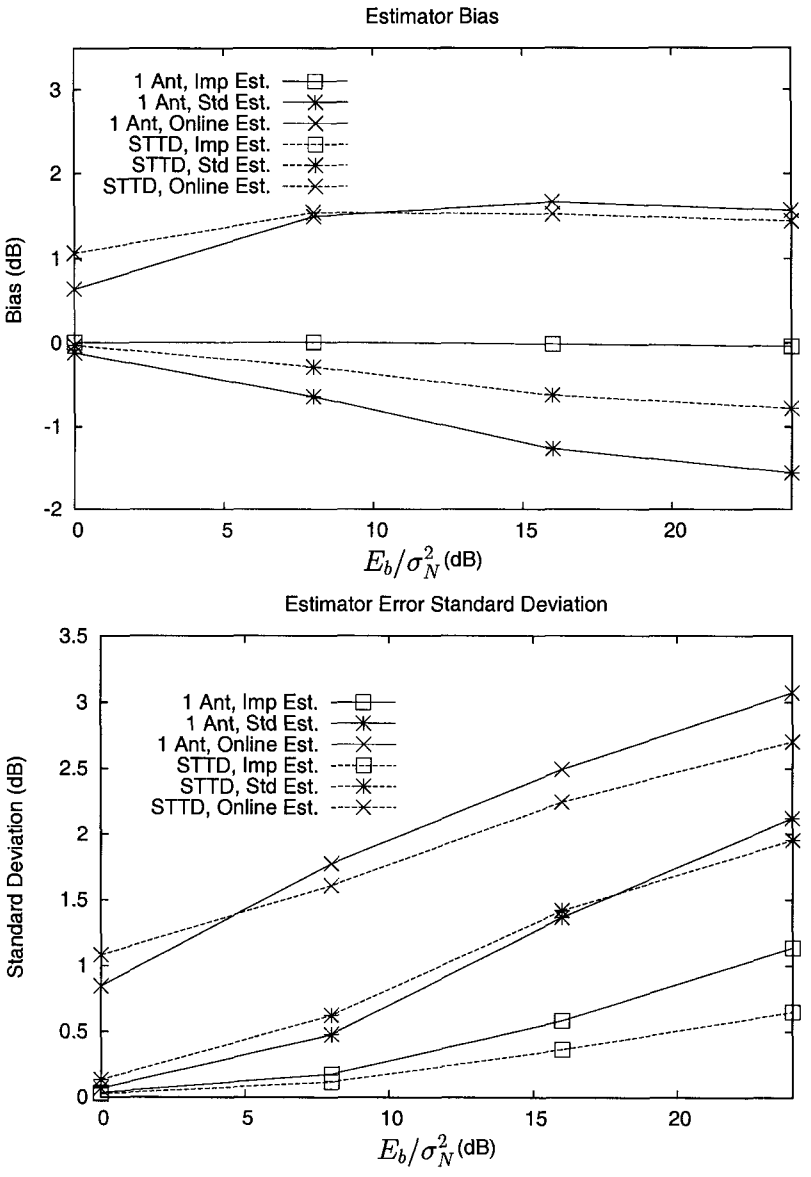

Figure 3.15: Channel state estimation accuracy, 100 km/h.

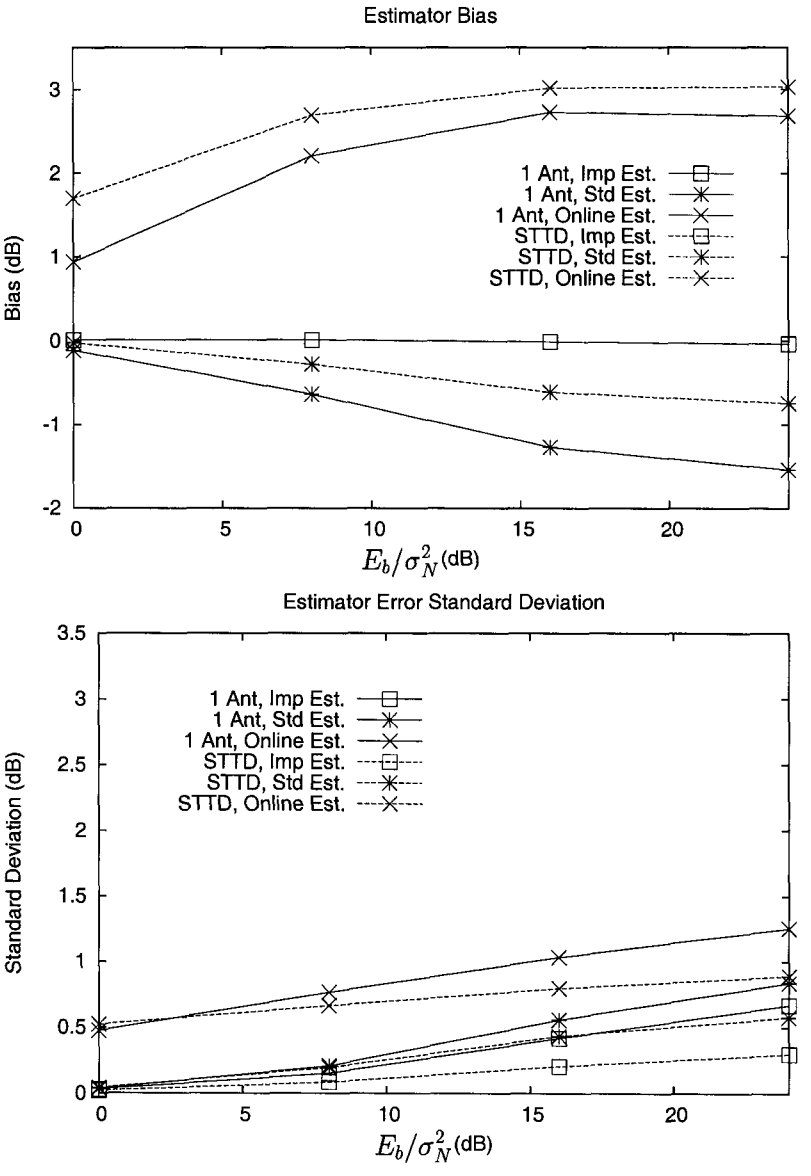

Figure 3.16: Channel state estimation accuracy, 5 km/h.

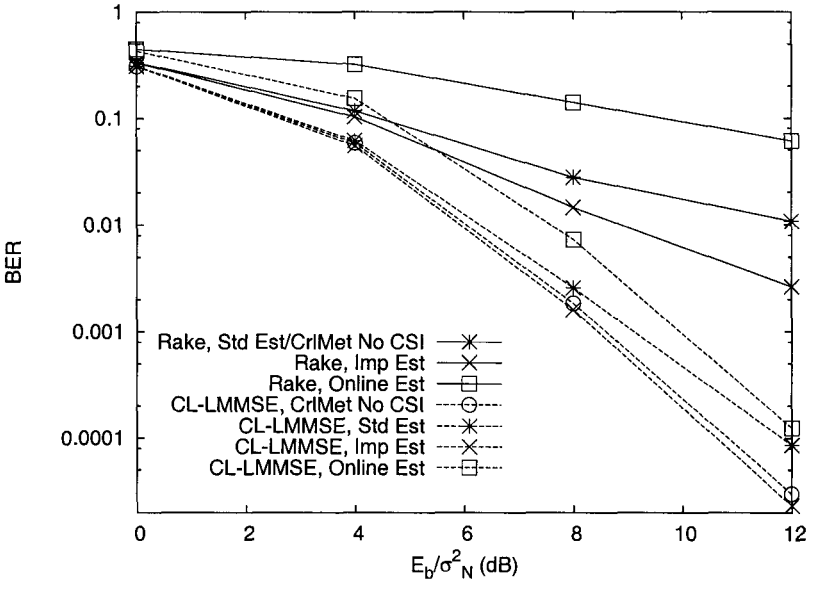

Figure 3.17: Forward link performance with convolutional codes.

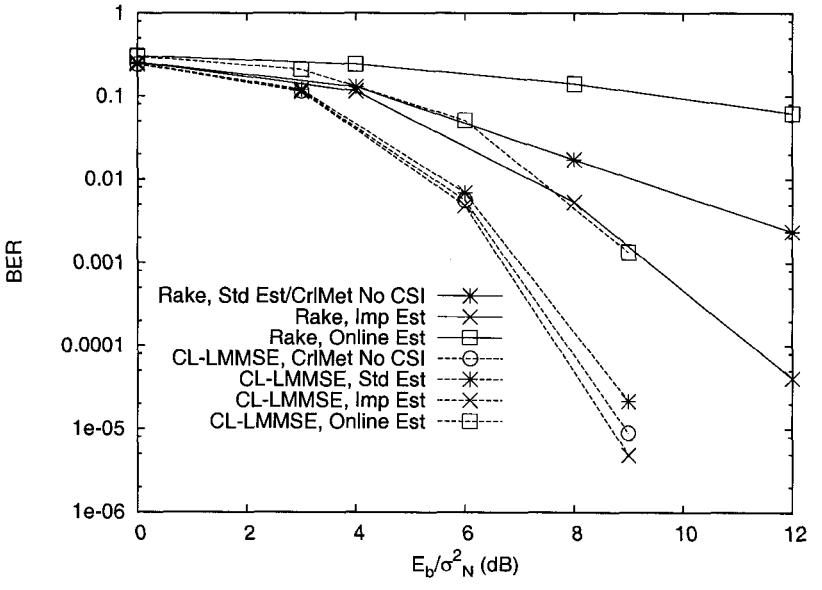

Figure 3.18: Forward link performance with turbo codes, SOVA decoding.

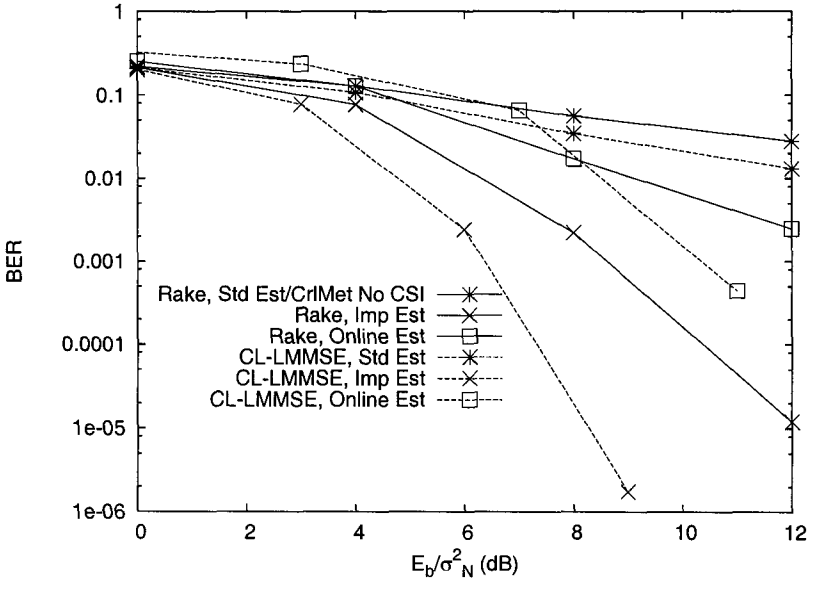

Figure 3.19: Forward link performance with turbo codes, LogMAP decoding.

Chapter 4

Rake Receiver Channel Estimation Error Compensation using the MAP Metric

This chapter presents new techniques for using the CDMA mobile turbo decoder MAP metric calculation to compensate for Rake receiver channel estimation error in a frequency selective channel.

Uncertainty in the symbol samples at the output of a CDMA mobile Rake receiver comes from several sources: interference, thermal noise, radio channel fading and estimation error in the Rake receiver combining weights. In order to provide optimal error correction, the trellis path metrics calculated by the mobile channel decoder must account for all these sources of uncertainty. However, Chapter 1 shows that the conventional MAP metric is derived assuming that the only uncertainty in the received symbol samples is due to an additive Gaussian interference plus noise process. This chapter will present two strategies for modifying the turbo decoder MAP metric evaluation to accommodate for the additional uncertainty due to radio channel fading and Rake finger combining weight estimation error.

The first strategy starts by estimating desired signal amplitude, $\zeta(i)$, and interference plus noise variance, $\sigma^2(i)$, for each received symbol interval and in-

corporating this information into the conventional MAP metric calculation. This estimation of $\zeta(i)$ and $\sigma^2(i)$ is discussed in detail in Chapter 3. However, Chapter 3 assumes that estimation error in the mobile's Rake finger combining weights is negligible. In many practical systems, this assumption is not valid.

Forward link channel estimation in a commercial CDMA system is typically performed using a base station pilot signal. In some systems, the base station pilot can be allocated as much as 20% of the maximum forward channel power [74]. Since this considerably reduces the forward link capacity available for traffic transmission, there is a clear incentive to reduce the transmit power of the pilot. As this is done, channel estimation error in the mobile will increase to a point where its effect on the Rake finger combining weights can no longer be ignored.

This chapter will show that it is possible to account for the uncertainty this Rake finger combining weight error adds to the received symbols by adding a bias term to the $\sigma^2(i)$ estimates used in the conventional MAP metric calculation. Estimating the instantaneous values of $\zeta(i)$ and $\sigma^2(i)$ removes any uncertainty in the received symbols due to small scale radio channel fading and adding this bias term accounts for any uncertainty due to Rake finger combining weight estimation error. As a result, the only remaining source of uncertainty is the additive interference plus noise process at the output of the Rake receiver.

Chapter 2 showed that both the intracell interference and intercell interference plus thermal noise processes can be considered Gaussian for moderate spreading factors and link loads. Therefore, since the conventional MAP metric calculation is based on an additive Gaussian interference plus noise assumption, it remains optimal for use in the mobile. In this chapter, using the conventional MAP metric calculation with a biased estimate of $\sigma^2(i)$ to account for estimation error in the Rake finger combining weights will be referred to as *conventional metrics with bias.*

The second approach to evaluating the MAP metric to account for estimation error in the Rake finger combining weights is to derive a received symbol sample distribution that incorporates uncertainty not only due to the additive Gaussian interference and noise process but also to radio channel fading and error in the complex channel gain estimates. A new MAP metric is then derived based on this distribution. Since the small scale fading process is now incorporated into the received symbol sample distribution, it is no longer necessary to perform the symbol-by-symbol channel state estimation described in Chapter 3. This metric will be referred to as an *inclusive metric* since it is based on a received symbol sample distribution that includes all sources of received symbol uncertainty.

The use of both conventional metrics with bias and inclusive metrics has been explored in previous research. Ling and Xiao *et. al.* investigate the use of conventional metrics that incorporate symbol-by-symbol estimates of channel state information (CSI) and also include a bias term to account for uncertainty due to channel estimation error at the mobile receiver [43, 82]. Frenger and Li *et. al.* derive received symbol sample distributions that incorporate the uncertainty of an additive noise process, small scale fading and random channel estimation error [20, 42]. These distributions are then used to find new inclusive metrics.

The contributions of this chapter address two important omissions in the previous research. First, this work is the first to develop inclusive metrics and conventional metrics with bias for use in a frequency selective fading channel. All previous work in this area has considered only a frequency flat fading channel [43, 82, 20, 42]. This is an important contribution since the wideband nature of modern CDMA systems implies that they are almost always subject to frequency selective fading. Second, this work is the first to develop inclusive metrics and conventional metrics with bias for use on the CDMA forward link. Previous research into these metrics has only considered channels with AWGN [43, 82, 20, 42]. This

chapter will show that the unique nature of CDMA forward link intracell interference changes both the derivation and performance of these techniques.

In the following, Section 4.1 presents a symbol-level system model for the CDMA forward link with Rake receiver channel estimation error that is based on the symbol-level model discussed in Section 2.3. The technique of using conventional MAP metrics with a CSI bias to account for Rake combining weight estimation error is developed in Section 4.2. Section 4.3 derives a new distribution that accounts for interference, noise, small scale fading and Rake combining weight estimation error in a frequency selective channel. That distribution is then used to develop an inclusive MAP channel decoder metric. CDMA forward link simulations are used in Section 4.4 to compare the performance of the techniques presented in Sections 4.2 and 4.3.

4.1 CDMA System Model

At the start of Chapter 3, the output of the mobile Rake receiver during symbol interval i, y_i, is written as

$$y_i = \sum_{f=0}^{F-1} \left[c(iR, z_f) A x_i + U_{f,i} \right] \hat{c}(iR, z_f)^* \tag{4.1}$$

where R is the number of spreading chips per channel encoded symbol, $c(iR, z_f)$ is the small scale complex channel gain at Rake finger delay z_f during symbol interval i, x_i is the channel encoded symbol, $U_{f,i}$ is the noise and interference at the output of the despreading stage in finger f during symbol interval i and $\hat{c}(iR, z_f)$ is the mobile's estimate of the complex channel gain at delay z_f. In this chapter, the term A is an amplitude that represents the transmit amplitude of the CDMA signal, the despreading gain of the receiver and large scale channel attenuation.

When the Rake receiver combining weights in (4.1) are subject to channel

estimation error, the channel estimate term $\hat{c}(iR, l) = c(iR, l) + V_{l,i}$, where $V_{l,i}$ is a zero mean complex Gaussian random variable with variance $\sigma_V^2(l)$. Using this notation, the equation (4.1) can be rewritten as

$$y_i = \sum_{f=0}^{F-1} \left[c(iR, z_f)Ax_i + U_{f,i}\right] \left[c(iR, z_f) + V_{z_f,i}\right]^* \tag{4.2}$$

On the CDMA forward link, the noise and interference term $U_{f,i} = N_{z_f,i} + I_{z_f,i}$. The intercell interference plus thermal noise term, $N_{z_f,i}$, is shown in Section 2.3 to be a zero-mean complex Gaussian random variable with variance σ_N^2. As explained in Chapter 2, the intracell interference term $I_{z_f,i}$ can be written as

$$I_{z_f,i} = \sum_{l=0}^{L-1} c(iR, l)I_i(z_f - l)[1 - \delta(l - z_f)] \tag{4.3}$$

where $I_i(r)$ represents the composite forward link signal during symbol interval i after large scale channel attenuation and despreading with a time offset of r. The $[1 - \delta(l - z_f)]$ term represents the Walsh sequence cancellation of the intracell interference that is synchronous with finger time offset z_f, where $\delta(z)$ equals 1 if $z = 0$ and is 0 otherwise. For moderate to heavy traffic loading, it is shown in Section 2.3.3 that $I_i(r)$ can be considered a zero mean complex Gaussian random variable with variance σ_I^2. Note that the definition of the intracell interference random variable in (4.3) is slightly different than in Section 2.3 because it does not include the Rake finger combining weight.

Since both the intercell interference plus noise and intracell interference components of $U_{f,i}$ can be considered Gaussian, $U_{f,i}$ is also a complex Gaussian random variable with zero mean and a variance given by

$$
\begin{aligned}
\sigma_U^2(f,i) &= \left\langle (N_{z_f,i} + I_{z_f,i})(N_{z_f,i} + I_{z_f,i})^* \right\rangle \\
&= \left\langle \left(N_{z_f,i} + \sum_{l=0}^{L-1} c(iR,l) I_i(z_f - l)[1 - \delta(l - z_f)]\right) \right. \\
&\quad \left. \left(N_{z_f,i} + \sum_{q=0}^{L-1} c(iR,q) I_i(z_f - q)[1 - \delta(q - z_f)]\right)^* \right\rangle \\
&= \left\langle N_{f,i} N_{f,i}^* \right\rangle + \sum_{l=0}^{L-1} \sum_{q=0}^{L-1} c(iR,l) c^*(iR,q) \left\langle I_i(z_f - l) I_i(z_f - q)^* \right\rangle \\
&\quad \cdot [1 - \delta(l - z_f)]\,[1 - \delta(q - z_f)] \\
&= \sigma_N^2 + \sigma_I^2 \sum_{l=0}^{L-1} \sum_{q=0}^{L-1} c(iR,l) c^*(iR,q) \delta[(l - z_f) - (q - z_f)] \\
&\quad \cdot [1 - \delta(l - z_f)]\,[1 - \delta(q - z_f)]\,.
\end{aligned}
\tag{4.4}
$$

The purpose of this chapter is to present new ways of evaluating the MAP metric to deal with Rake finger combining weight estimation error. In order to determine the variance of this error process, $\sigma_V^2(l)$, some typical values for CDMA forward link received pilot signal to noise plus interference ratio (SNIR) must be calculated. A seven cell hexagonal topology is assumed with one tier of neighboring cells and a middle cell with co-ordinates $(0, 0)$. Received pilot SNIR is calculated according to

$$
\gamma_P = \frac{\rho_R G_{CE} P_D}{\rho_W P_D + \sum_{k=0}^{5} P_{N,k} + P_{Th}} \tag{4.5}
$$

where G_{CE} is the processing gain of the channel estimation scheme, P_D is the received power from the desired base station, ρ_R is the fraction of total forward link power allocated to the pilot, $P_{N,k}$ is the received interference power from the kth neighboring base station, P_{Th} is thermal noise power and ρ_W is a Walsh code orthogonality factor.

The received base station powers are calculated assuming a maximum base station transmit power of 44 dBm, a path loss exponent of 4, cells with an $R =$ 1km radius, mobiles and base stations with omni antennas and a 1.9 GHz carrier frequency. Thermal noise is -113 dBm, $\rho_P = 0.16$, $\rho_W = 0.5$ and chip rate is 1.2288 Mcps. It is assumed that the pilot signal is processed with a moving average filter that has a 1 ms observation window such that $G_{CE} = 30.9\ dB$.

With these parameters and the worst case mobile co-ordinates of $(0, R)$, the ratio of channel estimate to interference plus noise is approximately 18 dB.

4.2 Conventional Metrics with Bias

Calculating the conventional MAP channel decoder metric discussed in Chapter 1 requires desired signal amplitude, $\zeta(i)$, and interference plus noise variance, $\sigma^2(i)$, to be estimated for each received symbol at the channel decoder input. This section will illustrate how a bias term can be added to the estimates of $\sigma^2(i)$ to account for the additional received symbol uncertainty caused by Rake finger combining weight estimation error.

In (4.2), the output of a Rake receiver subject to channel estimation error is written in terms of the actual channel impulse response $c(iR, l)$. However, since the mobile has knowledge of $c(i\hat{R}, l)$ and not $c(iR, l)$, the expression for y_i can be equivalently written as

$$\begin{aligned} y_i &= \sum_{f=0}^{F-1} \left\{ \left[\hat{c}(iR, z_f) - V_{z_f,i} \right] Ax_i + U_{f,i} \right\} \hat{c}(iR, z_f)^* \\ &= \sum_{f=0}^{F-1} \left[|\hat{c}(iR, z_f)|^2 Ax_i - V_{z_f,i} Ax_i \hat{c}(iR, z_f)^* + U_{f,i} \hat{c}(iR, z_f)^* \right] \\ &= \sum_{f=0}^{F-1} \left[|\hat{c}(iR, z_f)|^2 Ax_i + W_{f,i} \right] \end{aligned} \tag{4.6}$$

where $W_{f,i} = V_{z_f,i} Ax_i \hat{c}(iR, z_f)^* + U_{f,i} \hat{c}(iR, z_f)^*$ is the effective noise term in finger f for symbol i. Since both $V_{z_f,i}$ and $U_{f,i}$ are zero mean complex Gaussian terms, $W_{f,i}$ is also zero mean complex Gaussian with variance

$$\sigma_W^2(f, i) = \sigma_U^2(f, i) |\hat{c}(iR, z_f)|^2 + \sigma_V^2(z_f) A^2 |\hat{c}(iR, z_f)|^2 \tag{4.7}$$

Note that the first term in (4.7) is the variance of the interference and noise process and the second is an additional bias term, which accounts for the Rake combining weight estimation error.

When the mobile is using conventional metrics with a bias to account for Rake receiver channel estimation error, the desired signal amplitude term, $\zeta(i)$,

required by the MAP metric calculations can be estimated in a straightforward manner using pilot symbols embedded in the data stream or by averaging the envelope of the information bits. The interference plus noise variance required for the metric, $\sigma^2(i)$, is estimated by the mobile using the expression for $\sigma_W^2(f,i)$ in (4.7). This is equivalent to the improved estimation technique presented in Chapter 3 with an additional Rake finger channel estimation error bias term.

The $\hat{c}(iR, z_f)$ terms required in (4.7) are estimated using the forward link pilot signal and A can be estimated by averaging pilot symbols embedded in the data stream or the envelope of the information bits over many wavelengths. The variance of the interference plus noise, $\sigma_U^2(f,i)$, is calculated by the mobile using (4.4). The small scale channel impulse response terms required in (4.4) are estimated using the forward link pilot signal and the variance terms σ_I^2 and σ_N^2 can be determined using the least squares estimation technique presented in Section 3.2.4.

4.3 Inclusive Metrics

The conventional MAP metric derivation discussed in Chapter 1 assumes the only uncertainty in the received symbol is due to the additive interference plus noise process. The inclusive MAP metric derived in this section is based on a received symbol distribution that incorporates not only the additive interference plus noise process $U_{f,i}$ in (4.2) but also the small scale fading process $c(iR, l)$ and the Rake finger combining weight error process $V_{l,i}$

In Sections 4.1 and 4.2, it was established that $U_{f,i}$ and $V_{l,i}$ can be considered zero mean complex Gaussian random variables. If Rayleigh fading is assumed, $c(iR, l)$ is also a zero mean complex Gaussian process with variance $\sigma_C^2(l)$. This variance is equivalent to the average received power of the multipath component at delay l.

With these assumptions, each of the F terms added together in (4.2) can be considered a product of two correlated complex Gaussian processes. In this section, the distribution of the real and imaginary components of y_i will be derived using this observation as a starting point. This new distribution will then be used to develop the inclusive MAP channel decoder metric. Since the real and imaginary components of y_i are independent and identically distributed, only the distribution for the real component will be derived in the following.

Proakis provides a joint characteristic function for the real and imaginary components of the product of two zero mean correlated Gaussians X and Y [60]. Under the assumption that the real and imaginary components of X and Y are uncorrelated, this function can be written as

$$\Phi(j\omega_1, j\omega_2) = \frac{4[m_{xx}m_{yy}(1-\mu^2)]^{-1}}{\left[\omega_1 - j\frac{2\mu}{\sqrt{m_{xx}m_{yy}}(1-\mu^2)}\right] + \omega_2^2 + \frac{4}{m_{xx}m_{yy}(1-\mu^2)^2}} \tag{4.8}$$

where $m_{xx} = \langle |X|^2 \rangle$, $m_{yy} = \langle |Y|^2 \rangle$ and $\mu = \langle XY^* \rangle / \sqrt{m_{xx}m_{yy}}$.

The characteristic function of the real component of the product of X and Y, $\Phi_R(j\omega)$ can be determined from (4.8) by setting $\omega = \omega_1$ and $\omega_2 = 0$ such that $\Phi_R(j\omega) = \Phi(j\omega, 0)$ [58]. Algebraic manipulation can then be used to express $\Phi_R(j\omega)$ in the following form

$$\Phi_R(j\omega) = \frac{\alpha}{(\rho_N + j\omega)(\rho_P - j\omega)} \tag{4.9}$$

where

$$\begin{aligned} \rho_N &= \frac{4\mu}{\sqrt{m_{xx}m_{yy}}(1-\mu^2)} + \sqrt{\frac{16}{m_{xx}m_{yy}(1-\mu^2)^2}} \\ \rho_P &= \frac{4\mu}{\sqrt{m_{xx}m_{yy}}(1-\mu^2)} - \sqrt{\frac{16}{m_{xx}m_{yy}(1-\mu^2)^2}} \\ \alpha &= \frac{4}{m_{xx}m_{yy}(1-\mu^2)} \end{aligned} \tag{4.10}$$

The real component of y_i in (4.2) is equal to the sum of the real components

of the F correlated Gaussian product terms in (4.2). The characteristic function of the real component of the fth product term in this sum is given by (4.9), where $X = c(iR, z_f)Ax_i + U_{f,i}$ and $Y = c(iR, z_f) + V_{z_f,i}$. In order to use (4.10) to calculate ρ_P and ρ_N, it is noted that

$$\begin{aligned} m_{xx} &= \langle |c(iR, z_f)Ax_i + U_{f,i}|^2 \rangle = A^2\sigma_C^2(z_f) + \sigma_U^2(f) \\ m_{xx} &= \left\langle |c(iR, z_f) + V_{z_f,i}|^2 \right\rangle = \sigma_C^2(z_f) + \sigma_V^2(z_f) \\ \mu &= \frac{\left\langle [c(iR,z_f)Ax_i+U_{f,i}][c(iR,z_f)+V_{z_f,i}]^* \right\rangle}{\sqrt{(A^2\sigma_C^2(z_f)+\sigma_U^2(f))(\sigma_C^2(z_f)+\sigma_V^2(z_f))}} \\ &= \frac{A\sigma_C^2(z_f)}{\sqrt{(A^2\sigma_C^2(z_f)+\sigma_U^2(f))(\sigma_C^2(z_f)+\sigma_V^2(z_f))}} \end{aligned} \tag{4.11}$$

The terms α, ρ_P and ρ_N in (4.10) found using the relationships in (4.11) are denoted α_f, $\rho_{P,f}$ and $\rho_{N,f}$.

Note that the interference plus noise variance $\sigma_U^2(f)$ in (4.11) is different than the interference plus noise variance $\sigma_U^2(f,i)$ calculated in (4.4). CDMA intracell interference is a non-stationary process with a variance that changes from symbol-to-symbol due to the fluctuations in the small scale radio channel impulse response. The variance $\sigma_U^2(f,i)$ calculated in (4.4) captures these variations. In contrast, the variance $\sigma_U^2(f)$ represents the interference plus noise variance averaged over many wavelengths and is calculated according to

$$\sigma_U^2(f) = \sigma_N^2 + \sigma_I^2 \sum_{\substack{l=0 \\ l \neq z_f}}^{L-1} \sigma_C^2(l). \tag{4.12}$$

The overall characteristic function of a sum of complex Gaussian products is equal to the product of the characteristic functions of the individual terms making up the sum [58]. Therefore, using (4.9), the characteristic function of the real component of y_i in (4.2) can be written as

$$\Phi_{R,Y}(j\omega) = \prod_{f=0}^{F-1} \frac{\alpha_f}{(\rho_{N,f} + j\omega)(\rho_{P,f} - j\omega)} \tag{4.13}$$

In order to find the inverse transform of (4.13) the equation can be expanded using partial fraction expansion such that

$$\Phi_{R,Y}(j\omega) = \sum_{f=0}^{F-1} \left[\frac{N_f}{(\rho_{N,f} + j\omega)} + \frac{P_f}{(\rho_{P,f} - j\omega)} \right] \tag{4.14}$$

where the partial fraction expansion coefficients P_f and N_f are calculated according to

$$\begin{aligned} N_f &= [\rho_{N,f} + j\omega]\, \Phi_{R,Y}(j\omega)|_{j\omega = -\rho_{N,f}} \\ P_f &= [\rho_{P,f} - j\omega]\, \Phi_{R,Y}(j\omega)|_{j\omega = \rho_{P,f}} \end{aligned} . \tag{4.15}$$

Once the partial fraction expansion is complete, the PDF of the real component of y_i, $f_{R,Y}(y)$, is found by summing the inverse transforms of the individual terms making up the sum in (4.14). These inverse transforms are found using the relationships [12]

$$\begin{aligned} \tfrac{1}{p+j\omega} &\overset{\text{CF}^{-1}}{\rightarrow} e^{px} u(-x) \\ \tfrac{1}{p-j\omega} &\overset{\text{CF}^{-1}}{\rightarrow} e^{-px} u(x). \end{aligned} \tag{4.16}$$

Using (4.16), the PDF $f_{R,Y}(y)$ can be written as

$$f_{R,Y}(y) = \sum_{f=0}^{F-1} \left[N_f \exp(\rho_{N,f} y) u(-y) + P_f \exp(-\rho_{P,f} y) u(y) \right]. \tag{4.17}$$

The inclusive MAP metric that incorporates the new distribution in (4.17) is calculated the same way as the conventional MAP metric described in Chapter 1 except that the calculation for $\gamma_k^\theta(l, l')$ in (1.5) is replaced with

$$\gamma_k^\theta(l, l') = \begin{cases} p_\theta(k) \prod_{j=kN_s}^{(k+1)N_s - 1} f_{R,Y}(y_j), & (l, l') \in B_k^\theta \\ 0, & \text{otherwise} \end{cases} \tag{4.18}$$

This metric can be implemented in the mobile with a reasonable amount of complexity. The final expression for $f_{R,Y}(y)$ in (4.17) is a summation of exponentials where the value of F is generally quite low for conventional Rake receivers

and the exponential function itself can be implemented with a lookup table. Also, the mutually exclusive step functions in (4.17) ensure that only half of the terms inside the braces need to be evaluated to calculate a particular point on the PDF.

Part of the complexity required to implement this metric is performing the partial fraction expansion necessary to determine the coefficients in (4.17). The partial fraction expansion must be performed each time either the numerator term or the poles of (4.13) change significantly. The terms that make up the numerator and poles of (4.13) consist of the average received power of a particular channel tap, $\sigma_C^2(l)$, the transmit amplitude and large scale attenuation of the desired signal A, the variance of the channel estimation error, $\sigma_V^2(l)$ and the average interference plus noise variance in each finger, $\sigma_U^2(f)$. These quantities will remain approximately constant for the duration of an encoded frame. Therefore, the partial fraction expansion need only be performed at the beginning of each frame.

It should be noted that a conventional MAP metric requires symbol-by-symbol estimates of the small scale fading process. This limits the observation window used to determine these estimates to less than the channel coherence time. However, the CSI required for this inclusive metric remains constant for many wavelengths. This allows the observation window used to calculate inclusive metric CSI to be as long as the encoded frame, resulting in improved accuracy and better performance.

4.4 Metric Performance

In this section, CDMA forward link simulations are used to compare the performance of the conventional MAP metric, the conventional MAP metric with bias as presented in Section 4.2 and the inclusive metric as presented in Section 4.3.

The simulation results show bit error rate (BER) plotted versus signal to noise ratio, E_b/σ_N^2, where E_b is energy per bit and σ_N^2 is intercell interference plus

thermal noise variance at the mobile receiver input. A spreading factor of 16 is assumed. The level of intracell interference used in the simulation is equivalent to 16 equal power traffic transmissions and is kept constant for all values of E_b/σ_N^2. Data rate is 38.4 kbps, frames are 40 ms long and BPSK is used. The turbo code used by the base station is rate 1/2 with punctured rate 1/2 RSC (1,17/15) component encoders and the mobile uses the LogMAP turbo decoder. The turbo encoder uses a random interleaver and the decoder uses a maximum of 8 iterations.

A frequency selective Rayleigh fading radio channel is considered with three different channel profiles. The first is a three path channel where the average received powers of the multipath components decay in 4 dB steps, the second a 2 path channel with the average received power of the second path 3 dB below the main path and the third a 5 path channel where the average received power of the multipath components decays in 2 dB steps.

The simulation results are shown in Figs. 4.1 through 4.5. Figs. 4.1 through 4.3 show results for the 3 path channel model with received pilot SNIR, γ_P, values of 15 dB, 18 dB and 21 dB, where received pilot SNIR is defined in (4.5). Figs. 4.4 and 4.5 both use a received pilot SNIR of 18 dB with the 2 path and 5 path channel models, respectively. These received pilot SNIR values are used to determine the variance, $\sigma_V^2(l)$ of the estimation error in each of the Rake finger combining weights. Assuming that the received channel impulse response is normalized such that $\sum_{l=0}^{L-1} \sigma_C^2(l) = 1$, then the channel estimation error variance $\sigma_V^2(l) = \sigma_C^2(l)/\gamma_P$.

Each simulation plot shows 5 BER curves. The first BER curve represents conventional MAP metric performance with improved estimation and no compensation for Rake finger channel estimation error. The estimates of $\zeta(i)$ required by the metric calculations are obtained using a 1 ms moving average filter that operates on the envelope of the data symbols. The required interference plus noise variance values, $\sigma^2(i)$, are calculated by the mobile using (4.4). The chan-

nel impulse response terms required in this equation are estimated using a 1 ms moving average filter on a forward link pilot signal that is transmitted at 16% of the maximum base station transmit power. The variances σ_N^2 and σ_I^2 required in (4.4) are estimated using the LSE presented in Section 3.2.4, where the estimator observation window is 40 ms.

The second BER curve on the simulation plots is generated using the conventional MAP metric and the same techniques for estimating $\zeta(i)$ and $\sigma^2(i)$ as described above. However, a bias term is added to $\sigma^2(i)$, as described in Section 4.2, to account for Rake finger weight estimation error.

The third BER curve is also generated using the conventional MAP metric and represents the artificial case where the channel decoder operates with perfect CSI but estimation error is still present in the Rake finger combining weights. The simulation used to generate this curve has perfect knowledge of $\zeta(i)$, $\sigma^2(i)$ and the bias factor to account for Rake finger weight estimation error.

The simulation used to generate the fourth BER curve uses the inclusive metric, as described in Section 4.3. In the derivation of this metric, it is assumed that the interference and noise terms $U_{f,i}$ in (4.2) are independent between fingers. However, the equation for CDMA forward link intracell interference in (4.3) shows that there is some intracell interference correlation between fingers. As a result, the distribution derived in Section 4.3 will deviate from the true distribution for y_i when intracell interference is present. The result will be some degradation in the performance of the inclusive MAP metric presented in Section 4.3.

In order to quantify this degradation, the true distribution of the real component of y_i is found using a histogram of 10^6 samples of y_i generated according to (4.2). The histogram function found using this approach, $f_{R,H}(y)$, is then used in (4.18) in place of $f_{R,Y}(y)$ to calculate the LogMAP trellis path metrics. The result is the fifth BER curve in the simulation plots. This numerical technique clearly

isn't practical to implement in a mobile. However, it does provide a lower performance bound that could be achieved if the inclusive metric was derived using an exact expression for the received symbol distribution.

Fig. 4.1 shows that conventional LogMAP metric performance is very poor at low pilot SNIR without any compensation to account for Rake finger combining weight estimation error. Adding a bias term to the interference plus noise variance estimates to account for this error, as described in Section 4.2, provides a significant improvement. However, even after adding this bias, forward link performance is still considerably worse than when the conventional MAP metric is calculated with perfect channel state information. This is because, in addition to degrading the Rake finger combining weights, channel estimation error also degrades the interference plus noise variance estimate $\sigma_U^2(f,i)$ evaluated using (4.4).

Fig. 4.1 also shows that while the conventional MAP metric with perfect channel state information outperforms the inclusive metrics, the inclusive metric approach is better than conventional MAP metrics that are calculated with estimated channel state information. The channel state information used by the conventional MAP metric requires estimates of the instantaneous value of the small scale fading process. As a result, the observation window of the moving average filters used to estimate this small scale fading information have to be less than the channel coherence time. In contrast, the inclusive metrics operate using information that remains constant for many wavelengths. The estimators used to determine this information can use observation windows much longer than the channel coherence time, resulting in better accuracy.

As expected, as received pilot SNIR improves, the benefit of modifying the MAP metric calculation to compensate for Rake finger channel estimation error will decrease. While the benefit of using the techniques described in Sections 4.2 and 4.3 remains significant even at an 18 dB pilot SNIR, they offer much the same

performance as the conventional MAP metric with no modification at a pilot SNIR of 21 dB.

Comparing Figs. 4.2, 4.4 and 4.5 show that multipath channel profile also affects the benefit of using the techniques presented in Sections 4.2 and 4.3. As the number of resolvable multipath components increases, the benefit of using the inclusive metric or the conventional metric with bias also increases. Therefore, the techniques presented in this chapter will provide more benefit when used with wideband CDMA systems, like UMTS, and slightly less benefit when used with more narrowband CDMA systems, like IS-95 or IS-2000.

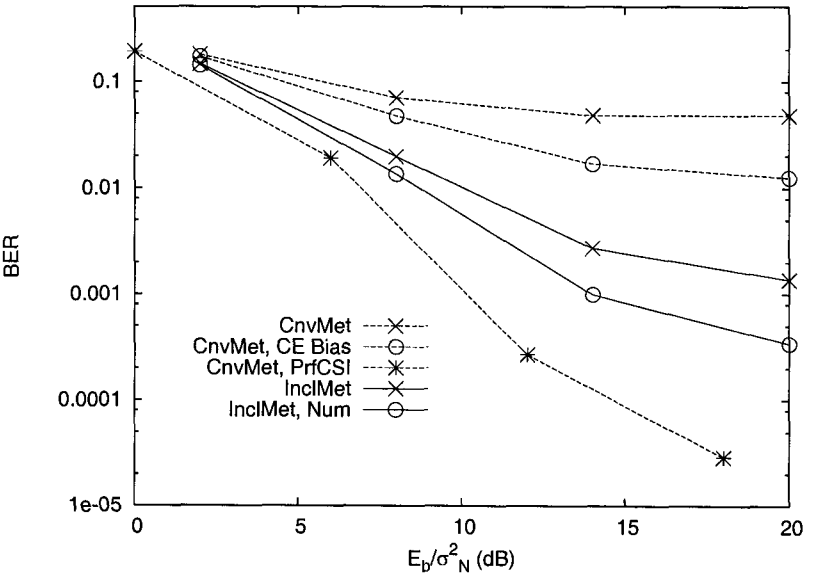

Figure 4.1: 15 dB pilot SNIR, 3 path channel.

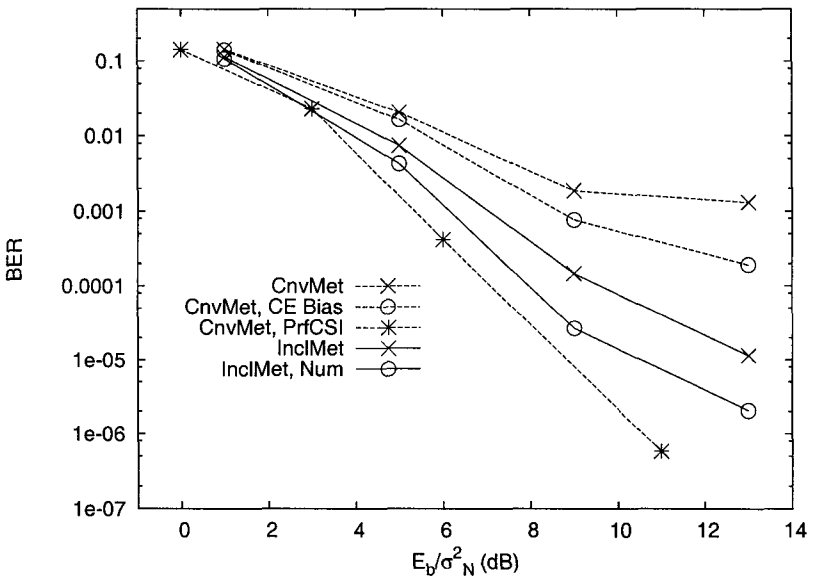

Figure 4.2: 18 dB pilot SNIR, 3 path channel.

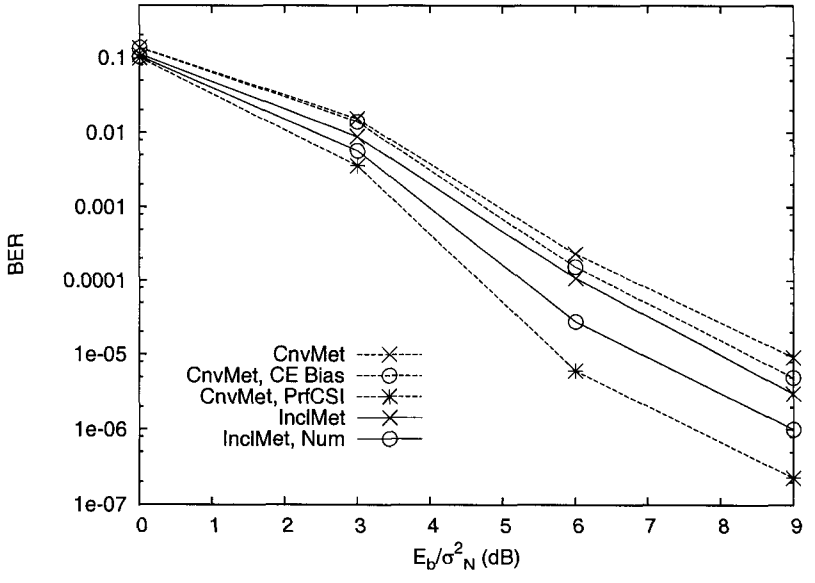

Figure 4.3: 21 dB pilot SNR, 3 path channel.

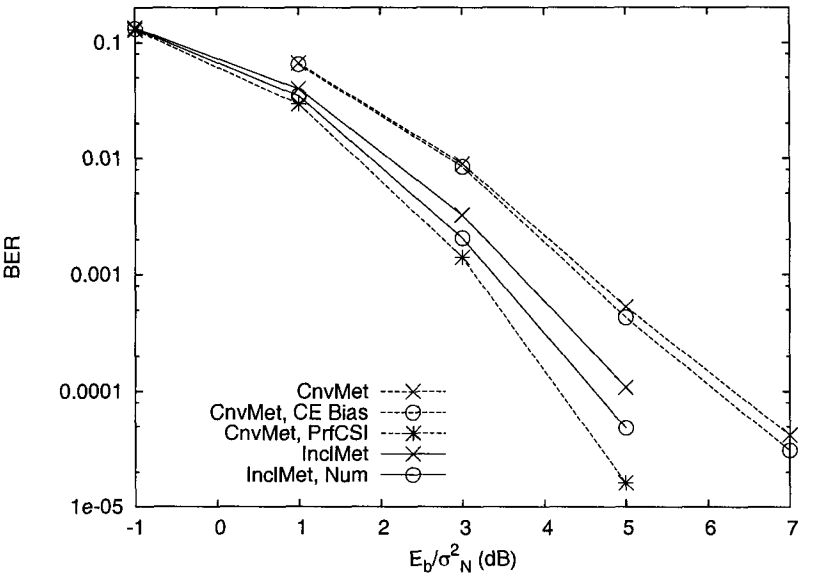

Figure 4.4: 18 dB pilot SNIR, 2 path channel.

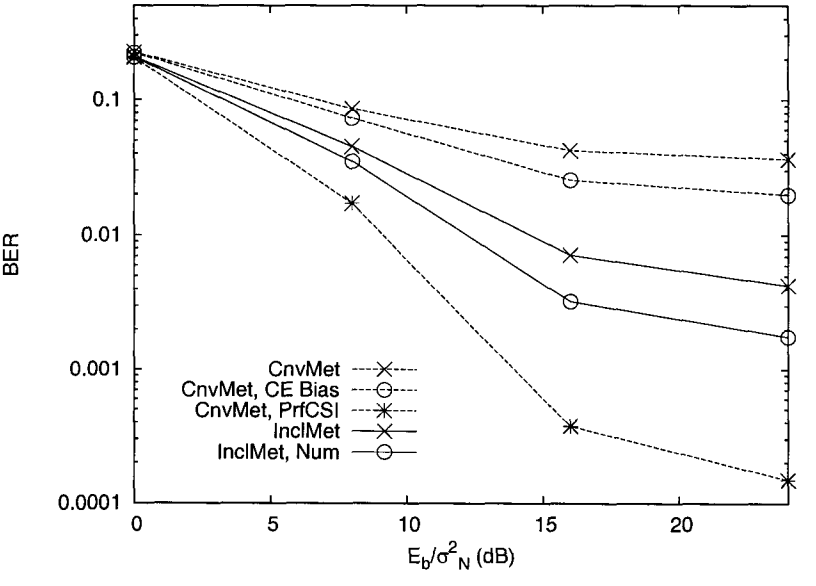

Figure 4.5: 18 dB pilot SNIR, 5 path channel.

Chapter 5

Conclusions and Future Work

5.1 Concluding Remarks

This thesis has presented several techniques for improving CDMA forward link physical layer performance by improving the trellis path metric calculations performed by the CDMA mobile channel decoder. This section will summarize the important observations made in this thesis and the contributions this work has made to new research.

This thesis topic is very relevant to the wireless industry. Chapter 1 has explained that CDMA is used extensively in current cellular systems and promises to become even more prominent in future wireless networks. This chapter also has showed that forward link performance is an extremely important issue when working with CDMA systems. It is typically the forward link that limits the voice capacity of current CDMA networks. This problem will become even more serious with the introduction of download-intensive wireless data applications that promise to make even heavier demands on the forward link.

The importance of the CDMA forward link makes enhancing its performance a very active area of research. Chapter 1 presented a survey of some of the different techniques being proposed for improving the forward link physical layer. While these ideas all have advantages, there are several reasons why enhancing the

mobile is a particularly attractive way to improve the forward link. The design of the mobile receive chain is not regulated by the CDMA industry standards. This means it is easier to implement and deploy mobile receive chain improvements than it is to make changes to the base station transmit chain. The turnover of mobiles is also much higher than it is for network infrastructure, making it easier and cheaper to distribute phones with new technology.

Much of the research into improving CDMA forward link performance by making changes to the mobile has dealt with interference cancellation. This research uses detailed knowledge of CDMA forward link signal and interference statistics to develop advanced receiver designs capable of canceling interference. However, there has not been adequate research into determining if knowledge of the unique conditions that exist on the CDMA forward link can also be used to improve the mobile channel decoder. This investigation was the focus of this thesis.

The channel coding discussion in Chapter 1 showed that the mobile channel decoder recovers the transmitted information by comparing samples of the received channel encoded symbol stream to symbols that correspond to all possible paths through the channel code trellis diagram. The decoder selects the path with the best metric as the one most likely to correspond to the transmitted information. Regardless of the particular channel decoder algorithm, the conventional derivation of this metric calculation is always based on the assumption that the probability distribution of the symbol samples at the input to the channel decoder is Gaussian.

When investigating how the CDMA mobile channel decoder can be improved, it must first be established whether it is valid to assume that the symbol samples at the input to the mobile channel decoder are Gaussian distributed. This can be determined by establishing whether the forward link interference and noise processes causing uncertainty in the received symbol samples are Gaussian at the

channel decoder. It is commonly assumed that the combined intercell interference and thermal noise processes have a Gaussian distribution. However, previous research has not established whether CDMA forward link intracell interference can also be considered Gaussian for the range of spreading factors and link loads experienced in a modern CDMA system. In addition to presenting the CDMA forward link models used throughout this thesis, the primary contribution of Chapter 2 is to establish that the Gaussian distribution can be used to accurately describe intracell interference for moderate spreading factors and link loads.

At the beginning of Chapter 3, it was established that, as long as channel estimation error is small, the Gaussian distributed CDMA forward link interference and noise processes result in a Gaussian received symbol sample distribution at the mobile channel decoder input. This Gaussian received symbol distribution means that the conventional channel decoder metrics are optimal for use on the CDMA forward link. However, the calculation of these metrics still requires values of desired signal amplitude and interference plus noise variance to be estimated at the channel decoder input. This is referred to as channel state estimation. The complex nature of CDMA forward link interference can make channel state estimation difficult. The primary contribution of this thesis towards the use of conventional channel decoder metrics in the CDMA mobile is to recognize this fact and then to present three channel state estimation schemes suitable for use in a CDMA mobile.

The first technique, standard estimation, assumes all CDMA forward link interference and noise can be modeled as an AWGN process at the mobile receiver input. This is a common assumption that results in a simple but somewhat inaccurate estimator.

The second technique, online estimation, calculates received signal to noise plus interference ratio at the input to the channel decoder using the second order

statistics of the received symbol samples. This is a technique originally developed for use on the time invariant AWGN channel that is applied in a new way in this thesis for use on the CDMA forward link.

The third technique, improved estimation, is a novel channel state estimation technique that separately accounts for the intracell interference and intercell interference plus thermal noise processes at the Rake output when calculating interference plus noise variance. This estimator is more complex than standard and online estimation but also much more accurate. The complexity of improved estimation comes partly from the equations used to calculate variance and partly from the requirement of needing to know the proportion of intracell interference and intercell interference plus thermal noise at the input to the mobile. Chapter 3 presents a new least-squares estimation technique that determines these input interference levels using the signal at the mobile receiver input. It is shown in Chapter 3 that improved estimation is the most accurate of the three channel state estimation schemes and results in the best CDMA forward link performance.

CDMA forward link simulations are used to compare forward link performance when the mobile uses standard, online and improved channel state estimation. In all cases, the more accurate improved channel state estimation results in the best performance. However, the extent of this improvement depends on several factors, including the channel decoder algorithm, mobile velocity, receiver architecture and base station transmission scheme. Another contribution made by this thesis is the detailed investigation of these tradeoffs. New observations are made not only concerning channel state estimation on the CDMA forward link but also about channel decoder algorithms behave when affected by different types of channel state estimation error.

When considering a Viterbi or SOVA channel decoder, the relative forward link performance difference between the different channel state estimation schemes is

dependent on velocity. Fluctuations in both intracell interference variance and desired signal level become more stationary as mobile velocity is reduced. This means that the different channel state estimates produced by standard, online and improved estimation are all approximately stationary over the encoded frame duration at low velocities. Since any factor that remains constant in the Viterbi or SOVA metric calculations does not affect decoder performance, all three channel state estimation schemes perform approximately the same at low mobile speeds. Therefore, the more accurate improved estimation techniques provide the most benefit for these decoders when used at higher mobile velocities.

Using the more accurate improved channel state estimation scheme with the LogMAP decoder results in a very large forward link performance improvement relative to online and standard estimation. This improvement is mostly independent of velocity. The LogMAP decoder is more sensitive to metric parameter estimation errors than the Viterbi and SOVA decoders. Unlike the Viterbi and SOVA decoders, the LogMAP decoder requires accurate channel state estimates even when these values are stationary over the encoded frame duration. Since improved estimation accounts for the partial Walsh-sequence cancellation of intracell interference, it always produces a more accurate channel state estimate, even at low mobile velocities. The result is better LogMAP performance. Providing the LogMAP decoder with the most accurate channel state estimates possible clearly results in a significant performance improvement, regardless of velocity.

In order for this work to be relevant not only for current generation CDMA systems but also for future systems, the standard, online and improved channel state estimation schemes are also applied to CDMA forward links that incorporate multiple antenna transmission and interference cancellation in the mobile. Space Time Transmit Diversity (STTD) was selected for the multiple antenna transmission scheme since different versions of this technique have been incorporated into

both the IS-2000 and UMTS CDMA standards. A chip-level LMMSE equalizer was chosen for mobile receiver interference cancellation since it represents a good compromise between complexity and performance. Previous research has not investigated the issue of forward link channel state estimation for CDMA systems with either STTD or intracell interference cancellation. This is an important omission since the results in this thesis show that channel state estimation accuracy can significantly affect the performance of these systems.

When used in an STTD system, the relative differences between the CDMA performance achieved by the different channel state estimation schemes remain approximately the same for the Viterbi and SOVA decoders. However, an improvement is seen in how standard estimation performs with the LogMAP decoder. Walsh sequence cancellation has a smaller effect on the level of intracell interference in an STTD system. Since neglecting intracell interference cancellation is a major source of standard estimation inaccuracy, an improvement is seen in the combined performance of LogMAP decoding with standard estimation as this cancellation becomes less significant.

The benefit of using channel state estimation with a mobile chip-level LMMSE equalizer depends on channel decoder algorithm. The chip-level LMMSE receiver is designed to remove as much intracell interference as possible. Since the accuracy of improved channel state estimation is primarily due to a more accurate description of intracell interference, it is expected that the advantage of using improved estimation will decrease with the introduction of the chip-level LMMSE receiver. This is shown to be true for the Viterbi and SOVA decoders, where the correlation metric with no channel state information offers almost the same performance as the different channel state estimation schemes. However, the more accurate improved estimation still offers a significant performance improvement for the LogMAP decoder, even when the equalizer is used. Therefore, in mobiles

with some form of intracell interference cancellation, channel state estimation will likely be unnecessary for the Viterbi and SOVA decoders but will still offer a significant advantage when used with the LogMAP decoder.

Chapter 3 showed that conventional channel decoder metrics were optimal for use on the CDMA forward link by making the assumption that any uncertainty in the received symbol due to channel estimation errors is very small. This is a valid assumption for systems with a very strong forward link pilot signal or a small amount of interference. However, in many practical CDMA systems, channel estimation errors are too large to be ignored.

Chapter 4 considers the scenario when the channel estimates used for the mobile Rake finger combining weights are subject to a significant level of channel estimation error. It is shown that even with a random Gaussian estimation error process corrupting the Rake finger combining weights, the received symbol distribution is still Gaussian and conventional metrics are optimal for use in the mobile. A bias term can then be added to the channel state information used to calculate the conventional metric.

This chapter also showed that there is benefit to deriving an inclusive channel decoder metric based on a received symbol distribution that incorporates not only interference plus noise but also the small scale fading and Rake finger combining weight estimation error processes. While this metric is sub-optimal when the mobile has perfect channel state information knowledge, it performs better than the conventional metric when the channel state information required by the channel decoder must be estimated. This is because the CSI required by the inclusive metric can be estimated using observation windows much longer than the channel coherence time, resulting in improved accuracy.

Chapter 4 makes several new research contributions. It introduces the first channel decoder metrics derived for the frequency selective wireless channel that

account for receiver channel estimation error. All other research in this area has been restricted to the flat fading channel. This is also the first time that metrics accounting for receiver channel estimation error have been derived for the CDMA forward link. All other metrics of this type consider channels with AWGN only.

CDMA forward link simulations show that the conventional metric with bias and the inclusive metric both considerably improve CDMA forward link performance when channel estimation error is severe. The conventional metric with bias offers the best performance when the channel decoder operates with perfect CSI. However, the inclusive metric performs better when CSI must be estimated since the type of CSI required by the inclusive metric can be estimated with greater accuracy. As receiver channel estimation error is reduced, the performance gap between the new metric and a conventional MAP metric with improved channel state estimation starts to close. Simulation results also show that these new metrics offer a larger performance advantage over the conventional metric when the channel has a larger number of resolvable multipath components. Therefore, the techniques in Chapter 4 should be used for heavily loaded systems where the mobiles experience a high level of channel estimation error and for wideband CDMA systems that are able to resolve a larger number of multipath components.

To conclude, this thesis presents several new techniques for improving CDMA forward link performance. These techniques are all aimed at finding ways to improve the performance of the mobile channel decoder. It has been established that channel estimation error dictates whether the conventional channel decoder metrics are optimal for use on the CDMA forward link. When channel estimation errors are small and conventional metrics can be used, several channel state estimation schemes are presented that use knowledge of the CDMA forward link to better estimate the information required to calculate these metrics. The result is better forward link performance for a broad range of CDMA forward link con-

ditions and designs. When channel estimation errors are high and the received symbol sample distribution is no longer Gaussian, a new channel decoder metric is derived that accounts for this new distribution and results in better forward link performance.

The work in this thesis presents new techniques that can be used to improve CDMA forward link performance in both current and next generation cellular networks. This research has made a number of new contributions to the area of wireless communications systems. The new techniques developed in the course of this work offer a significant performance improvement while remaining practical to implement in real systems.

5.2 Future Work

The work presented in this thesis will result in two research initiatives that are based on the channel state estimation work in Chapter 3 and the new metric derivation work in Chapter 4.

The channel state estimation work in Chapter 3 will be extended to develop new techniques for improving the performance of adaptive transmission techniques. The designs of new wireless systems are starting to incorporate a large number of adaptive transmission techniques ranging from adaptive modulation and OFDM sub-carrier selection [23] to adaptive packet transmission scheduling [17].

All adaptive transmission schemes react to changes in the quality of the wireless link between the base station and mobile. Any technique that improves the estimation of this link quality will result in an overall improvement in the performance of adaptive transmission. The channel state estimation work in Chapter 3 is essentially an exploration of new ways to estimate CDMA forward link quality. Since there are many adaptive transmission schemes being proposed for the

CDMA forward link, many of the principles explored in Chapter 3 can be applied to link quality estimation for adaptive transmission.

The work in Chapter 4 demonstrated that it is important to carefully evaluate whether the Gaussian received symbol sample distribution assumption made by conventional channel decoder metrics is valid. When it is not, this chapter also demonstrated that channel decoder performance can be significantly improved by employing a new metric based on the actual received symbol distribution.

There are other cases where the samples of the received channel encoded symbols in a communications system might not be Gaussian distributed. Examples include wireless optical systems corrupted by shot noise, wireless LAN systems, such as 802.11, with a small number of high power interfering signals or wired systems that are subject to self interference or crosstalk. The results in Chapter 4 clearly show that new metrics derived specifically for the distributions of the received symbol samples in these systems could potentially offer a significant performance improvement.

Bibliography

[1] 3rd Generation Partnership Project. Technical specification group radio access network: Multiplexing and channel coding (FDD) (release 1999), 2000-03. V3.2.0.

[2] 3rd Generation Partnership Project. Technical specification group radio access network: Physical channels and mapping of transport channels onto physical channels (FDD) (release 1999), 2000-03. V3.2.0.

[3] 3rd Generation Partnership Project. Technical specification group radio access network: Spreading and modulation (FDD) (release 1999), 2000-03. V3.2.0.

[4] S. M. Alamouti. A simple transmit diversity technique for wireless communications. *IEEE Journal on Selected Areas in Communication*, 16(8):1451–1458, October 1998.

[5] N. Arora and D. George. Interference cancellation schemes for wideband CDMA downlink. In *2000 IEEE International Conference on Personal Wireless Communications*, pages 224–229, December 2000.

[6] P. Bender, P. Black, M. Grob, R. Padovani, N. Sindhushyana, and S. Viterbi. CDMA/HDR: a bandwidth efficient high speed wireless data service for nomadic users. *IEEE Communications Magazine*, 28(7):70–77, July 2000.

[7] N. Benvenuto, R. Sandre, and G. Sostrato. Reduced-state maximum-likelihood multiuser detection for down-link TD-CDMA systems. *IEEE Journal on Selected Areas in Communication*, 20(2):264–272, February 2002.

[8] C. Berrou, A. Glavieux, and P. Thitimajshima. Near Shannon limit error-correcting coding and decoding: Turbo-codes. In *Proceedings of the 1993 IEEE International Conference on Communications (ICC '93)*, volume 2, pages 1064–1070, May 1993.

[9] A. Bircan, O. M. Sunay, and A. N. Akansu. Multicode CDMA downlink in shadowed multipath fading. In *Proceedings of the 2001 IEEE International Conference on Communications (ICC 2001)*, volume 2, pages 462–466, June 2001.

[10] G. E. Bottomley, T. Ottosson, and Y. P. Wang. A generalized RAKE receiver for interference suppression. *IEEE Journal on Selected Areas in Communication*, 18(8):1536–1545, August 2000.

[11] I. N. Bronshtein and K. A. Semendyayev. *Handbook of Mathematics.* Springer, 3 edition, 1957.

[12] G. A. Campbell and R. M. Foster. *Fourier Integrals for Practical Applications.* D. Van Nostrand Company, Inc., 1948.

[13] A. Chheda and D. Paranchych. Performance evaluation of two transmit diversity techniques for cdma2000. In *1999 IEEE Wireless Communications and Networking Conference (WCNC)*, volume 2, pages 893–897, September 1999.

[14] M. V. Clark. Linear receivers for spread spectrum communication over multipath dispersive channels. In *Proceedings of the 1999 IEEE Global Telecom-*

munications Conference (GLOBECOM 1999), volume 1b, pages 837–841, December 1999.

[15] J. De Vriendt, P. Laine, C. Lerouge, and X. Xu. Mobile network evolution: a revolution on the move. *IEEE Communications Magazine*, 40(4):104–111, April 2002.

[16] A. Elezabi and A. Duel-Hallen. Improved single-user decoder metrics for two-stage detectors in DS-CDMA. In *IEEE VTS Fall Vehicular Technology Conference*, volume 3, pages 24–28, Sept. 2000.

[17] R. C. Elliott and W. A. Krzymień. Scheduling algorithms for high throughput packet data service in cellular radio systems. *accepted to the Canadian Journal of Electrical and Computer Engineering.*

[18] P. Z. Fan, N. Suehiro, N. Kuroyanagi, and X. M. Deng. Class of binary sequences with zero correlation zone. *IEE Electronics Letters*, 35(10):777–779, May 1999.

[19] G. J. Foschini and M. J. Gans. On limits of wireless communications in a fading environment when using multiple antennas. *Wireless Personal Communications*, 6:311–335, 1998.

[20] P. Frenger. Turbo decoding for wireless systems with imperfect channel estimates. *IEEE Transactions on Communications*, 48(9):1437–1440, September 2000.

[21] I. Ghauri and D. T. M. Slock. Linear receivers for the DS-CDMA downlink exploiting orthogonality of spreading sequences. In *32nd Asilomar Conference on Signals, Systems and Computers*, volume 1, pages 650–654, November 1998.

[22] M. Ghosh. Adaptive chip-equalizers for synchronous DS-CDMA systems with pilot sequences. In *Proceedings of the 2001 IEEE Global Telecommunications Conference (GLOBECOM 2001)*, volume 6, pages 3385–3389, November 2001.

[23] L. Hanzo, C. H. Wong, and M. S. Yee. *Adaptive Wireless Transceivers*. Wiley, 1 edition, 2002.

[24] M. J. Heikkila, P. Komulainen, and J. Lilleberg. Interference suppression in CDMA downlink through adaptive channel equalization. In *Proceedings of the 1999 IEEE 49th Vehicular Technology Conference (VTC 1999)*, volume 2, pages 978–982, September 1999.

[25] A. H. Hmimy and S. C. Gupta. Performance of turbo-codes for WCDMA systems in frequency selective fading channels. In *Proceedings of the 1999 IEEE 49th Vehicular Technology Conference (VTC 1999)*, volume 2, pages 1459–1463, May 1999.

[26] K. Hooli, M. Juntti, M. J. Heikkila, P. Komulainen, M. Latva-aho, and J. Lilleberg. Chip-level channel equalization in W-CDMA downlink. In *EURASIP Journal on Applied Signal Processing*, volume 8, pages 1–14, 2002.

[27] K. Hooli, M. Latva-aho, and M. Juntti. Performance evaluation of adaptive chip-level channel equalizers in WCDMA downlink. In *Proceedings of the 2001 IEEE International Conference on Communications (ICC 2001)*, volume 6, pages 1974–1979, June 2001.

[28] M. R. Hueda, C. Rodriguez, and C. Marques. New interpath interference model for DS-CDMA indoor transmissions with distributed antennas. In *Proceedings of the 11th IEEE International Symposium on Personal, Indoor*

and Mobile Radio Communications (PIMRC 2000), volume 1, pages 92–97, September 2000.

[29] A. Jalali and A. Gutierrez. Performance comparison of direct spread and multicarrier CDMA systems. In *Proceedings of the 1998 IEEE 48th Vehicular Technology Conference (VTC 1998)*, volume 3, pages 2042–2046, May 1998.

[30] A. Jalali and P. Mermelstein. Effects of diversity, power control and bandwidth on the capacity of microcellular CDMA systems. *IEEE Journal on Selected Areas in Communication*, 12(5):952–961, June 1994.

[31] L. Jalloul, K. Rohani, K. Kuchi, and J. Chen. Performance analysis of CDMA transmit diversity methods. In *IEEE VTS 50th Vehicular Technology Conference, Fall*, volume 3, pages 1326–30, September 1999.

[32] D. N. Kalofonos, E. Kurtas, and G. J. Proakis. Performance of multi-code CDMA systems with concatenated coding and iterative decoding in multipath Rayleigh fading channels. In *Proceedings of the IEEE VTS 50th Vehicular Technology Conference (VTC 1999 - Fall)*, volume 5, pages 2566–2570, September 1999.

[33] S. M. Kay. *Fundamentals of Statistical Signal Processing: Estimation Theory.* Prentice Hall, 1993.

[34] S. M. Kay. *Fundamentals of Statistical Signal Processing: Detection Theory.* Prentice Hall, 1998.

[35] H. Kim, J. Koo, Y. Han, and C. Kang. Forward link capacity based on interference characteristics in CDMA systems. In *Proceedings of the 52nd IEEE VTS Fall Vehicular Technology Conference (VTC 2000 Fall)*, volume 2, pages 592–596, September 2000.

[36] A. Klein. Data detection algorithms specifically designed for the downlink of CDMA mobile radio systems. In *Proceedings of the IEEE 47th Vehicular Technology Conference (VTC '97)*, volume 1, pages 203–207, May 1997.

[37] T. P. Krauss, W. J. Hillery, and M. D. Zoltowski. MMSE equalization for forward link in 3G CDMA: Symbol-level versus chiplevel. In *10th IEEE Workshop on Statistical Signal and Array Processing*, pages 18–22, August 2000.

[38] T. P. Krauss, M. D. Zoltowski, and G. Leus. Simple MMSE equalizers for CDMA downlink to restore chip sequence: Comparison to zero-forcing and RAKE. In *Proceedings of the 2000 IEEE International Conference on Acoustics, Speech and Signal Processing (ICASSP '00)*, volume 5, pages 2865–2868, June 2000.

[39] L. L. Lapin. *Probability and Statistics for Modern Engineering.* PWS-Kent, 2 edition, 1990.

[40] M. Lenardi, A. Medles, and D. T. M. Slock. A SINR maximizing Rake receiver for DS-CDMA downlinks. In *Thirty Fourth Asilomar Conference on Signals, Systems and Computers*, volume 2, pages 1283–1287, October 2000.

[41] M. Lenardi and D. T. M. Slock. A RAKE receiver with intracell interference cancellation for a DS-CDMA synchronous downlink with orthogonal codes. In *Proceedings of the 2000 IEEE 51st Vehicular Technology Conference Spring (VTC 2000-Spring)*, volume 1, pages 430–434, May 2000.

[42] K. L. Li and S. W. Cheung. Modified branch metric for turbo codes using PSA technique in Ricean fading channels. *IEE Proceedings on Communications*, 149(4):227–231, August 2002.

[43] F. Ling. Optimal turbo decoding metric generation in a pilot assisted coherent wireless communication system. In *Proceedings of the 2000 IEEE 52nd Vehicular Technology Conference Fall (VTC 2000-Fall)*, volume 1, pages 298–302, September 2000.

[44] U. Madhow and M. L. Honig. MMSE interference supression for direct-sequence spread-spectrum CDMA. *IEEE Transactions on Communications*, 42(12):3178–3188, December 1994.

[45] M. F. Madkour and S. C. Gupta. Performance analysis of a wireless multirate DS-CDMA in multipath fading channels. In *Proceedings of the 2000 IEEE Emerging Technologies Symposium: Broadband, Wireless Internet Access*, pages 1–5, April 2000.

[46] M. F. Madkour, S. C. Gupta, and T. P. Wang. Successive interference cancellation algorithms for downlink W-CDMA communications. *IEEE Transactions on Wireless Communications*, 1(1):169–177, January 2002.

[47] L. Mailaender. CDMA downlink equalization with imperfect channel estimation. In *Proceedings of the 2001 IEEE 53rd Vehicular Technology Conference Spring (VTC 2001-Spring)*, volume 3, pages 1593–1597, May 2001.

[48] G. G. Messier and W. A. Krzymień. Improved forward link error correction for CDMA systems with space time transmit diversity. In *Proceedings of the 2002 IEEE Global Telecommunications Conference (GLOBECOM 2002)*, volume 1, pages 992–996, Taipei, Taiwan, November 2002.

[49] G. G. Messier and W. A. Krzymień. Improving convolutional code and turbo code performance on the CDMA forward link. In *Proceedings of the IEEE International Symposium on Spread Spectrum Techniques and Applications*

ISSSTA 2002, volume 1, pages 29–33, Prague, The Czech Republic, September 2002.

[50] G. G. Messier and W. A. Krzymień. Improving convolutional code performance on the CDMA forward link. In *Proceedings of the 12th Virginia Tech/MPRG Symposium on Wireless Personal Communications*, volume 1, pages 163–167, Blacksburg, U.S.A, June 2002.

[51] G. G. Messier and W. A. Krzymień. A coloured Gaussian model for CDMA forward link in-cell interference. In *Proceedings of the 2003 IEEE 57th Vehicular Technology Conference Spring (VTC 2003-Spring)*, volume 3, pages 2052–2056, Jeju, Korea, April 2003.

[52] G. G. Messier and W. A. Krzymień. Estimation of in-cell and out-of-cell interference levels for improved CDMA forward link error correction. In *Proceedings of the 2003 IEEE International Conference on Communications (ICC 2003)*, volume 1, pages 368–372, Anchorage, U.S.A., May 2003.

[53] G. G. Messier and W. A. Krzymień. Novel channel decoding for CDMA mobiles with linear MMSE receivers. In *Proceedings of the 15th Internation Conference on Wireless Communications (Wireless '03)*, volume 2, pages 417–441, Calgary, Canada, July 2003.

[54] G. G. Messier and W. A. Krzymień. A new MAP channel decoder trellis path metric for a CDMA mobile subject to channel estimation errors. In *Proceedings of the 2004 IEEE International Conference on Communications (ICC 2004)*, Paris, France, June 2004.

[55] G. G. Messier, J. S. Nielsen, and W. A. Krzymień. CDMA forward link performance evaluation using propagation measurements. In *Proceedings of*

the 2001 IEEE International Conference on Communications (ICC 2001), volume 10, pages 2995–2999, Helsinki, Finland, June 2001.

[56] L. Mucchi, M. Latva-aho, E. Del Re, and R. Fantacci. Sensitivity of blind adaptive LMMSE single-user receivers to path delay and phase estimation errors in multipath fading channel. In *Proceedings of the 2001 IEEE 53rd Vehicular Technology Conference Spring (VTC 2001-Spring)*, volume 4, pages 1814–1818, May 2001.

[57] D. L. Noneaker. Optimal combining for Rake reception in mobile cellular CDMA forward links. In *Proceedings of the 1998 IEEE Military Communications Conference MILCOM 1998*, volume 3, pages 842–846, October 1998.

[58] A. Papoulis. *Probability, Random Variables, and Stochastic Processes.* McGraw-Hill, 3 edition, 1991.

[59] F. Petre, M. Moonen, M. Engels, N. Gyselinckx, and H. De Man. Pilot-aided adaptive chip equalizer receiver for interference suppression in DS-CDMA forward link. In *Proceedings of the 2000 IEEE 52nd Vehicular Technology Conference Fall (VTC 2000-Fall)*, volume 1, pages 303–308, September 2000.

[60] J. G. Proakis. Probabilities of error for adaptive reception of M-phase signals. *IEEE Transactions on Communications*, COM-16:71–81, February 1968.

[61] J. G. Proakis. *Digital Communications.* McGraw Hill, 4 edition, 2001.

[62] M. Rahnema and Y. Antia. Optimum soft decision decoding with channel state information in the presence of fading. *IEEE Communications Magazine*, 35(7):110–111, July 1997.

[63] A. Ramesh, A. Chockaligam, and L. B. Milstein. SNR estimation in generalized fading channels and its application to turbo decoding. In *Proceedings*

of the 2001 IEEE International Conference on Communications (ICC 2001), volume 4, pages 1094–1098, June 2001.

[64] A. Ramesh, A. Chockaligam, and L. B. Milstein. SNR estimation in Nakagami fading with diversity for turbo decoding. In *Proceedings of the 2001 IEEE Military Communications Conference MILCOM 2001*, volume 2, pages 1141–1145, 2001.

[65] P. B. Rapajic and B. S. Vucetic. Adaptive receiver structures for asynchronous CDMA. *IEEE Journal on Selected Areas in Communication*, 12(4):685–697, May 1994.

[66] T. S. Rappaport. *Wireless Communications, Principles and Practice.* Prentice Hall, 1996.

[67] D. T. M. Slock and I. Ghauri. Blind maximum SINR receiver for the DS-CDMA downlink. In *Proceedings of the 2000 IEEE International Conference on Acoustics, Speech and Signal Processing (ICASSP '00)*, volume 5, pages 2485–2488, June 2000.

[68] R. A. Soni, R. M. Buehrer, and J. Tsai. Open-loop transmit diversity in IS-2000 systems. In *33rd Asilomar Conference on Signals, Systems and Computers*, volume 1, pages 654–658, October 1999.

[69] T. A. Summers and S. G. Wilson. SNR mismatch and online estimation in turbo decoding. *IEEE Transactions on Communications*, 46(4):421–423, April 1998.

[70] J. S. Thompson, P. M. Grant, and B. Mulgrew. Downlink transmit diversity schemes for CDMA networks. In *IEEE VTS 50th Vehicular Technology Conference, Fall*, volume 3, pages 1382–1386, September 1999.

[71] TIA/EIA. *IS-95-B: TIA/EIA Interim Standard: Mobile Station Base Station Compatibility Standard for Dual-Mode Wideband Spread Spectrum Cellular System.* Telecommunications Industry Association, 1995.

[72] TIA/EIA. *IS-2000-2: TIA/EIA Physical layer standard for cdma2000 spread spectrum systems.* Telecommunications Industry Association, 1999.

[73] TIA/EIA. *cdma2000 High Rate Packet Data Air Interface Specification.* Telecommunications Industry Association, 2000.

[74] TIA/EIA/IS-97-C. *TIA/EIA Recommended Minimum Performance Standards for Dual-Mode Spread Spectrum Cellular Base Stations.* Telecommunications Industry Association, 1999.

[75] B. Unal. Performance of turbo-codes in time-synchronous BPSK/CDMA systems and Rayleigh fading channels. In *Proceedings of the IEEE VTS 50th Vehicular Technology Conference (VTC 1999 - Fall)*, volume 3, pages 1575–1579, September 1999.

[76] M. C. Valenti and B. D. Woerner. Performance of turbo codes in interleaved flat fading channels with estimated channel state information. In *Proceedings of the 1998 IEEE 48th Vehicular Technology Conference (VTC 1998)*, volume 1, pages 66–70, May 1998.

[77] S. Verdu. Minimum probability of error for asynchronous Gaussian multiple-access channels. *IEEE Transactions on Information Theory*, IT-32:85–96, January 1986.

[78] A. J. Viterbi. *CDMA: Principles of Spread Spectrum Communication.* Addison-Wesley, 1995.

[79] B. Vucetic and J. Yuan. *Turbo Codes: Principles and Applications.* Kluwer, 2000.

[80] Y. Wang, J. Wu, Z. Du, and W. Wu. Performance of MMSE multiuser detection for downlink CDMA. In *Proceedings of the 2000 IEEE International Conference on Communications (ICC 2000)*, volume 2, pages 919–923, June 2000.

[81] R. Wichman and A. Hottinen. Multiuser detection for downlink CDMA communications in multipath fading channels. In *Proceedings of the IEEE 47th Vehicular Technology Conference (VTC '97)*, volume 2, pages 572–576, May 1997.

[82] W. Xiao. Optimal detection of M-QAM signal with channel estimation error. In *Proceedings of the 2003 IEEE International Conference on Communications (ICC 2003)*, volume 5, pages 3251–3255, May 2003.

Appendix A

Advanced Mobile Receiver Structures

In Chapter 3, several techniques are presented for estimating the channel state information required by a CDMA mobile channel decoder. It is important to evaluate the performance of these techniques for mobiles using the Rake receiver since the Rake is commonly used in current CDMA systems. However, developing new CDMA mobile receiver structures capable of canceling interference is a very active area of research. As the processing capabilities of the handset improve, it is very likely that some of these receiver designs will be incorporated into commercial systems. Therefore, in order for the channel state estimation techniques investigated in Chapter 3 to be relevant to future CDMA systems, they must also be applied to mobiles capable of interference cancellation.

A large number of advanced receivers have been proposed for use on the CDMA forward link. The purpose of this appendix is to provide a brief survey of some of these receivers and to select a design that represents a reasonable compromise between complexity and performance. The channel state estimation techniques presented in Chapter 3 will then be adapted for use with this receiver.

A selection of the receiver designs being proposed for the CDMA forward link are discussed in Section A.1. They are divided into two groups: linear receivers and non-linear receivers. The evaluation in this appendix will focus primarily on

linear designs because their lower complexity makes them a more practical choice for implementation.

Section A.2 provides a description of the linear receiver designs selected for evaluation. The description of each receiver includes what assumptions the design makes about forward link interference and whether the receiver requires any additional information beyond the received signal vector. Section A.2 uses the mathematical notation developed for the chip-level CDMA forward link model in Section 2.2 to illustrate the structure and operation of each receiver design.

Simulation is used in Section A.3 to compare the performance of the receivers presented in Section A.2 for high data rate, low spreading factor applications. Simulated channels are used to evaluate the performance of the receivers for both random spreading sequence and Walsh/PN-sequence concatenated spreading schemes. Comparing receivers using these two different spreading schemes provides some insight into how each design deals with interference.

Measured channels are also used for the simulations in Section A.3. A key component of comparing advanced receiver performance is choosing an appropriate multipath channel profile. Most advanced receiver structures improve CDMA forward link performance through some type of intracell interference cancellation or mitigation. The amount of intracell interference present on the forward link of a commercial CDMA system using Walsh/PN-sequence concatenated spreading depends on the extent of multipath dispersion causing Walsh sequence orthogonality degradation. This means that choosing a channel model with excessive multipath dispersion will increase the amount of intracell interference in the system and make interference cancellation look artificially more attractive. Using measured channels ensures a more realistic comparison of receiver designs.

For some of the receiver structures compared in Section A.3, there is a clear tradeoff between performance and complexity. Simulations using measured chan-

nels are used to investigate this tradeoff in Section A.4. Complexity for this comparison is measured in terms of the number of taps used by the receiver. This is generally proportional to the number of computational operations required to detect each symbol.

Final comments related to this survey of receiver designs are made in Section A.5.

A.1 A Survey of CDMA Forward Link Receiver Research

A.1.1 Linear Receivers

The standard Rake receiver is the simplest receiver design used on the CDMA forward link. It was the first receiver used in commercial CDMA mobiles and is still widely used today [78]. The standard Rake has a number of parallel structures called fingers that are used to despread different multipath components of the received signal. After despreading, a finger will multiply its received signal by the conjugate estimate of the complex channel gain of the multipath component it is tracking [61]. After this multiplication, the outputs of all the fingers are time aligned and added together. Under the assumption that all interference and noise on the CDMA forward link can be represented using an AWGN process at the mobile receiver input, this maximal ratio combining maximizes the signal to noise plus interference ratio (SNIR) of the desired signal at the Rake output assuming that the interference plus noise level on each finger is the same.

The Rake receiver with optimal combining has a standard Rake structure but uses finger weights that have a magnitude proportional to the SNIR at the output of each finger [30, 57]. The combining weight phases are equal to the conjugate of the estimated phase of the multipath component complex channel gain tracked by the Rake finger. This receiver structure is based on the observation that the

Walsh spreading sequences allow the despreading stage in each finger to cancel any synchronous intracell interference. The intracell interference that remains at the output of each finger is due to contributions from the other, asynchronous multipath components. As a result, the amount of intracell interference at the output of each finger is different and the desired signal magnitude alone no longer fully represents the finger reliability. Therefore, scaling each finger by the square root of the SNIR at the finger output results in better receiver performance. This technique maximizes the signal to noise plus interference ratio at the output of the Rake receiver under the assumption that the interference and noise in each finger is independent and that the signal to noise ratios at the output of each finger are different.

The Generalized Rake receiver also has a standard Rake structure but uses finger combining weights that satisfy the Neyman-Pearson requirements for a maximum-likelihood detector in coloured Gaussian noise [10, 40]. It is assumed that the interference plus noise at the CDMA mobile finger outputs can be represented using a coloured Gaussian process. The calculation of the covariance matrix of this process accounts for intracell interference correlation caused by multipath dispersion and for the partial Walsh sequence cancellation of that interference. The correlation of intracell interference across different fingers allows the Neyman-Pearson finger combining weight calculation to perform some interference cancellation through the use of a whitening matrix. The authors therefore observe that there is some benefit to having fingers in locations with no desired signal energy is present at all since they provide information that aids in this interference cancellation.

A symbol-level linear minimum mean squared error (LMMSE) receiver has been proposed for the CDMA mobile [44, 65, 14, 37, 80]. This linear receiver minimizes the mean squared error between the receiver output and the desired

data symbol. This operation accounts for the desired signal and interference dispersion caused by the multipath channel and for correlation between forward link spreading codes. While this receiver provides excellent performance, it is quite complex. It requires a large number of taps, estimates of the multipath channel and knowledge of the covariance matrices of all forward link spreading codes. As a result, this receiver is useful for this comparison as a bound on the best performance possible with a linear receiver operating on a single symbol but does not lend itself to practical implementation.

A second LMMSE receiver design proposed for the CDMA forward link, often called the chip-level LMMSE, seeks to minimize the mean squared error between the received signal and the CDMA chip sequence transmitted by the base station [36, 21, 26, 14, 38, 67, 37, 41]. This equalizes multipath channel dispersion and restores the orthogonality of the Walsh spreading sequences. The equalizer is followed by a single despreading stage that recovers the desired data symbol. It can be shown that this receiver is equivalent to the symbol-level LMMSE. However, the dependence on knowledge of the forward link spreading codes can be removed by approximating the codes as white, random processes. This makes the receiver much more practical to implement and has resulted in considerable research being performed on this particular receiver structure. Extensive work has been done on how to best implement this receiver using adaptive or recursive algorithms for both the pilot-assisted [59, 47, 22, 24] and blind scenarios [56].

A.1.2 Non-linear Receivers

Verdu has shown that the maximum likelihood receiver for CDMA systems is implemented by simultaneously detecting all CDMA signals [77]. This approach is referred to as multi-user detection. Multi-user detection has been considered mainly for the reverse link where the base station needs to detect all the signals it

receives and has knowledge of the spreading codes for each user. A CDMA mobile receiver generally decodes only a small subset of the signals transmitted on the forward link and has knowledge only of the spreading codes assigned to it. As a result, it is more difficult to justify multi-user detection for the forward link.

Despite its complexity, multi-user detection has been shown to significantly improve forward link performance [81]. As a result, work has been done to simplify forward link multi-user detection through successive interference cancellation [5, 46] and reduced trellis searches [7].

A.2 Receiver Designs

A.2.1 Selecting Receivers for this Comparison

The receiver structures evaluated in this appendix are all linear. While progress is being made to reduce the complexity of multi-user detection for the CDMA downlink, linear receivers remain the more practical choice for implementation. Blind techniques are not considered since it is assumed that the channel impulse response can be determined using the forward link pilot signal.

When implementing more advanced receivers, like the chip-level LMMSE or generalized Rake receiver, an adaptive or recursive algorithm is typically used to calculate the receiver tap weights. These adaptive algorithms will not be considered for this study. Instead, receiver combining weights are calculated directly from the receiver equations. This is too computationally intensive for implementation in a real mobile but will allow the simulation results in this appendix to reflect the best possible performance that can be obtained using each receiver technique.

A.2.2 Rake Receivers

As defined in Section 2.2.2, the output of a Rake receiver with F fingers is given by

$$y_i = \frac{1}{\sqrt{R}} \boldsymbol{s}_{i,0}^H \boldsymbol{W}_i^H \boldsymbol{M}_i(a,b)^H \boldsymbol{r}_i(a,b) \tag{A.1}$$

The standard Rake receiver, Rake receiver with optimal combining and generalized Rake receiver all share this common structure. They differ only in how the Rake receiver combining weights in $\boldsymbol{W}_i$ are calculated. These calculations are discussed in the following sections.

Standard Rake Receiver (Rake)

The standard Rake receiver uses combining weights $w_i(f) = c_{i,0}(z_f)$ to make up the matrix $\boldsymbol{W}_i$. The finger delays $z_0, \ldots z_{F-1}$ correspond to the arrivals of the strongest signal multipath components during symbol interval i.

Rake Receiver with Optimal Combining (ORake)

The Rake receiver with optimal combining also uses finger delays that track the arrival of the strongest multipath components. However, the receiver combining weights are calculated according to

$$w_i(f) = \left(\sqrt{|\zeta(i)_f|^2 / \sigma^2(i)_f} \right) \angle \left(c_{i,0}(z_f) \right) \tag{A.2}$$

where $\zeta(i)_f$ is the magnitude of the desired signal at the output of finger f and $\sigma^2(i)_f$ is the interference plus noise variance at the output of finger f. The magnitude of $w_i(f)$ is therefore equal to the square root of the SNIR at the output of the despreading stage in finger f and the angle of $w_i(f)$ is equal to the angle of $c_{i,0}(z_f)$.

The signal envelope, $\zeta(i)_f$ can be determined using pilot symbols or fixed transmit energy power control bits embedded in the traffic transmission. The

variance of the interference plus noise at the output of finger f can be calculated according to

$$\sigma^2(i)_f = \sigma_I^2 \sum_{l=0}^{L-1} |c_{i,0}(l)|^2 [1 - \delta(z_f - l)] + \sigma_N^2 \tag{A.3}$$

where σ_I^2 represents the variance of intracell interference at the Rake receiver input and σ_N^2 is the variance of the intercell interference plus thermal noise process at the mobile receiver input.

Generalized Rake Receiver (GRake)

The finger combining weights of the Generalized Rake receiver are determined according to the Neyman-Pearson detection criterion for a generalized matched filter in coloured Gaussian noise [34].

The weights are calculated by considering the desired signal and interference plus noise components at the output of the despreading stage in each finger. The desired signal at the finger outputs is equal to $\boldsymbol{h}_i\sqrt{R}b_{i,0}$ where $\boldsymbol{h}_i = [c_{i,0}(z_0), \ldots c_{i,0}(z_{F-1})]$ and R is the number of spreading chips per encoded information symbol. The combining weights are calculated according to $\boldsymbol{w}_i = \boldsymbol{R}_{IN,i}^{-1}\boldsymbol{h}_i$, where $\boldsymbol{R}_{IN,i}$ is the covariance matrix of the interference and noise across the Rake finger outputs. The element r_{mn} at the mth row and nth column of the covariance matrix is calculated according to

$$\begin{aligned} r_{mn} = \; & \sigma_I^2 \textstyle\sum_{l=0}^{L-1} \sum_{q=0}^{L-1} c_{i,0}^*(z_m) c_{i,0}(l) c_{i,0}(z_n) c_{i,0}^*(q) \\ & \cdot\delta\left[(z_m - l) - (z_n - q)\right] [1 - \delta(z_m - l)][1 - \delta(z_n - q)] \\ & + \sigma_N^2 \delta(m - n). \end{aligned} \tag{A.4}$$

When the GRake receiver structure was originally presented, the authors noted that placing fingers at time offsets without desired signal energy can improve overall receiver performance [10]. This is because these fingers contribute interference

information to the calculation of $\boldsymbol{w}_i$ that improves the cancellation of that interference. However, the authors do not actually present an algorithm to manage the placement of the GRake fingers. For the receiver comparison in this appendix, a simple finger placement algorithm is used where fingers are divided into two groups: signal fingers and interference fingers. The signal fingers are assigned to track the strongest multipath components of the received signal. The interference fingers are spaced in increments of 1 chip to the left and right of the cluster of signal fingers.

A.2.3 Linear Minimum Mean Squared Error (LMMSE) Receivers

Symbol-Level

The symbol-level LMMSE receiver seeks to find the receiver tap weight vector $\boldsymbol{E}_i \in \mathcal{C}^{(b-a)}$ for data symbol i that minimizes $E\left\{|\boldsymbol{E}_i^H \boldsymbol{r}_i(a,b) - b_{i,0}|^2\right\}$. By this definition, the symbol-level LMMSE receiver produces an estimate of $b_{i,0}$ by simultaneously processing all samples of the received signal containing a multipath component of $b_{i,0}$. Therefore, the values of a and b defining the received signal vector size for the LMMSE receiver are $a = iSR$ and $b = (i+1)SR + (L-S)$, where S is the number of samples per chip and $(L-S)$ is the number of samples overlapping with the next symbol interval due to multipath dispersion. This corresponds to a receiver with $SR + (L-S)$ taps. The tap weight vector of an LMMSE receiver is determined according to $\boldsymbol{E}_i = \boldsymbol{C}_{br}\boldsymbol{C}_{rr}^{-1}$, where $\boldsymbol{C}_{br}$ is the cross-covariance matrix between the desired data symbol and received signal and $\boldsymbol{C}_{rr}$ is the covariance matrix of the received signal [33].

The LMMSE receiver is a Bayesian estimator for data symbol $b_{i,0}$ and incorporates some *a priori* knowledge of $b_{i,0}$ into the tap weight calculation. This *a priori* information takes the form of the cross-covariance vector of the desired data symbol with the received symbol vector, $\boldsymbol{C}_{br}$. In this application, $\boldsymbol{C}_{br}^T \in \mathcal{C}^{(b-a)}$ is

a row vector calculated according to

$$\boldsymbol{C}_{br} = [\ 0\ \cdots\ 0\ \boldsymbol{s}_{i,0}^H\ 0\ \cdots\ 0\ ]\boldsymbol{C}_i^H \boldsymbol{D}_i(a,b)^H \tag{A.5}$$

where $[\ 0\ \cdots\ 0\ \boldsymbol{s}_{i,0}^H\ 0\ \cdots\ 0\ ]$ has length 3R and is the spreading code for $b_{i,0}$, $\boldsymbol{s}_{i,0}^H$, padded on either side by R zeros. The channel tap matrix, $\boldsymbol{C}_i$, and the chip waveform matrix, $\boldsymbol{D}_i(a,b)$, are defined in Section 2.2.1.

The covariance matrix of the received signal, $\boldsymbol{C}_{rr}$, is calculated in Chapter 2 from the received signal according to (2.13) and is written as

$$\boldsymbol{C}_{rr} = \boldsymbol{D}_i(a,b)\boldsymbol{C}_i\boldsymbol{R}_{SS}(i)\boldsymbol{C}_i^H\boldsymbol{D}_i(a,b)^H + \sigma_N^2\boldsymbol{I}. \tag{A.6}$$

The matrix $\boldsymbol{R}_{SS}(i) \in \mathcal{C}^{3R\times 3R}$ is the covariance matrix of the data symbols multiplied by their spreading codes. The calculation of this matrix requires knowledge of the spreading codes and data symbols of all users on the forward link. Generally, it is assumed that the forward link spreading codes during the desired symbol interval are known but the information bits of the other users are not [26]. Under these conditions, the matrix $\boldsymbol{R}_{SS}(i)$ is written as

$$\begin{aligned}\boldsymbol{R}_{SS}(i) &= \operatorname{diag}\left\{2K,\ldots,2K,\textstyle\sum_{k=0}^{K-1}\boldsymbol{s}_{i,k}\boldsymbol{s}_{i,k}^H,2K,\ldots,2K\right\}\\ &= \begin{bmatrix} 2K & 0 & \ldots & 0 & \ldots & 0 & 0\\ 0 & 2K & \ldots & 0 & \ldots & 0 & 0\\ \vdots & \vdots & \vdots & \vdots & \vdots & \vdots & \vdots\\ \vdots & \vdots & \vdots & \sum_{k=0}^{K-1}\boldsymbol{s}_{i,k}\boldsymbol{s}_{i,k}^H & \vdots & \vdots & \vdots\\ \vdots & \vdots & \vdots & \vdots & \vdots & \vdots & \vdots\\ 0 & 0 & \ldots & 0 & \ldots & 2K & 0\\ 0 & 0 & \ldots & 0 & \ldots & 0 & 2K \end{bmatrix}.\end{aligned} \tag{A.7}$$

This is a $3R \times 3R$ matrix with a $R \times R$ matrix in the middle, $\sum_{k=0}^{K-1}\boldsymbol{s}_{i,k}\boldsymbol{s}_{i,k}^H$, equal to the summation of covariance matrices of each spreading code used in symbol interval i. This center matrix is surrounded on all sides by a band of zeros with diagonals equal to 2K. The width of this band is equal to R on all four sides. This

unusual structure is due to the lack of knowledge of the data symbols causing ISI which results in the band of zeros surrounding $\sum_{k=0}^{K-1} \boldsymbol{s}_{k,i}\boldsymbol{s}_{k,i}^H$.

The symbol-level LMMSE yields excellent performance but is very difficult to implement in practice. The mobile requires knowledge of all forward link spreading sequences in order to calculate $\boldsymbol{R}_{SS}(i)$. The large number of receiver taps in the symbol-level LMMSE also means that calculating the receiver tap weights requires intensive computation. As a result, the symbol-level LMMSE is considered in this report mainly as a bound indicating the best performance possible with a linear receiver that processes samples over a single symbol interval.

Chip-Level

The chip-level LMMSE receiver seeks to recover the chips of the CDMA waveform transmitted by the base station by equalizing the multipath dispersion of the radio channel. This restores the orthogonality of the forward link Walsh spreading sequences and reduces the level of intracell interference. The data symbols are then recovered with a single despreading stage. The derivation of this receiver is part of the chip level model presented in Chapter 2 and is included in Section 2.2.3.

A.3 Receiver Performance Comparison

A.3.1 Simulation Description

The CDMA forward link is simulated using the chip-level model presented in Section 2.2. The number of spreading code chips per symbol, R, is 8 and 5 equal power forward channel users are assumed. The chip rate is equal to 1.2288 Mcps, data rate is 153.6 kbps and frame length is 20 ms. Channel coding is not used. White Gaussian noise is added to input of the mobile receiver with a variance equal to $R/(E_b/N_o)$, where E_b/N_o is the ratio of bit energy to thermal noise power spectral density. The simulation results show the forward link bit error

rate (BER) of user 0 plotted versus E_b/N_o. The level of intracell interference remains constant for all values of E_b/N_o.

A performance comparison is conducted in Section A.3.2 using a simulated channel model that considers both random spreading sequences and the Walsh/PN sequence concatenated spreading scheme commonly used in commercial CDMA systems [72, 3]. Section A.3.4 presents a performance comparison of different receivers conducted using measured channels and Walsh/PN-sequence concatenated spreading. The technique used to collect the radio channel measurements is discussed in Section A.3.3

A.3.2 Simulated Channel Results

A three path, Rayleigh fading channel model with average relative received path powers equal to -2 dB, -6 dB and -10 dB is used to compare the performance of different receivers. The Rake and ORake receivers use 3 fingers and the GRake uses 3 signal fingers with 2 interference fingers. The chip-level LMMSE equalizer uses 5 taps. Simulation results for random spreading sequences are shown in Fig. A.1 and results for Walsh/PN-sequence concatenated spreading are shown in Fig. A.2.

Walsh/PN-sequence concatenated spreading offers partial intracell interference cancellation, even in the presence of multipath dispersion. As a result, receiver performance in Fig. A.2 is generally better than in Fig. A.1. The figures also indicate that the relative performance of the different receiver structures will change depending on the type of spreading scheme being used.

The ORake uses combining weights with magnitudes proportional to the SNIR at the output of each finger. These weights offer a slight improvement when the interference levels at the output of each finger are different. However, this only happens when Walsh/PN-sequence spreading is used and partial cancellation of

intracell interference occurs in each finger. When random spreading sequences are used, no interference cancellation occurs in the fingers and the interference level is the same at all the finger outputs. As a result, ORake and standard Rake performance is equivalent in Fig. A.1.

The GRake and chip-level LMMSE receiver performance is much better when the Walsh/PN-sequence concatenated spreading is used. An advanced receiver structure is only able to compensate for an impairment when it has information describing that impairment. The GRake and chip-level LMMSE are only given information describing the multipath channel and therefore can only cancel the interference caused by multipath dispersion by equalizing the channel. This provides a significant improvement for Walsh/PN-sequence spreading since Walsh sequences are able to remove all intracell interference once multipath dispersion is removed. However, the improvement provided by the GRake and chip-level LMMSE is less significant for random spreading sequences that offer no synchronous intracell interference cancellation.

These results also indicate that the performance of the GRake and chip-level LMMSE equalizer is approximately equivalent for the simulated channel. Both receivers employ a whitening matrix inversion that attempts to remove interference caused by multipath dispersion. The difference is that the chip-level LMMSE performs the whitening before despreading and the GRake whitens after despreading. However, since both receivers are linear, the resulting performance is the same.

Figs. A.1 and A.2 indicate that the symbol-level LMMSE receiver performance remains fairly consistent, regardless of whether random spreading sequences or Walsh/PN-sequence concatenated spreading is being used. Like the GRake and chip-level LMMSE, the symbol level LMMSE receiver uses channel information to compensate for multipath dispersion. However, the symbol-level LMMSE also has information describing the correlation properties of the forward link spread-

ing codes. This further improves its ability to cancel interference, yielding good performance even when random spreading codes are used.

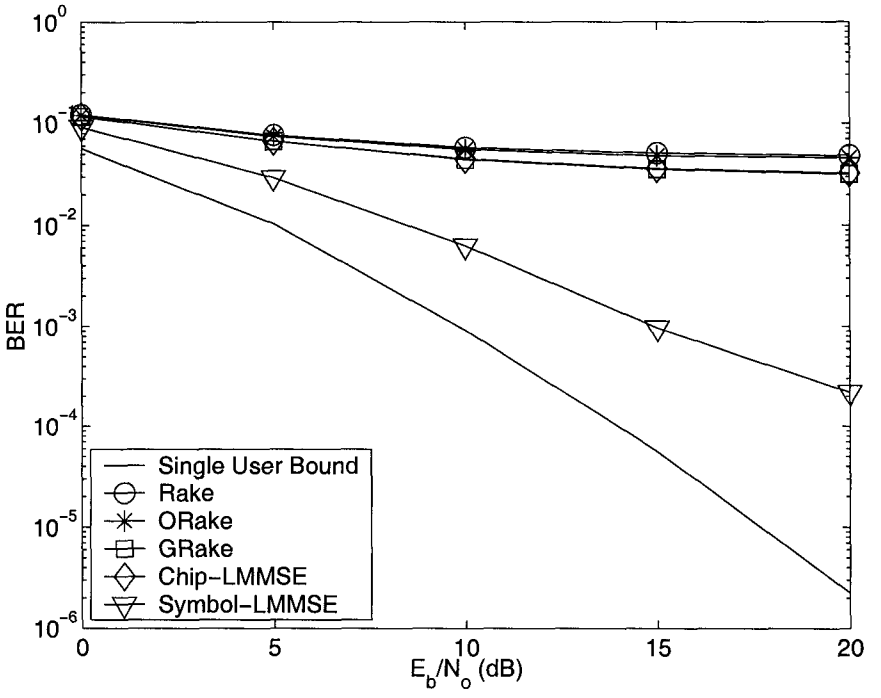

Figure A.1: Simulated channel, random spreading sequences.

A.3.3 Collecting Radio Channel Measurements using Base Station Pilot Signals

The measurement system used for collecting the radio channel measurements used in Section A.3.4 uses a PN sequence to determine the impulse response of the radio channel. A PN sequence is transmitted through the radio channel and the baseband quadrature components of the received signal are correlated with a locally generated copy of the PN sequence. The result of the correlation operation is the complex impulse response of the channel [66].

In order to capture time variations in the channel, a continuously repeating PN sequence is transmitted. The receiver records a T_m second snapshot of the

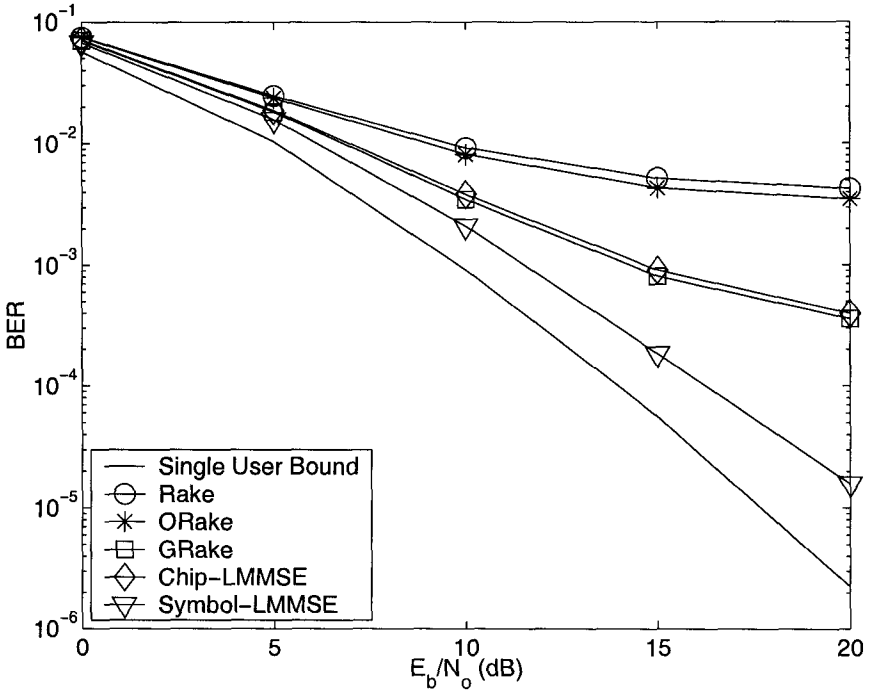

Figure A.2: Simulated channel, Walsh/PN-sequence concatenated spreading.

PN sequence, illustrated in Fig. A.3. The received signal is then divided into several consecutive segments of duration T_{seg}. The value of T_{seg} must be long enough to provide sufficient processing gain in the correlation but shorter than the channel coherence time in order to not obscure time variations in the channel. As a compromise, T_{seg} is set to half the channel coherence time. A correlation is performed over each segment using a locally generated copy of the transmitted PN sequence. The impulse responses generated by the correlation operations characterize propagation conditions for each segment interval. Once the impulse responses are generated, they can be grouped together to form a complex-valued channel impulse response surface. The surface is normalized such that large scale propagation effects are removed. The magnitude of an example surface collected in an urban area of Calgary, Canada using this technique is shown in Fig. A.4.

When collecting forward link propagation data in several different environ-

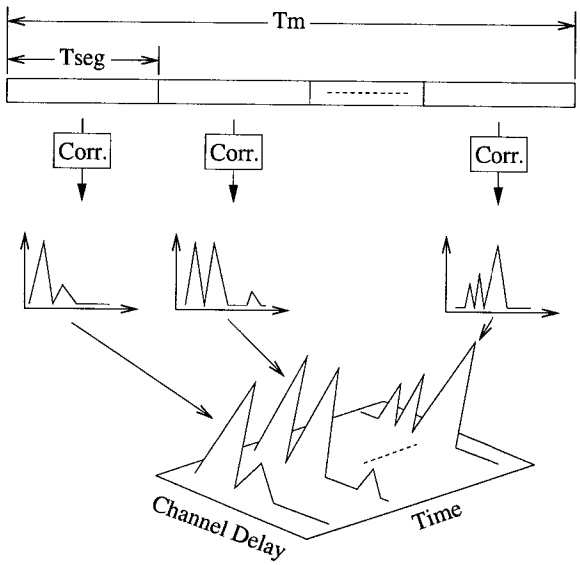

Figure A.3: Dynamic channel characterization.

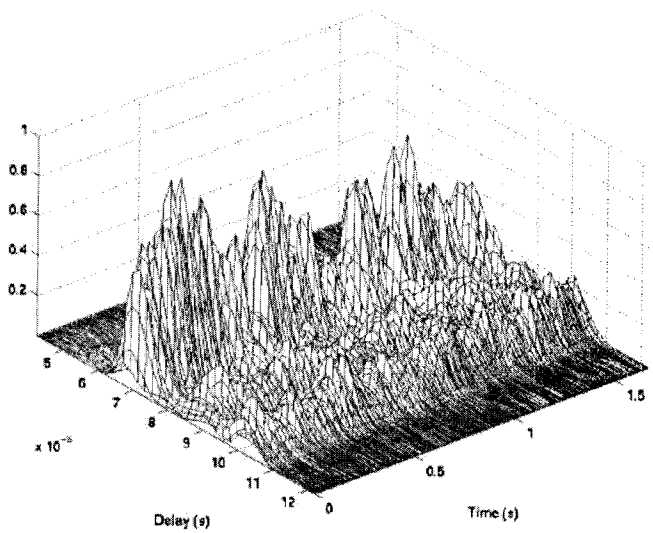

Figure A.4: Urban forward channel impulse response.

ments, it can be time consuming to deploy and adjust transmit antennas to ensure the measurements characterize channel conditions for a realistic base station configuration. To avoid this problem, the measurements considered in this study are collected using the pilot signals transmitted by IS-95 base stations in the 2 GHz PCS band. This allows propagation data to be easily collected in a wide variety of environments for realistic base station antenna configurations and transmit powers.

When using IS-95 pilot signals for channel measurements, there is some interference from the other spread spectrum signals transmitted by the base station. The maximum vehicle velocity used to collect measurements for this work is 70 km/h. Assuming channel coherence time is the inverse of the maximum Doppler frequency, a radio channel at PCS frequencies remains approximately stationary for 8 ms at this speed. The length of the correlation interval used to extract the measurements, T_{seg}, is therefore 4 ms. At the IS-95 chip rate of 1.2288 Mcps, this provides a processing gain of 37 dB which is sufficient to ensure forward link interference does not significantly corrupt the measurements. For lower velocity measurements, T_{seg} is increased and the processing gain is further improved.

A.3.4 Measured Channel Results

In order to compare the receiver structures using realistic multipath profiles and fading statistics, forward link simulations are also conducted using measured channel responses instead of a statistical channel model. The technique described in Section A.3.3 was used to collect a series of dynamic channel impulse response measurements in the downtown core of Calgary, Canada [55].

The simulations described in Section A.3.2 are rerun with the measured channels replacing the simulated channel model. The simulation parameters are the

same except that the Rake and ORake are now simulated with 3 fingers, the GRake uses 3 signal fingers with 3 interference fingers and the Chip-LMMSE uses 6 taps. The simulation results are shown in Fig. A.5.

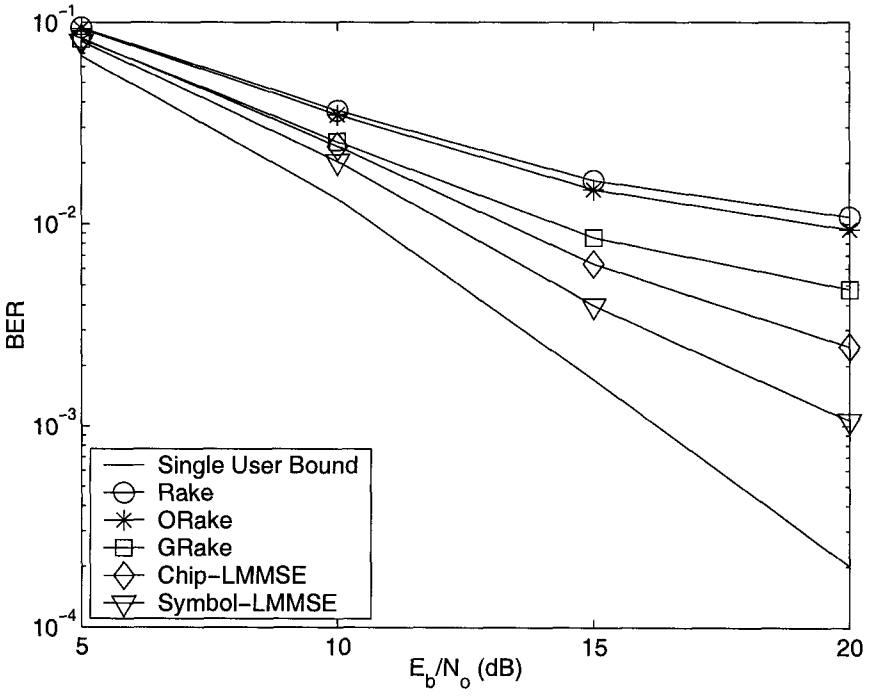

Figure A.5: Measured channel, Walsh/PN-sequence concatenated spreading codes.

It is clear that the performance benefit of using more advanced receiver structures is smaller for the measured channel than for the simulated channel presented in Section A.3.2. This is a result of the smaller delay spread of the measured urban channel.

Calgary's downtown core is a dense cluster of 30 to 50 story office buildings. However, despite the rich scattering environment, the mean value of the measurement RMS delay spreads is only 1.1 μs. The relatively small delay spread is not due to a lack of scattering objects but rather to small cell size. In a dense urban environment, cell size is reduced to handle increased user density. The average

radius of the cells were the measurements were collected is approximately 400 m. If a cellular service provider decides on a cell radius of 400 m, great care will be taken with antenna tilting and transmit power adjustments to ensure the base station pilot signal is not transmitted beyond that region. As a result, channel impulse response measurements collected using base station pilot signals will generally have small delay spreads in dense urban environments.

At a chip rate of 1.2288 Mcps and average delay spread of 1.1 μs, the number of resolvable multipath components will be approximately two. Under these conditions, the Walsh sequence intracell interference cancellation achieved with a standard Rake receiver is quite good and the benefit of canceling additional intracell interference with more advanced receiver structures is reduced.

Fig. A.5 also shows that the chip-level LMMSE performs better than the GRake on measured channels. The degradation of the GRake is caused by the algorithm used to position the GRake fingers. The chip-level LMMSE always uses equally spaced taps. However, the GRake positions its signal fingers on the largest multipath components and then equally spaces its interference fingers to the left and right of the signal finger cluster. This algorithm performed well on the regularly spaced channel path delays of the simulated channel but performs poorly on a realistic channel profile. The inventors of the GRake indicate that determining optimal finger positions is still an outstanding problem [10]. Since the chip-level LMMSE has similar computational complexity to the GRake without the finger positioning problems, it is a better structure for use in realistic channels.

A.4 The Complexity vs. Performance Tradeoff

This section illustrates the benefit of adding extra complexity to advanced receiver structures when used in realistic channels. Only the chip-level LMMSE receiver is considered. Adding additional fingers to the Rake and ORake receivers considered

in Section A.3.2 would not result in an improvement since 3 fingers are sufficient to capture all the desired signal energy from the measured channels. Changing the number of taps in the symbol-level LMMSE is not possible since, by the definition provided in Section A.2.3, it must simultaneously process all received signal samples that contain desired symbol energy. Finally, the GRake is not considered due to the difficultly assigning finger positions that was discussed in Section A.3.4.

Simulations of the chip-level LMMSE receiver are performed using the measured channels and the simulation parameters described in Section A.3.2. Simulations are conducted for 6, 7 and 8 receiver taps and the results are shown in Fig. A.6.

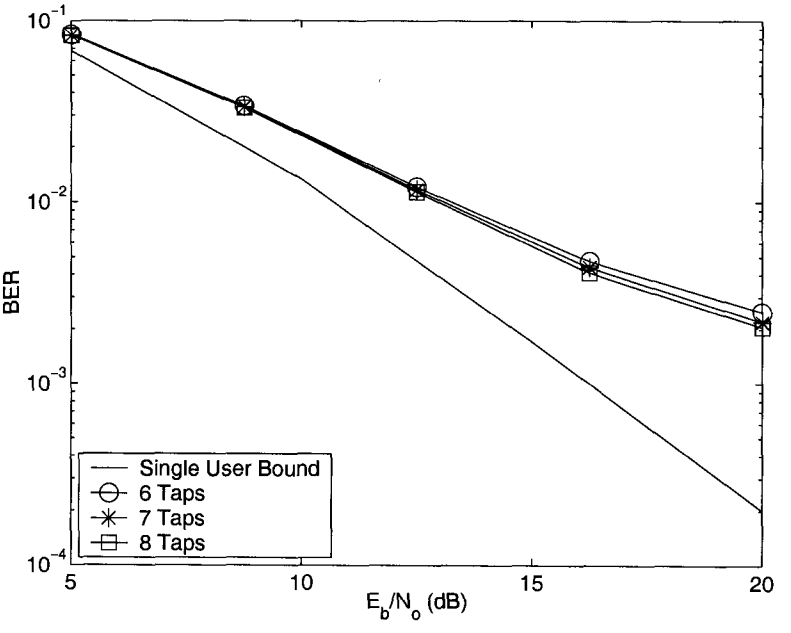

Figure A.6: Measured channel, varied chip-level LMMSE complexity.

Fig. A.6 indicates that the benefit of increasing the number of taps in the chip-level LMMSE equalizer is quite small. This is due to the relatively short delay spread of the measured channel. If delay spread is small, the channel can

be equalized with a small number of taps. If the channel was more dispersive, increasing the number of receiver taps to deal with this multipath would show a more dramatic improvement than indicated in Fig. A.6.

A.5 Selection of a Receiver Design

Advanced receiver structures have received considerable attention as one way to improve CDMA forward link performance. Both linear and non-linear receiver designs have been proposed but the lower complexity of the linear receivers make them the most likely candidates for implementation. The linear receiver structures considered in this report are the Rake receiver, Rake receiver with optimal combining, generalized Rake receiver, chip-level LMMSE receiver and symbol-level LMMSE receiver.

The performance of these receivers is considerably different when used on simulated and measured channels. Simulation results for a three path simulated channel model indicate that the interference cancellation of the advanced receiver structures offer a significant performance improvement. However, when the same receivers are used on measured channels, the improvement is more modest. This is because the smaller delay spread of the particular measured channel results in less intracell interference. As a result, using receivers that are able to cancel that interference provides less of a benefit.

As pointed out in Section A.3.4, cellular channels with extremely large delay spreads are uncommon. In dense urban areas with lots of clutter, cells tend to be very small. Since the base stations are only illuminating a small area, channel delay spreads are short. In residential or rural regions with larger cell sizes, the amount of clutter is typically less. This serves to maintain shorter delay spread values. As a result, if advanced receiver structures are deployed in real mobiles, the overall capacity improvement will likely be significant but may be less than

suggested by some simulated channel models.

Small delay spreads also mean that it may not be worthwhile to increase receiver complexity by using a large number of receiver taps. Simulations using measured channels indicate that most of the benefit of using interference cancellation can be realized with a relatively small number of taps.

The results in this appendix indicate that some receiver structures can perform poorly when used on the irregularly shaped multipath profiles of measured channels. In simulated channels, the GRake performance is equivalent to the chip-level LMMSE. However, the GRake performance degrades when its finger positioning algorithm is applied to a measured radio channel.

Overall, these results indicate that interference cancellation through advanced receiver structures may significantly improve CDMA forward link performance. The chip-level LMMSE receiver, in particular, stands out as a good compromise between performance and complexity. However, it is important to consider realistic propagation conditions when attempting to quantify the performance improvement.